

DEPARTAMENTO DE ASTROFÍSICA

Universidad de La Laguna

*From sketch to painting: multiwavelength analysis of  
low-mass X-ray binaries*

Thesis submitted by  
D. Daniel Mata Sánchez  
As a requirement for the degree of  
Doctor by the University of La Laguna

Supervisors:  
Dr. Teodoro Muñoz Darias  
and  
Dr. Jorge Casares Velázquez



INSTITUTO D' ASTROFÍSICA D' CANARIAS  
June 2017

Este documento incorpora firma electrónica, y es copia auténtica de un documento electrónico archivado por la ULL según la Ley 39/2015.  
*Su autenticidad puede ser contrastada en la siguiente dirección <https://sede.ull.es/validacion/>*

Identificador del documento: 970342

Código de verificación: pkuTTaUi

Fecha: 29/06/2017 10:41:42

Firmado por: DANIEL MATA SÁNCHEZ  
UNIVERSIDAD DE LA LAGUNA

29/06/2017 11:14:09

JORGE CASARES VELAZQUEZ  
UNIVERSIDAD DE LA LAGUNA

TEODORO MUÑOZ DARIAS  
UNIVERSIDAD DE LA LAGUNA

ERNESTO PEREDA DE PABLO  
UNIVERSIDAD DE LA LAGUNA

29/06/2017 12:50:38

04/07/2017 18:28:11

Examination date: September, 2017  
Thesis supervisor: Teodoro Muñoz Darias  
Thesis supervisor: Jorge Casares Velázquez

©Daniel Mata Sánchez 2017

ISBN: xx-xxx-xxxx-x

Depósito legal: TF-xxxx/2017

Some of the figures included in this document have already been published in *Monthly Notices of the Royal Astronomical Society*.

Este documento incorpora firma electrónica, y es copia auténtica de un documento electrónico archivado por la ULL según la Ley 39/2015.  
*Su autenticidad puede ser contrastada en la siguiente dirección <https://sede.ull.es/validacion/>*

Identificador del documento: 970342

Código de verificación: pkuTTaUi

Firmado por: DANIEL MATA SÁNCHEZ UNIVERSIDAD DE LA LAGUNA	Fecha: 29/06/2017 10:41:42
JORGE CASARES VELAZQUEZ UNIVERSIDAD DE LA LAGUNA	29/06/2017 11:14:09
TEODORO MUÑOZ DARIAS UNIVERSIDAD DE LA LAGUNA	29/06/2017 12:50:38
ERNESTO PEREDA DE PABLO UNIVERSIDAD DE LA LAGUNA	04/07/2017 18:28:11

*A mis padres;  
a mi abuela Eudoxia;  
a Xana.*

Este documento incorpora firma electrónica, y es copia auténtica de un documento electrónico archivado por la ULL según la Ley 39/2015.  
*Su autenticidad puede ser contrastada en la siguiente dirección <https://sede.ull.es/validacion/>*

Identificador del documento: 970342

Código de verificación: pkuTTaUi

Firmado por: DANIEL MATA SÁNCHEZ  
UNIVERSIDAD DE LA LAGUNA

Fecha: 29/06/2017 10:41:42

JORGE CASARES VELAZQUEZ  
UNIVERSIDAD DE LA LAGUNA

29/06/2017 11:14:09

TEODORO MUÑOZ DARIAS  
UNIVERSIDAD DE LA LAGUNA

29/06/2017 12:50:38

ERNESTO PEREDA DE PABLO  
UNIVERSIDAD DE LA LAGUNA

04/07/2017 18:28:11

Este documento incorpora firma electrónica, y es copia auténtica de un documento electrónico archivado por la ULL según la Ley 39/2015.  
*Su autenticidad puede ser contrastada en la siguiente dirección <https://sede.ull.es/validacion/>*

Identificador del documento: 970342

Código de verificación: pkuTTaUi

Firmado por: DANIEL MATA SÁNCHEZ UNIVERSIDAD DE LA LAGUNA	Fecha: 29/06/2017 10:41:42
JORGE CASARES VELAZQUEZ UNIVERSIDAD DE LA LAGUNA	29/06/2017 11:14:09
TEODORO MUÑOZ DARIAS UNIVERSIDAD DE LA LAGUNA	29/06/2017 12:50:38
ERNESTO PEREDA DE PABLO UNIVERSIDAD DE LA LAGUNA	04/07/2017 18:28:11

## Agradecimientos

Parece mentira que hayan pasado ya 4 años desde que comencé la tesis. Durante este tiempo, he conocido a mucha gente que me ha ayudado de una forma u otra a llegar hasta aquí.

En primer lugar quiero dar las gracias a mi familia, sobre todo a mis padres, Marisa y Jose, por su continuo apoyo y paciencia. Especialmente cuando cambié los veranos calurosos e inviernos nevados de Salamanca por el “particular” clima lagunero. Siempre me han animado a hacer lo que me gustara, aunque fuera a más de 1500 kilómetros de casa y mirando al firmamento. Gracias también a todos mis tíos, primos, sobrinos segundos, abuelos y “arrimados”, por interesarse durante las comidas familiares en qué era eso de las binarias de rayos X. Sobre todo a mi abuela Eudoxia, a quien, cuando le contaba que estudiaba física, temía que me fuera a dedicar a hacer bombas. Por suerte salí a ella gracias a su papel como madrina; y así he acabado, escribiendo una tesis.

Gracias también a mi otra familia, la científica, empezando por mis directores Teo y Jorge. Durante todo este tiempo, han sido una fuente de conocimiento, motivación e inspiración continua. Me gustaría pensar que he heredado algo de su dedicación y paciencia: siempre están al pie del cañón, a pesar de que a las binarias de rayos X les guste hacerse notar en plenas vacaciones de verano o en Navidad. Y cómo olvidar al grupo de binarias de rayos X: Montse, Nacho, Manu Linares, Pablo (gracias por tu labor como árbitro de esta tesis; espero que algún día me perdone por hacerte trabajar en fin de semana), Tariq e incluso Juan (nuestro infiltrado de AGNs). También a Manu Torres, que me hizo sentirme como en casa durante mi estancia en Utrecht; y a Ali, cuyo fugaz paso por el grupo dejó huella. Gracias a Felipe, que me convirtió en “hermano mayor” a pesar de ser hijo único; siempre recordaré dónde está el Este, no te preocupes. Con todos ellos he compartido incontables reuniones de trabajo acompañadas, como no podía ser de otra manera, de sus correspondientes comidas de trabajo... que a veces llevaban a sobremesas (de trabajo)... e incluso a cenas (de trabajo también, por supuesto). También agradezco su cálida acogida al Instituto de Astrofísica de Canarias, al Netherlands Institute for Space Research (SRON); y también a la Universidad de Oxford. Gracias ellos pude conocer a científicos como Jonay, Peter Jonker o Phil Charles, que me ayudaron mejorar durante mis inicios en el mundo de la investigación.

Firmado por: DANIEL MATA SÁNCHEZ UNIVERSIDAD DE LA LAGUNA	29/06/2017 11:14:09
JORGE CASARES VELAZQUEZ UNIVERSIDAD DE LA LAGUNA	29/06/2017 12:50:38
TEODORO MUÑOZ DARIAS UNIVERSIDAD DE LA LAGUNA	04/07/2017 18:28:11
ERNESTO PEREDA DE PABLO UNIVERSIDAD DE LA LAGUNA	

Y por último, pero no por ello menos importante, quiero agradecer su inigualable compañía a los que han sido mis compañeros de fatigas en esta odisea llamada tesis. A Marcos, contador profesional de chistes malos, y mi cupido personal; y a Ernest, compañero de frikismo y cervezas. A Morate, Ferra, Awe, Pryzia y Ray; que me ayudaron a descubrir tantos juegos de mesa y de rol que ahora tendré problemas en la mudanza. A Ismael; Sara y Javi (junto a Drogon, por supuesto); Rebeca, que me soportó como compañero de piso; Sergio, Víctor, Dani... En La Topa siempre recordarán nuestras discusiones sobre lengua y filosofía. Y en especial, muchas gracias a Xana, por haberme apoyado durante este último año de doctorado, más aún teniendo en cuenta que también era su último año de tesis. *Me has conocido en un momento extraño de mi vida.*

No me olvido de todos los demás amigos que he conocido durante mi vida en las islas. Artemi, Alejandra y Andrés, Isa, Ana, David, Cristina, Inés, Júlia... La lista es interminable y sin duda me dejo mucha gente, pero confío en que os déis por agradecidos.

En definitiva, gracias a todos los que habéis sido parte de mi vida hasta ahora. Nos vemos al otro lado de la tesis.

Daniel

Este documento incorpora firma electrónica, y es copia auténtica de un documento electrónico archivado por la ULL según la Ley 39/2015.  
Su autenticidad puede ser contrastada en la siguiente dirección <https://sede.ull.es/validacion/>

Identificador del documento: 970342

Código de verificación: pkTTaUi

Fecha: 29/06/2017 10:41:42

Firmado por: DANIEL MATA SÁNCHEZ  
UNIVERSIDAD DE LA LAGUNA

JORGE CASARES VELAZQUEZ  
UNIVERSIDAD DE LA LAGUNA

TEODORO MUÑOZ DARIAS  
UNIVERSIDAD DE LA LAGUNA

ERNESTO PEREDA DE PABLO  
UNIVERSIDAD DE LA LAGUNA

29/06/2017 11:14:09

29/06/2017 12:50:38

04/07/2017 18:28:11

# Resumen

Las binarias de rayos X están formadas por un objeto compacto (bien un agujero negro de masa estelar o una estrella de neutrones) y una estrella compañera, que transfiere material al primero a través de un disco de acreción. Estos sistemas fueron descubiertos por primera vez gracias a su intensa radiación en la banda de los rayos X, pero para poder comprender y caracterizar su fenomenología extrema es necesario observar en otras longitudes de onda. En esta tesis presentamos un estudio observacional multifrecuencia de cinco binarias de rayos X poco masivas (del inglés, LMXB); una subclase definida por tener compañeras de tipo espectral tardío ( $\lesssim 1 M_{\odot}$ ). Las binarias observadas contienen tanto estrellas de neutrones como agujeros negros.

Comenzaremos analizando dos sistemas transitorios recientemente descubiertos cuyos parámetros fundamentales aún están siendo debatidos.

El primero es MAXI J1957+032, una binaria de rayos X transitoria recientemente descubierta y que ha entrado en erupción hasta en 4 ocasiones en sólo 16 meses, siendo cada erupción igualmente corta (< 5 días). Estas frecuentes y cortas erupciones (comparadas con otros sistemas transitorios), en combinación con el espectro sin líneas que obtuvimos durante el evento de septiembre de 2016, sugieren que es una nueva LMXB de periodo orbital corto. En esta tesis proporcionamos algunas de sus propiedades principales, como la distancia y la luminosidad. La naturaleza de su objeto compacto, sin embargo, es aún desconocida.

El segundo sistema, Swift J1357.2-0933, fue descubierto durante una erupción en 2011 que permitió clasificarlo como una LMXB con un agujero negro. Obtuvo espectroscopía con el telescopio GTC durante el estado de quietud, momento en el cual el disco de acreción contribuye menos al flujo en el rango visible. Sin embargo, no encontramos ningún rastro de los rasgos de absorción de la estrella compañera. No obstante, nuestro análisis espectroscópico impuso nuevas restricciones a la contribución al flujo en el rango visible de origen no estelar, lo que nos permitió estimar la distancia y altura sobre el plano Galáctico de esta fuente. También presentamos un límite restrictivo a la masa del agujero negro ( $> 9.3 M_{\odot}$ ). Por tanto, Swift J1357.2-0933 contiene uno de los agujeros negros estelares más masivos jamás encontrados en nuestra Galaxia y es un nuevo miembro de la población recientemente descubierta a más de  $> 1 \text{ kpc}$  del plano Galáctico.

A continuación, analizamos dos sistemas binarios canónicos que albergan una estrella de

neutrones con el objetivo de estudiar sus estrellas compañeras, que hasta el momento nunca habían sido detectadas.

Scorpius X-1 es la LMXB canónica con estrella de neutrones. A pesar de que fue descubierta durante los inicios de la astronomía de rayos X (hace más de 50 años), su naturaleza persistente ha evitado que se realizara un estudio dinámico sobre su estrella compañera (dado que sólo es posible durante la quietud). En este trabajo obtuvimos espectroscopía en el infrarrojo cercano y realizamos un análisis Monte Carlo que nos permitió establecer restricciones más férreas sobre las masas de este sistema prototípico.

Aquila X-1 es también una LMXB con estrella de neutrones, pero en este caso del subtipo transitorio. Exhibe erupciones recurrentes cada dos años, y ha sido exhaustivamente estudiada desde su descubrimiento hace más de 40 años. A pesar de su brillo relativamente elevado (tanto en el rango visible como en el infrarrojo cercano), su estudio dinámico en quietud no ha sido posible debido a la presencia de una estrella de campo cercana (a sólo 0.4 segundos de arco). Usando el espectrógrafo de campo integral SINFONI instalado en el telescopio VLT y su módulo de óptica adaptativa conseguimos aislar Aquila X-1 y obtener espectros en distintas fases orbitales. Esto nos permitió detectar, por primera vez, los rasgos de absorción de su estrella compañera, así como medir su curva de velocidad radial. Asimismo, hemos podido establecer nuevas restricciones a la distancia al sistema, así como a la inclinación orbital, que no favorece la presencia de una estrella de neutrones masiva.

Para completar esta muestra también presentamos los resultados de la mayor campaña espectroscópica en el rango visible jamás realizada (de la que tengamos conocimiento) sobre la erupción de una binaria transitoria de rayos X. V404 Cygni es una LMXB que alberga un agujero negro y exhibe erupciones cada  $\sim 25$  años. Sus parámetros dinámicos han sido medidos y refinados durante las últimas décadas. La nueva base de datos obtenida, formada por 651 espectros y que cubre por completo la erupción experimentada en junio de 2015, nos permite *retocar la imagen* establecida para este sistema transitorio. En particular, detectamos continuas eyeciones de masa desde el disco de acreción en forma de vientos fríos (perfles P Cygni), así como una nebulosa en expansión. Nuestro estudio sugiere que las eyeciones juegan un papel principal en la regulación de la erupción.

A través del análisis de estas cinco LMXBs, esta tesis proporciona nuevos resultados sobre sus parámetros fundamentales así como sobre los procesos físicos relacionados con la acreción. También hemos empleado una colección extensa de técnicas observacionales a lo largo de las distintas etapas del proceso de investigación; desde el *boceto* del sistema dibujado con la detección inicial en los rayos X, hasta una *pintura* más elaborada que las observaciones multifrecuencia (tanto en erupción como en quietud) nos permiten elaborar.

Este documento incorpora firma electrónica, y es copia auténtica de un documento electrónico archivado por la ULL según la Ley 39/2015.  
Su autenticidad puede ser contrastada en la siguiente dirección <https://sede.ull.es/validacion/>

Firmado por:	Identificador del documento:	Código de verificación:	Fecha:
DANIEL MATA SÁNCHEZ UNIVERSIDAD DE LA LAGUNA	970342	pkuTTaUi	29/06/2017 10:41:42
JORGE CASARES VELAZQUEZ UNIVERSIDAD DE LA LAGUNA			29/06/2017 11:14:09
TEODORO MUÑOZ DARIAS UNIVERSIDAD DE LA LAGUNA			29/06/2017 12:50:38
ERNESTO PEREDA DE PABLO UNIVERSIDAD DE LA LAGUNA			04/07/2017 18:28:11

# Abstract

X-ray binaries are formed by a compact object (either a stellar-mass black hole or a neutron star) and a donor star, which transfers mass onto the former via an accretion disc. They are usually discovered thanks to their bright X-ray radiation, but observations at other wavelengths are mandatory to fully understand and characterise their extreme phenomenology. In this thesis, we present a multiwavelength observational study of five low mass X-ray binaries (LMXBs); a subclass defined by their late spectral type companion stars ( $\lesssim 1 M_{\odot}$ ). The selected binaries contain both accreting neutron stars and black holes.

We first study two recently discovered transient systems whose fundamental parameters are still under debate.

The first is MAXI J1957+032, a recently discovered X-ray transient which has been detected in outburst 4 times in  $\sim 16$  months, each outburst with equally short duration ( $< 5$  days). These frequent and short outbursts (when compared with other transients), combined with the featureless spectrum that we obtained during the September 2016 event, suggest this may be a new short orbital period LMXB. In this thesis, we report on some of its main properties, such as the distance and luminosity. However, the nature of the compact star remains unknown.

The second system, Swift J1357.2-0933, was discovered during an outburst in 2011 and classified as a LMXB harbouring a black hole. We obtained optical spectroscopy with GTC during quiescence, when the disc contribution to the optical flux is at its minimum. However, we did not find any trace of the donor star absorption features. Our spectroscopic analysis set new constraints on the non-stellar contribution to the optical flux, which allows us to estimate the distance and the height of the system above the Galactic plane. We also present a restrictive limit to the black hole mass ( $> 9.3 M_{\odot}$ ). Therefore, Swift J1357.2-0933 is one of the most massive stellar-mass black holes ever found in our Galaxy, as well as a member of the new population of the thick disc, located  $> 1$  kpc outside the Galactic plane.

Subsequently, we analysed two canonical binaries that harbour neutron stars with the aim to study their donor stars, which have never been detected before.

Scorpius X-1 is the canonical persistent neutron-star LMXB. Despite it was discovered at the dawn of X-ray astronomy (more than 50 years ago), its persistent nature has prevented

Firmado por: DANIEL MATA SÁNCHEZ UNIVERSIDAD DE LA LAGUNA	29/06/2017 11:14:09
JORGE CASARES VELAZQUEZ UNIVERSIDAD DE LA LAGUNA	29/06/2017 12:50:38
TEODORO MUÑOZ DARIAS UNIVERSIDAD DE LA LAGUNA	04/07/2017 18:28:11
ERNESTO PEREDA DE PABLO UNIVERSIDAD DE LA LAGUNA	

a proper dynamical study as it requires the detection of the donor star (only possible during the quiescence phase). We obtained near-infrared spectroscopy and performed a Monte Carlo analysis that allows us to set tighter constraints on the masses of this prototypical system.

Aquila X-1 is also a canonical neutron-star LMXB, but in this case of the subtype of transient systems. It exhibits recurrent outbursts every two years, and has been exhaustively studied since its discovery more than 40 years ago. In spite of its accessible quiescent brightness (both in the optical and near-infrared), its dynamical study has been hampered so far by the presence of a brighter nearby (0.4 arcsec away) field star. Combining the integral field spectrograph SINFONI attached to the VLT telescope with its adaptive optics module, we singled out Aquila X-1 and obtained phase-resolved spectra. This allowed us to detect, for the first time, its donor star absorption features, as well as to measure its radial velocity curve. We set new constraints on the distance to the system, as well as the orbital inclination which discards high neutron star masses.

To complete this sample, we also present the results of the most extensive optical spectroscopic campaign ever performed (to our knowledge) on an outburst of a transient X-ray binary system. V404 Cygni is a LMXB which contains a black hole. The system exhibits outbursts every  $\sim 25$  years. Its dynamical parameters have been measured and refined over the course of the last decades. Our new large database of 651 spectra covering the entire June 2015 outburst allows us to touch up the *painting* of this transient. In particular, we detect continuous mass outflows from the accretion disc in the form of a cold wind (P-Cygni profiles), as well as an expanding nebula. Our study suggests that the outflow plays a major role in regulating the outburst evolution.

Through the analysis of these five low mass X-ray binaries, this thesis provides new results on both their fundamental parameters and the relevant accretion-related physical processes at work. It also presents an extensive collection of the observational techniques employed along the different stages of the research process, that is, from the rough *sketch* of the system depicted by the initial detection in the X-rays, to a more detailed *painting* that detailed multiwavelength follow-up (both in outburst and quiescence) enables to elaborate.

Este documento incorpora firma electrónica, y es copia auténtica de un documento electrónico archivado por la ULL según la Ley 39/2015.  
Su autenticidad puede ser contrastada en la siguiente dirección <https://sede.ull.es/validacion/>

Identificador del documento: 970342

Código de verificación: pkuTTaUi

Firmado por: DANIEL MATA SÁNCHEZ UNIVERSIDAD DE LA LAGUNA	Fecha: 29/06/2017 10:41:42
JORGE CASARES VELAZQUEZ UNIVERSIDAD DE LA LAGUNA	29/06/2017 11:14:09
TEODORO MUÑOZ DARIAS UNIVERSIDAD DE LA LAGUNA	29/06/2017 12:50:38
ERNESTO PEREDA DE PABLO UNIVERSIDAD DE LA LAGUNA	04/07/2017 18:28:11

# Contents

Agradecimientos	v
Resumen	vii
Abstract	ix
<b>1 Introduction</b>	<b>1</b>
1.1 The LMXB population . . . . .	4
1.1.1 LMXB evolution . . . . .	4
1.1.2 Characterising the LMXB population . . . . .	6
1.1.3 Cataclysmic variables: the same, but different . . . . .	7
1.2 The physics of LMXBs . . . . .	7
1.2.1 Anatomy of an LMXB . . . . .	8
1.2.2 X-ray evolution and accretion states . . . . .	11
1.3 Optical and near infrared view of LMXBs . . . . .	14
1.3.1 Quiescence . . . . .	14
1.3.2 Outburst . . . . .	18
1.4 Dynamical studies . . . . .	19
1.4.1 Orbital period and inclination . . . . .	19
1.4.2 Donor star radial velocity . . . . .	22
1.4.3 Donor star rotational velocity . . . . .	23
1.4.4 Compact object orbital velocity . . . . .	25
1.4.5 Measuring masses: state of the art . . . . .	27
<b>2 Multiple outbursts of MAXI J1957+032</b>	<b>29</b>
<b>3 The quiescence of the black hole transient Swift J1357.2-0933</b>	<b>37</b>
<b>4 Scorpius X-1: the canonical neutron-star LMXB</b>	<b>45</b>
<b>5 The donor of Aquila X-1 revealed</b>	<b>51</b>

xi

Este documento incorpora firma electrónica, y es copia auténtica de un documento electrónico archivado por la ULL según la Ley 39/2015.  
Su autenticidad puede ser contrastada en la siguiente dirección <https://sede.ull.es/validacion/>

Identificador del documento: 970342	Código de verificación: pkuTTaUi
Firmado por: DANIEL MATA SÁNCHEZ UNIVERSIDAD DE LA LAGUNA	Fecha: 29/06/2017 10:41:42
JORGE CASARES VELAZQUEZ UNIVERSIDAD DE LA LAGUNA	29/06/2017 11:14:09
TEODORO MUÑOZ DARIAS UNIVERSIDAD DE LA LAGUNA	29/06/2017 12:50:38
ERNESTO PEREDA DE PABLO UNIVERSIDAD DE LA LAGUNA	04/07/2017 18:28:11

---

<b>6</b>	<b>The 2015 outburst of the black hole transient V404 Cygni</b>	<b>57</b>
6.1	Introduction . . . . .	57
6.2	Observations . . . . .	59
6.3	Methods . . . . .	60
6.4	Results and discussion . . . . .	62
6.5	Conclusions and future work . . . . .	74
6.6	Appendix . . . . .	75
<b>7</b>	<b>Conclusions</b>	<b>79</b>

Este documento incorpora firma electrónica, y es copia auténtica de un documento electrónico archivado por la ULL según la Ley 39/2015.  
Su autenticidad puede ser contrastada en la siguiente dirección <https://sede.ull.es/validacion/>

Identificador del documento: 970342

Código de verificación: pkuTTaUi

Firmado por: DANIEL MATA SÁNCHEZ UNIVERSIDAD DE LA LAGUNA	Fecha: 29/06/2017 10:41:42
JORGE CASARES VELAZQUEZ UNIVERSIDAD DE LA LAGUNA	29/06/2017 11:14:09
TEODORO MUÑOZ DARIAS UNIVERSIDAD DE LA LAGUNA	29/06/2017 12:50:38
ERNESTO PEREDA DE PABLO UNIVERSIDAD DE LA LAGUNA	04/07/2017 18:28:11

---

# 1

---

## Introduction

X-RAY binaries were first detected almost 60 years ago at the very dawn of X-ray astronomy with the discovery of Sco X-1 (Giacconi et al. 1962). Later, further observations found the corresponding counterparts at different wavelength ranges, which led to the development of the canonical model for X-ray binaries (Shklovsky 1967). This model states that X-ray binaries are formed by two stellar bodies in a gravitationally bound orbit: a compact stellar remnant, either a neutron star (NS) or a stellar-mass black hole (BH), and a companion (donor) star. Their X-ray radiation is powered by accretion of material from the companion star onto the compact object, as it forms an accretion disc that heats up to  $\sim 10^7$  K.

The population of X-ray binaries includes a wide variety of compact accreting binaries (see Sec. 1.1). In order to understand their specific peculiarities, they can be initially classified attending to general criteria.

Attending to the companion star mass:

- Low mass X-ray binaries (LMXBs): those with a late spectral type companion ( $\lesssim 1 M_\odot$ ). To understand the accretion process in this case, one needs to consider the gravitational equipotential surfaces of a binary system, which are represented in the left panel of Fig. 1.1. The most noticeable features in this diagram are the Lagrangian points (L1 to L5), spatial locations in the binary rest frame where a small mass could maintain a stable position relative to the two binary components. Among the equipotential surfaces, the most relevant are the Roche lobes, which confine the regions of space gravitationally bounded to either main body (see Fig. 1.1, right panel). In LMXBs, mass transfer occurs when the donor star overflows its Roche lobe and its outermost parts are ripped off by the gravitational attraction of the compact object. In order to conserve angular momentum, the transferred material forms an accretion disc around the NS or BH after leaving the inner Lagrangian point (L1).

- High mass X-ray binaries (HMXBs): they contain an early-type donor star ( $\gtrsim 10 M_\odot$ ).

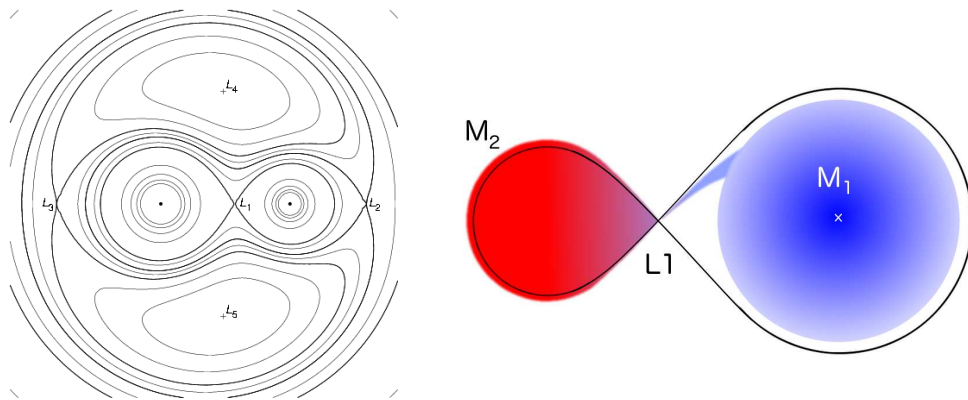


FIGURE 1.1— Left panel: gravitational equipotential surfaces in a binary system (picture by Dipankar Bhattacharya). Right panel: the black, solid line defines the Roche lobe of both the companion ( $M_2$ , red) and the compact object ( $M_1$ , white cross). The accretion disc surrounding the compact object (oriented face-on in this picture) is shown in blue. The mass transfer from the donor to the accretion disc occurs through the Lagrangian point L1.

Their main attribute, when compared to LMXBs, is the strong stellar wind characteristic of the early type companions. These winds are driven through light scattering by the metal ions present in the stellar atmosphere of the companion (line driven wind, see Kudritzki & Puls 2000 for a review). The material ejected through the stellar wind is able to provide matter for the accretion process before the companion fills its Roche lobe.

On the other hand, HMXBs with Be companion stars form excretion discs, as a result of the ejection of material due to the rapid rotation of the star. Accretion takes place when the compact object (bounded in an elliptical orbit) passes through the disc and produces periodic X-ray bursts. B(e) X-ray binaries have NS accretors (e. g. Negueruela 1998) with the exception of the recently discovered system MWC 656, which hosts a BH (Casares et al. 2014).

In this thesis we focus on LMXBs, which based on their long-term variability can be classified as:

- X-ray transients (XRTs): they exhibit extreme luminosities during short periods of time known as outbursts (e.g. the  $V$ -band magnitude of V404 Cygni varies from  $V = 18.4$  to  $V = 11.7$ ; see Corral-Santana et al. 2016 and references therein). XRT outbursts last from a few days (e.g. N6440 X2, see Sec. 2) to years (e.g. Swift J1753.5-0127 is still in outburst since 2005, Palmer et al. 2005), and have recurrence times of months (e.g. MAXI J1957+032, see Sec. 2) to decades (e.g. V404 Cygni, see Sec. 6).
- Persistent systems: these are always X-ray active, that is, they are permanently in “outburst” (e.g. Sco X-1, see Sec. 4). Most of the persistent LMXBs harbour NSs, and exhibit

Este documento incorpora firma electrónica, y es copia auténtica de un documento electrónico archivado por la ULL según la Ley 39/2015.  
Su autenticidad puede ser contrastada en la siguiente dirección <https://sede.ull.es/validacion/>

Identificador del documento: 970342

Código de verificación: pkuTTaUi

Firmado por: DANIEL MATA SÁNCHEZ  
UNIVERSIDAD DE LA LAGUNA

Fecha: 29/06/2017 10:41:42

JORGE CASARES VELAZQUEZ  
UNIVERSIDAD DE LA LAGUNA

29/06/2017 11:14:09

TEODORO MUÑOZ DARIAS  
UNIVERSIDAD DE LA LAGUNA

29/06/2017 12:50:38

ERNESTO PEREDA DE PABLO  
UNIVERSIDAD DE LA LAGUNA

04/07/2017 18:28:11

typical X-ray luminosities of  $\sim 10^{36-39}$  erg s $^{-1}$ . Nevertheless, in recent years a new population of very faint persistent X-ray sources has been found, with maximum luminosities in the 2 – 10 keV band of  $\sim 10^{34-36}$  erg s $^{-1}$  (e.g. Armas Padilla, Degenaar & Wijnands 2013).

This thesis focusses on the study of 1 persistent and 4 transient LMXBs from an observational point of view. We will go through the different stages of the characterisation process, from the rough *sketch* depicted with the initial detection in the X-rays, to the detailed *painting* that multiwavelength observations (both in outburst and quiescence) allow us to elaborate.

Este documento incorpora firma electrónica, y es copia auténtica de un documento electrónico archivado por la ULL según la Ley 39/2015.  
*Su autenticidad puede ser contrastada en la siguiente dirección <https://sede.ull.es/validacion/>*

Identificador del documento: 970342

Código de verificación: pkuTTaUi

Firmado por: DANIEL MATA SÁNCHEZ UNIVERSIDAD DE LA LAGUNA	Fecha: 29/06/2017 10:41:42
JORGE CASARES VELAZQUEZ UNIVERSIDAD DE LA LAGUNA	29/06/2017 11:14:09
TEODORO MUÑOZ DARIAS UNIVERSIDAD DE LA LAGUNA	29/06/2017 12:50:38
ERNESTO PEREDA DE PABLO UNIVERSIDAD DE LA LAGUNA	04/07/2017 18:28:11

## 1.1 The LMXB population

### 1.1.1 LMXB evolution

LMXBs are born from stellar binary systems with extreme ratios between their component masses. They are composed of a low-mass star ( $\lesssim 1 M_{\odot}$ , the companion star) and a massive star ( $\gtrsim 10 M_{\odot}$ ). The high-mass star evolves faster than the late-type companion and expands, filling its Roche lobe. The mass transfer from the massive star to the low-mass star is dynamically unstable and leads to the so-called common envelope phase (Paczynski 1976). During this phase, the binary would effectively orbit inside a common envelope of material expelled by the massive star. This envelope is heated by friction, as well as spun up. It enables the binary to lose angular momentum, which is transferred to the envelope, and finally expelled before the massive star reaches the final stage of its evolution, leaving a collapsed core (either a NS or a BH) behind.

Different studies, as those of the proper motion of pulsars (e.g. Hobbs et al. 2005), have led to the commonly accepted scenario of isolated NSs being formed as a result of a supernova (SN) explosion. These proper motions (typically a few hundred  $\text{km s}^{-1}$ ) are interpreted as natal kicks produced by an asymmetric ejection during the SN. On the other hand, the distribution of LMXBs in the Galaxy concentrates around the Galactic plane, but some systems have been observed outside this region, and therefore, natal kick velocities are necessary in order to explain such heights. For LMXBs, even symmetric mass ejections during the SN event can result in high systemic velocities (Blaauw kick; Blaauw 1961).

The presence of natal kicks is not fully confirmed for BH LMXBs due to both the smaller sample available so far (17 dynamically confirmed BHs) and the differing results found over this small population (e.g. Repetto, Davies & Sigurdsson 2012). Nevertheless, in the last years evidence for this phenomenon in BHs has been reported (e.g. Repetto, Igoshev & Nelemans 2017). Additionally, the detection of a new population of high Galactic latitude BHs (see Fig. 1.2 and Jonker & Nelemans 2004) favours this scenario. However, more members must be found in order to confidently constrain the models. In this regard, this thesis has contributed by constraining the fundamental parameters of one of the most recent members (Swift J1357.2-0933; see Sec. 3).

Once the compact object is formed, there are three standard evolutive scenarios that would yield a contact binary (King, Kolb & Burderi 1996) depending on the evolution time-scale of the companion star ( $t_{\text{MS}}$ ) and the angular momentum loss time-scale ( $t_{\text{AML}}$ ).

- $t_{\text{MS}} \ll t_{\text{AML}}$ : when the hydrogen core of the companion is exhausted (i.e. converted into a helium core), it collapses and hydrogen starts to be burnt in the outer layers. This expands the star atmosphere, overflowing its Roche lobe and starting the transfer of matter onto the compact object. This results in a long orbital period ( $P_{\text{orb}}$  hereafter) LMXB with a subgiant companion.
- $t_{\text{MS}} \gg t_{\text{AML}}$ : the binary loses angular momentum through magnetic braking and gravitational radiation (see below) until the low-mass companion fills its Roche lobe. This requires a severe shrinking of the binary orbit before mass transfer occurs, resulting in a short  $P_{\text{orb}}$  LMXB with a non-evolved companion.

Este documento incorpora firma electrónica, y es copia auténtica de un documento electrónico archivado por la ULL según la Ley 39/2015.  
Su autenticidad puede ser contrastada en la siguiente dirección <https://sede.ull.es/validacion/>

Identificador del documento: 970342

Código de verificación: pkuTTaUi

Fecha: 29/06/2017 10:41:42

Firmado por: DANIEL MATA SÁNCHEZ  
UNIVERSIDAD DE LA LAGUNA

JORGE CASARES VELAZQUEZ  
UNIVERSIDAD DE LA LAGUNA

TEODORO MUÑOZ DARIAS  
UNIVERSIDAD DE LA LAGUNA

ERNESTO PEREDA DE PABLO  
UNIVERSIDAD DE LA LAGUNA

29/06/2017 11:14:09

29/06/2017 12:50:38

04/07/2017 18:28:11

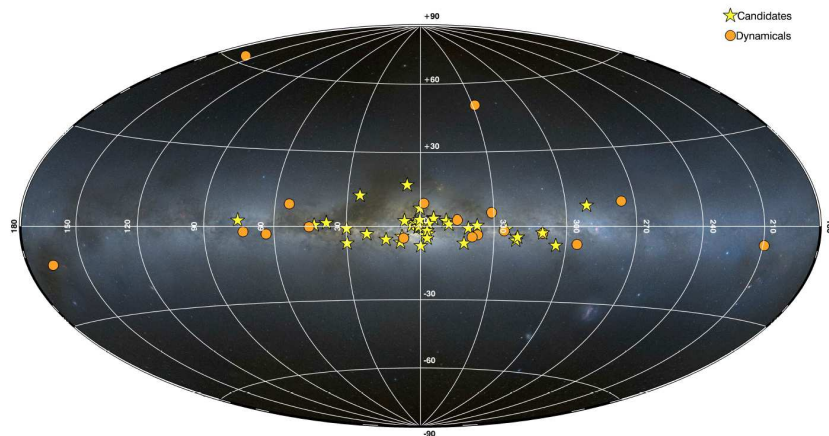


FIGURE 1.2— Galactic distribution of LMXBs with dynamically confirmed BHs (orange dots) and BH candidates (yellow stars). From Corral-Santana et al. 2016.

- $t_{\text{MS}} \sim t_{\text{AML}}$ : this is an intermediate case, where the final LMXB ends up with a short  $P_{\text{orb}}$ , as in the previous case. The donor star evolves and increases its radius significantly (compared to that of zero-age main sequence stars), but this process is frozen when the transfer of matter starts.

In LMXBs, mass transfer from the secondary ( $\lesssim 1 M_{\odot}$ ) to the primary (now a compact object; i. e.  $\gtrsim 1.2 M_{\odot}$ ) is expected to be stable. In order to conserve angular momentum, the orbit of the binary should stretch as a result of mass transfer, detaching the system and stopping the process. This is not actually the case, since shrinking of the binary orbit over time has been observed in several systems, and therefore, the total angular momentum would not be conserved. Therefore, angular momentum should somehow be extracted from the system. Besides non-conservative mass transfer, there are two main mechanisms that can account for this angular momentum loss:

- Magnetic braking: single, late-type stars are known to exhibit magnetic activity. Despite small mass losses via stellar wind, the magnetic field forces the wind to corotate with the star at a long distance from the surface. This produces an effective loss of angular momentum, which slows down the star rotation. Since donor stars in LMXBs are tidally locked to the orbit, the loss of angular momentum is transferred to the whole system, thereby shrinking the binary orbit.
- Gravitational radiation: the changing quadrupole moment of the orbiting bodies produces gravitational waves, which ultimately leads to a loss of energy and angular momentum (e.g. Kraft, Mathews & Greenstein 1962). Its strong dependence with the size of the orbit makes this effect important only in very close binaries (separation  $< 1 R_{\odot}$ ) with short  $P_{\text{orb}}$ .

Este documento incorpora firma electrónica, y es copia auténtica de un documento electrónico archivado por la ULL según la Ley 39/2015.  
Su autenticidad puede ser contrastada en la siguiente dirección <https://sede.ull.es/validacion/>

Identificador del documento: 970342

Código de verificación: pkuTTaUi

Fecha: 29/06/2017 10:41:42

Firmado por: DANIEL MATA SÁNCHEZ  
UNIVERSIDAD DE LA LAGUNA

JORGE CASARES VELAZQUEZ  
UNIVERSIDAD DE LA LAGUNA

TEODORO MUÑOZ DARIAS  
UNIVERSIDAD DE LA LAGUNA

ERNESTO PEREDA DE PABLO  
UNIVERSIDAD DE LA LAGUNA

29/06/2017 11:14:09

29/06/2017 12:50:38

04/07/2017 18:28:11

We note that recent measurements on several LMXBs reveal that  $P_{\text{orb}}$  may be shrinking much faster than predicted by the previously described phenomena (e.g. Burderi et al. 2010, González Hernández et al. 2017, Ponti et al. 2017). This points towards alternative scenarios such as non-conservative mass transfer, where most of the mass transferred from the companion is instead expelled out of the system, or an erratic  $P_{\text{orb}}$  evolution due to magnetic activity changing the gravitational quadrupole momentum of the companion (Applegate mechanism; Applegate 1992).

### 1.1.2 Characterising the LMXB population

#### *Neutron-star LMXBs*

A total of  $\sim 200$  LMXBs have been found so far, the majority with NS accretors (e.g. Liu, van Paradijs & van den Heuvel 2007). Identifying the compact object as a NS can be made by two main methods:

- i) Thermonuclear X-ray bursts: during outburst, LMXBs harbouring NSs can exhibit very abrupt rises in their X-ray luminosity followed by a characteristic cooling decay phase, with recurring timescales of  $\sim$  hours. These are called thermonuclear bursts, which last tens to hundreds of seconds and are produced by the ignition of accumulated material on the NS crust (see Galloway et al. 2008 for a review). The burst shape, intensity and duration vary depending on several parameters. In particular, the mass accretion rate onto the NS surface determines whether the fusion of helium or hydrogen is unstable, which would produce a burst (Fujimoto, Hanawa & Miyaji 1981). Helium bursts are faster and brighter than those triggered by hydrogen. Finally, when carbon is burnt on the NS surface, a superburst occurs, with a longer duration ( $\sim 3 - 14$  h) and longer recurrence times ( $\sim 1$  yr) than those characteristic of regular bursts (Cornelisse et al. 2000).
- ii) X-ray pulsars: LMXBs harbouring NSs with strong magnetic fields have their accretion discs truncated at a certain inner radius (typically a half of Alfvén radius). When reaching this radius, the stream of material is redirected towards the magnetic poles. This, in case of misalignment of the poles with the spin axis of the NS, yields X-ray flux pulsations. These are the so-called accretion-powered pulsars (see Sec. 2).

#### *Black-hole LMXBs*

If none of the previous phenomena is observed, determining the nature of the compact object in an LMXB becomes a difficult task. The X-ray properties (see Sec. 1.2.2) can be used to constrain the presence of a BH (these are known as BH candidates, see e.g. Belloni, Motta & Muñoz-Darias 2011), but only through dynamical studies (where the compact object mass is constrained) can the BH nature of the accretor be unambiguously confirmed (see Sec. 1.4). Only 17 systems (plus 1, see Sec. 3) out of  $\sim 60$  candidates possess dynamically confirmed BHs (see Casares & Jonker 2014, Corral-Santana et al. 2016).

Este documento incorpora firma electrónica, y es copia auténtica de un documento electrónico archivado por la ULL según la Ley 39/2015.  
Su autenticidad puede ser contrastada en la siguiente dirección <https://sede.ull.es/validacion/>

Firmado por:	Identificador del documento:	Código de verificación:	Fecha:
DANIEL MATA SÁNCHEZ UNIVERSIDAD DE LA LAGUNA	970342	pkuTTaUi	29/06/2017 10:41:42
JORGE CASARES VELAZQUEZ UNIVERSIDAD DE LA LAGUNA			29/06/2017 11:14:09
TEODORO MUÑOZ DARIAS UNIVERSIDAD DE LA LAGUNA			29/06/2017 12:50:38
ERNESTO PEREDA DE PABLO UNIVERSIDAD DE LA LAGUNA			04/07/2017 18:28:11

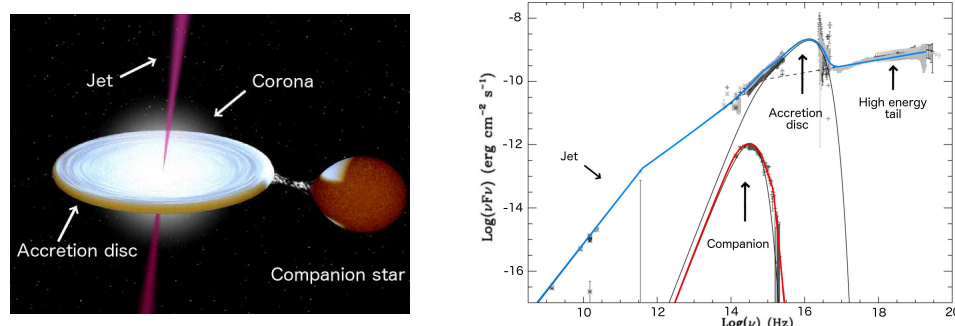


FIGURE 1.3— Left panel: artistic impression of an LMXB and its different components (artistic impression by Rob Hynes). Right panel: example of a spectral energy distribution (SED) from XTE J1118+480 (an LMXB which contains a BH). The lower, red curve represents the quiescent state (companion star plus small disc contribution). The upper, blue curve corresponds to the outburst SED. It can be fitted by combining a multicolour black-body to account for the disc (black, upper line) and three power laws in the radio, near-infrared (jet) and hard X-rays (high energy tail) bands (dashed line, mainly under the blue curve). Adapted from Chaty et al. (2003).

### 1.1.3 Cataclysmic variables: the same, but different

Cataclysmic variables (CVs) are fairly similar systems to LMXBs. These compact binaries are formed by a white dwarf and a late-type companion star. In particular, the so-called non-magnetic CVs form an accretion disc. They are classified as dwarf novae if they exhibit outburst behaviour (similar to transient LMXBs), while those always exhibiting high ultraviolet and optical luminosities are nova-like variables (similar to persistent LMXBs). We note that, even among the magnetic CVs, those known as intermediate polars also form accretion discs whose inner regions are truncated by the white dwarf magnetic field. For a review of CV evolution, see Knigge (2011).

CVs are far more abundant (by several thousands, e.g. Downes et al. 2006) but their accretion luminosities are lower than those observed in LMXBs. Indeed, the inner regions of their accretion discs produce significantly lower X-ray emission than we observe in LMXBs. This is due to the presence of a WD, which is less compact than either a NS or a BH. CVs do not produce significant X-ray irradiation of the accretion disc, and therefore the disc emission is dominated by viscous dissipation.

## 1.2 The physics of LMXBs

The name “LMXBs” already anticipates that the bulk of their emission is released in the X-ray regime. However, they are also detected and studied over the whole electromagnetic spectrum, from radio to  $\gamma$ -rays (e.g. Markoff et al. 2015). The full spectral energy distribution (SED) varies from one system to the other, as well as from the quiescent state to outburst, as a result of the variable contribution of the different spectral components (see Fig. 1.3).

Este documento incorpora firma electrónica, y es copia auténtica de un documento electrónico archivado por la ULL según la Ley 39/2015.  
Su autenticidad puede ser contrastada en la siguiente dirección <https://sede.ull.es/validacion/>

Identificador del documento: 970342

Código de verificación: pkuTTaUi

Fecha: 29/06/2017 10:41:42

Firmado por: DANIEL MATA SÁNCHEZ  
UNIVERSIDAD DE LA LAGUNA

JORGE CASARES VELAZQUEZ  
UNIVERSIDAD DE LA LAGUNA

TEODORO MUÑOZ DARIAS  
UNIVERSIDAD DE LA LAGUNA

ERNESTO PEREDA DE PABLO  
UNIVERSIDAD DE LA LAGUNA

29/06/2017 11:14:09

29/06/2017 12:50:38

04/07/2017 18:28:11

### 1.2.1 Anatomy of an LMXB

The picture of an LMXB can be decomposed attending to the observational features observed at different wavelengths, both in quiescence and outburst. The quiescent state is only observed in XRT systems, and it is characterised by faint radio and X-ray emission, plus optical to near-infrared (Opt-NIR) emission from the companion star. However, during the outburst state (exhibited by both transient and persistent systems), the accretion disc completely outshines the donor star and dominates the Opt-NIR wavelength range. This state is also characterised by several orders of magnitude higher radio and X-ray luminosities than in quiescence, which are associated with the jet and the accretion flow, respectively. The different spectral components and their contribution to the SED are detailed below.

#### *Companion star*

The late-type companion of an LMXB is the main contributor to the Opt-NIR emission in quiescence. The main difference between the companion and an isolated late-type star is the distorted shape of the former due to the gravitational attraction of the compact object (see Fig. 1.1). This deformation implies that the projected area of the donor (perpendicular to the line of sight) changes along the orbit and produces modulations in the Opt-NIR light curves. The detection of the spectral absorption features of the companion in quiescence enables to obtain a dynamical solution for the system (see Sec. 1.4). During the outburst, the disc completely veils the donor star; however, in some systems, the X-ray radiation produced in the inner part of the disc is strong enough to generate fluorescence lines on the inner face of the donor, that can be detected in the optical spectrum (see Sec. 1.3).

#### *Accretion disc*

This structure is formed by the infalling material (mainly hydrogen and helium, as it is stripped from the donor's atmosphere) onto the compact object. The disc is formed naturally due to the initial angular momentum of the accreted mass and viscous dissipation, and it is usually considered to have a Keplerian distribution of velocities. The velocity gradient of the disc leads to viscous friction between the non-corotating adjacent orbits. This allows conversion of the potential energy of the gas into radiation, as well as produces a gradient of temperatures in the disc ( $T \propto r^{-3/4}$ , with  $r$  the distance to the compact object). This process ultimately results in the net outward transport of angular momentum and the spiral infall of the gas onto the compact object. The range of temperatures across the disc varies from  $\sim 10^3$  K (near-infrared emission) in the outer rings, where neutral hydrogen can be found, to  $\sim 10^7$  K in the innermost stable orbit, enough to emit soft ( $\sim 0.1 - 5$  keV) X-ray emission. This range of temperatures and, in particular, the presence or absence of a stable population of neutral hydrogen in the outer disc will determine the long-term behaviour of an LMXB (i.e. persistent or transient).

#### **The disc instability model**

The outbursts of LMXBs (and CVs, see e.g. Warner 1995 for a review) may be explained through the Disc Instability Model (DIM, Osaki 1974; see also Lasota 2001 and Fender

Este documento incorpora firma electrónica, y es copia auténtica de un documento electrónico archivado por la ULL según la Ley 39/2015.  
Su autenticidad puede ser contrastada en la siguiente dirección <https://sede.ull.es/validacion/>

Firmado por:	Identificador del documento:	Código de verificación:	Fecha:
DANIEL MATA SÁNCHEZ UNIVERSIDAD DE LA LAGUNA	970342	pkuTTaUi	29/06/2017 10:41:42
JORGE CASARES VELAZQUEZ UNIVERSIDAD DE LA LAGUNA			29/06/2017 11:14:09
TEODORO MUÑOZ DARIAS UNIVERSIDAD DE LA LAGUNA			29/06/2017 12:50:38
ERNESTO PEREDA DE PABLO UNIVERSIDAD DE LA LAGUNA			04/07/2017 18:28:11

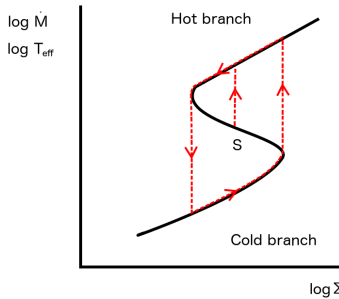


FIGURE 1.4— Thermal equilibrium curve (black, solid line) of a ring in the accretion disc.  $\Sigma$  is the surface density,  $\dot{M}$  the mass accretion rate and  $T_{\text{eff}}$  the effective temperature. Given a particular ring of the accretion disc in a stationary state “S” on the intermediate (unstable) branch, a local instability will force the material in the ring to the hot branch and then to the cold branch following a hysteresis pattern.

& Dubus 2012). The DIM is based on the simultaneous presence of both neutral and ionised hydrogen in the accretion disc due to its radial temperature profile. In the outer rings of the disc, lower temperatures are enough for hydrogen to start recombining ( $\lesssim 10^4$  K), and the electron scattering contribution (free-free) to the opacity is, therefore, greatly diminishing. On the other hand, free-free cooling dominates in the ionised, inner regions. This dramatic decrease of the overall opacity from the inner to the outer rings makes the disc thermally unstable. A small, local instability in the accretion rate of the intermediate rings makes them oscillate between the cold and the hot branches of their S-shaped thermal instability curve (see e.g. Cannizzo, Shafter & Wheeler 1988) following a hysteresis pattern (see Fig. 1.4). The instability propagates through the whole accretion disc, triggering the outburst of transient systems. The details of the outburst propagation (e.g. if its inwards, outwards or both) are still under debate.

The accretion disc gets hotter during the outburst, following the previously detailed mechanism. A fraction of the soft X-ray photons emitted by the hot innermost parts of the disc are also reprocessed by the colder external rings and re-emitted as optical light via Compton effect, producing an effective heating. The effective temperature at the outermost (and coldest) radius of an irradiated accretion disc is:  $T^4[R_d] \propto \dot{M}$ ; being  $\dot{M}$  the mass accretion rate and  $R_d$  the disc outer radius (see, e.g. King et al. 1996).

If we impose this temperature to be higher than the hydrogen ionisation temperature ( $\sim 7000$  K) it will result in a critical value of the mass accretion rate ( $\dot{M}_{\text{crit}}$ , which depends on  $R_d$  and, therefore, on  $P_{\text{orb}}$ ) above which neutral hydrogen can not be found in the outer radius. Given that any other ring will be hotter than the most external one, this condition applies to the whole accretion disc. Therefore, LMXBs with  $\dot{M} > \dot{M}_{\text{crit}}$  will be persistent systems. They will not be able to go back to quiescence since irradiation keeps the outer disc hot enough at all times. Those systems with  $\dot{M} < \dot{M}_{\text{crit}}$  will be transients (see Fig. 1.5).

Este documento incorpora firma electrónica, y es copia auténtica de un documento electrónico archivado por la ULL según la Ley 39/2015.  
Su autenticidad puede ser contrastada en la siguiente dirección <https://sede.ull.es/validacion/>

Identificador del documento: 970342

Código de verificación: pkuTTaUi

Fecha: 29/06/2017 10:41:42

Firmado por: DANIEL MATA SÁNCHEZ  
UNIVERSIDAD DE LA LAGUNA

JORGE CASARES VELAZQUEZ  
UNIVERSIDAD DE LA LAGUNA

TEODORO MUÑOZ DARIAS  
UNIVERSIDAD DE LA LAGUNA

ERNESTO PEREDA DE PABLO  
UNIVERSIDAD DE LA LAGUNA

29/06/2017 11:14:09

29/06/2017 12:50:38

04/07/2017 18:28:11

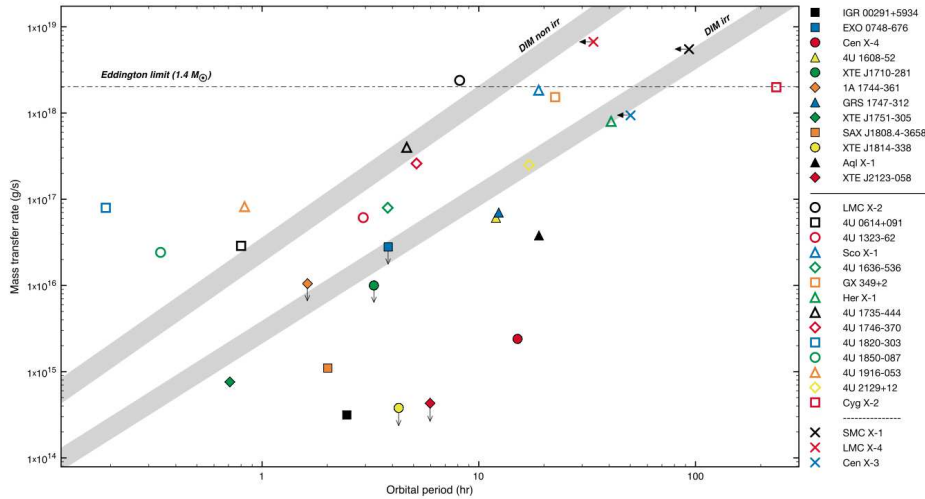


FIGURE 1.5— Mass transfer rate against  $P_{\text{orb}}$  for the known NS X-ray binaries. Filled and empty symbols refer to transient and persistent LMXBs, respectively, while crosses refer to persistent HMXBs. Grey-shaded areas define the mass accretion limit imposed by the DIM in the case of an irradiated (DIM irr) and non-irradiated (DIM non irr) disc. Systems with higher mass accretion rates are persistent, while those below the irradiated disc threshold are transient. The irradiated DIM seems to reproduce the transient-persistent division very well. Both this and a similar plot for BH LMXBs can be found in Coriat et al. (2012).

Este documento incorpora firma electrónica, y es copia auténtica de un documento electrónico archivado por la ULL según la Ley 39/2015.  
Su autenticidad puede ser contrastada en la siguiente dirección <https://sede.ull.es/validacion/>

Identificador del documento: 970342

Código de verificación: pkuTTaUi

Firmado por: DANIEL MATA SÁNCHEZ  
UNIVERSIDAD DE LA LAGUNA

Fecha: 29/06/2017 10:41:42

JORGE CASARES VELAZQUEZ  
UNIVERSIDAD DE LA LAGUNA

29/06/2017 11:14:09

TEODORO MUÑOZ DARIAS  
UNIVERSIDAD DE LA LAGUNA

29/06/2017 12:50:38

ERNESTO PEREDA DE PABLO  
UNIVERSIDAD DE LA LAGUNA

04/07/2017 18:28:11

*Compact object*

Some LMXB properties depend on the nature of the compact object. A BH will never contribute to the observed SED. On the other hand, NS LMXBs can exhibit an additional component: the so-called boundary layer. This is the region between the innermost stable orbit of the accretion disc and the surface of the NS. Infalling material needs to slow down from the high Keplerian velocities achieved at the innermost stable orbit of the disc to the rotational velocity of the NS. The energy released in the boundary layer is similar to that emitted by the rest of the accretion disc, and produces a new X-ray contribution to the SED which further complicates the spectral analysis of NS LMXBs (e.g. Mitsuda et al. 1989; Armas Padilla et al. 2017).

*Jet*

During outburst a strong increase in the radio emission is also observed. The emission in this band is dominated by the so-called jet, a collimated mass outflow which is formed by gas elements (electrons, and possibly some baryons) that reach the innermost parts of the accretion disc but, instead of being accreted, get expelled at relativistic velocities, emitting synchrotron radiation (see e.g. Fender 2001 for a review).

*High-energy tail*

During the hard state of the outburst (see below) and correlated with the jet radio emission (Gallo, Fender & Pooley 2004), a high-energy tail in the spectrum is observed. The origin of this emission is proposed to be thermal Comptonisation in a hot cloud of electrons, where the soft X-rays emitted by the disc are up-scattered via inverse Compton effect. This cloud is the so-called *corona*, but there is still strong debate on whether it is an independent structure or just the base of the jet (e.g. Markoff, Nowak & Wilms 2005).

## 1.2.2 X-ray evolution and accretion states

The outburst evolution has been widely studied in X-rays. The main reason is that the SED of an LMXB in outburst peaks in this regime (see Fig. 1.3). During outburst, the X-ray luminosity reaches up to  $10^7$  times that of quiescence. In some systems, this luminosity has been observed to reach the Eddington limit ( $L_{\text{Edd}}$ ), which is the maximum luminosity allowed just before the radiation pressure breaks the hydrostatic equilibrium and blows away the infalling material, stopping the accretion process. Considering pure hydrogen accreting material (under the assumption of spherical accretion):

$$L_{\text{Edd}} \simeq 1.26 \cdot 10^{38} M_1 \text{ erg s}^{-1}$$

where  $M_1$  is the compact object mass in solar masses ( $M_{\odot}$ ). For a canonical NS ( $\sim 1.4 M_{\odot}$ ) the Eddington luminosity is  $L_{\text{Edd}} \sim 2 \cdot 10^{38} \text{ erg s}^{-1}$ , while for a typical BH ( $\sim 10 M_{\odot}$ )  $L_{\text{Edd}} \sim 10^{39} \text{ erg s}^{-1}$ .

These high luminosities allow the detection of new LMXBs through X-ray monitoring of the sky. Current all-sky monitoring facilities are *INTEGRAL* (Kuulkers et al. 2007), *Swift* (Krimm et al. 2013) and *MAXI* (Matsuoka et al. 2009):

Este documento incorpora firma electrónica, y es copia auténtica de un documento electrónico archivado por la ULL según la Ley 39/2015. <i>Su autenticidad puede ser contrastada en la siguiente dirección <a href="https://sede.ull.es/validacion/">https://sede.ull.es/validacion/</a></i>		
Identificador del documento:	970342	Código de verificación: pkuTTaUi
Firmado por:	DANIEL MATA SÁNCHEZ UNIVERSIDAD DE LA LAGUNA	Fecha: 29/06/2017 10:41:42
	JORGE CASARES VELAZQUEZ UNIVERSIDAD DE LA LAGUNA	29/06/2017 11:14:09
	TEODORO MUÑOZ DARIAS UNIVERSIDAD DE LA LAGUNA	29/06/2017 12:50:38
	ERNESTO PEREDA DE PABLO UNIVERSIDAD DE LA LAGUNA	04/07/2017 18:28:11

- **MAXI** (Monitor for All-sky X-ray Image) is currently installed at the Japanese Experiment Module on the International Space Station. It has two detectors: *MAXI*/Gas Slit Camera (GSC), which covers the energy range  $\sim 2 - 30$  keV, and *MAXI*/Solid-state Slit Camera (SSC), which observes in the  $0.5 - 12$  keV band.
- **Swift** is a satellite equipped with different instruments. *Swift*/Burst Alert Telescope (BAT) is a hard X-ray detector used for the transient monitoring program, covering the energy range  $15 - 50$  keV. *Swift*/X-Ray Telescope (XRT) observes in the  $0.2 - 10$  keV band, and provides both high time-resolution light curves and X-ray spectroscopy. This is complemented with the Ultraviolet/Optical Telescope (UVOT) covering  $1500 - 8000$  Å with six broad-band filters.
- **INTEGRAL** (INTERnational Gamma-Ray Astrophysics Laboratory) is a space satellite dedicated to spectroscopy and imaging of gamma-ray sources in the range  $15$  keV –  $10$  MeV. However, it also possesses an X-ray monitor ( $4 - 35$  keV) and an optical ( $V$ -band,  $550$  nm) camera, useful for the detection of new XRTs.

Thanks to these and previous X-ray missions, X-ray spectral variations have been observed during the outburst of many LMXBs, allowing the identification of different accretion states. They can be characterised using the hardness ratio, that is, the ratio between the X-ray luminosity integrated over a “hard” band (e.g.  $5 - 50$  keV) to that of a “soft” band (e.g.  $0.1 - 5$  keV). Moreover, the fast X-ray variability exhibited during the outburst also traces the accretion state (Muñoz-Darias, Motta & Belloni 2011; Muñoz-Darias et al. 2014).

On the other hand, it has been shown that XRTs in outburst typically show two types of outflow: collimated radio-jets and highly-ionised X-ray winds; whose properties are coupled with those of the X-ray states (Fender & Muñoz-Darias 2016 for a review). In BHs, we can define 3 main states (Remillard & McClintock 2006, Belloni et al. 2011):

- Hard state: this state is characterised by a high ratio of hard to soft X-rays, high levels of fast variability and Comptonised emission dominating the SED. Quasi-steady radio emission showing a flat spectrum is also found, revealing the presence of a compact jet. This is observed at the initial rise of an XRT, as well as during the decay.
- Intermediate state: typically above 10% of the Eddington luminosity, a brief phase of discrete ejections is observed in radio. Indeed, in several cases spatially resolved blobs moving away from the central source have been detected. The observation of these blobs of plasma sometimes enable an independent measurement of the system orbital inclination (e.g. H 1743-322, Steiner, McClintock & Reid 2012). X-ray binaries that display discrete plasma ejections are usually dubbed “microquasars” (e.g. Mirabel et al. 1992).
- Soft state: a lower ratio of hard to soft X-rays is observed, as well as lower fast variability levels. A thermal component that can be modelled by the accretion disc dominates the SED. No radio emission (and therefore, no jet) is detected, but instead, a hot accretion disc wind is observed in the X-rays. This wind is detected as blue-shifted, highly-ionised

Este documento incorpora firma electrónica, y es copia auténtica de un documento electrónico archivado por la ULL según la Ley 39/2015.  
Su autenticidad puede ser contrastada en la siguiente dirección <https://sede.ull.es/validacion/>

Identificador del documento:	970342	Código de verificación:	pkuTTaUi
Firmado por:	DANIEL MATA SÁNCHEZ UNIVERSIDAD DE LA LAGUNA	Fecha:	29/06/2017 10:41:42
	JORGE CASARES VELAZQUEZ UNIVERSIDAD DE LA LAGUNA		29/06/2017 11:14:09
	TEODORO MUÑOZ DARIAS UNIVERSIDAD DE LA LAGUNA		29/06/2017 12:50:38
	ERNESTO PEREDA DE PABLO UNIVERSIDAD DE LA LAGUNA		04/07/2017 18:28:11

(Fe xxv, Fe xxvi) absorption lines (see Neilsen & Lee 2009, Ponti et al. 2012). The wind-launching mechanism may be a combination of radiation pressure (Proga 2000), as it is usually observed in high-luminosity systems (e.g. GRS 1915+105), and thermal pressure, given that the X-ray heating increases the disc temperature enough for atoms to reach a thermal velocity larger than the escape velocity. The total mass outflow associated with this wind might be comparable to the amount of mass accreted during the whole outburst (see Fender & Muñoz-Darias 2016).

On the other hand, NS LMXBs are more complex due to the extra spectral component from the boundary layer. These can be divided in two groups, as initially proposed by Hasinger & van der Klis (1989):

- Bright NSs (Z sources): they are all persistent systems accreting at near-Eddington luminosities ( $L_X \sim 0.5 - 1 L_{\text{Edd}}$ ). They display Z-shaped tracks in the hardness-intensity diagram, hence the name “Z sources”. The best examples of this class are Sco X-1 (see Sec. 4) and Cyg X-2 (Kuulkers et al. 1994).
- Faint NSs (atoll sources): they exhibit fainter luminosities due to their lower accretion rates ( $L_X \sim 0.01 - 0.5 L_{\text{Edd}}$ ), and show the same three main X-ray states observed in BH XRTs (hard, intermediate and soft). The best example of this behaviour is Aql X-1 (see Sec. 5).

By analysing the fast variability properties of a large sample of NS LMXBs ( $\sim 50$ ; Muñoz-Darias et al. 2014) it has been established that faint NSs are similar to BH XRTs, showing the three main states described above. On the contrary, bright NSs only sample the soft and intermediate states. Recently, more similarities between BH and NS LMXBs have been observed through a systematic search for quasi-periodic oscillations (Motta 2016) in their X-ray fluxes (Motta et al. 2017).

Este documento incorpora firma electrónica, y es copia auténtica de un documento electrónico archivado por la ULL según la Ley 39/2015.  
Su autenticidad puede ser contrastada en la siguiente dirección <https://sede.ull.es/validacion/>

Identificador del documento: 970342

Código de verificación: pkuTTaUi

Firmado por: DANIEL MATA SÁNCHEZ UNIVERSIDAD DE LA LAGUNA	Fecha: 29/06/2017 10:41:42
JORGE CASARES VELAZQUEZ UNIVERSIDAD DE LA LAGUNA	29/06/2017 11:14:09
TEODORO MUÑOZ DARIAS UNIVERSIDAD DE LA LAGUNA	29/06/2017 12:50:38
ERNESTO PEREDA DE PABLO UNIVERSIDAD DE LA LAGUNA	04/07/2017 18:28:11

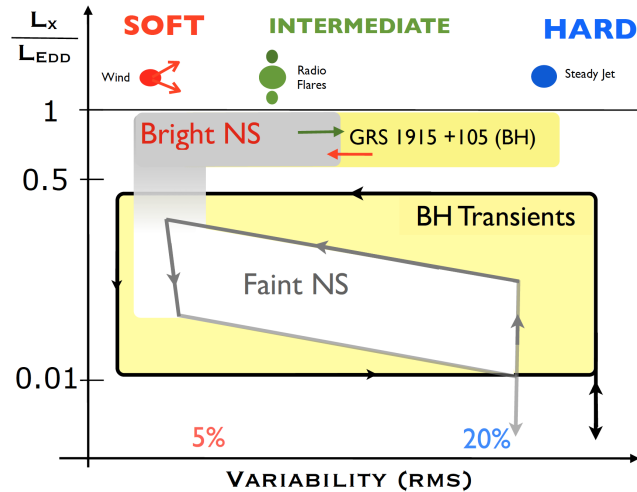


FIGURE 1.6— X-ray variability versus outburst luminosity for BH transients and faint NSs. Bright, persistent NSs as well as the only persistent BH known (GRS 1915+105) are also depicted in the diagram. Original image from Fender & Muñoz-Darias (2016).

### 1.3 Optical and near infrared view of LMXBs

The main focus of this thesis is the Opt-NIR spectroscopic analysis of LMXBs, both in outburst and quiescence. In this section, we will detail the different features observed in this wavelength range as well as provide their physical interpretation.

#### 1.3.1 Quiescence

##### *Donor star*

During quiescence, the Opt-NIR light is dominated by the companion star. Therefore, a classical LMXB quiescent spectrum will exhibit the absorption features from the donor star superimposed on the weak accretion disc contribution (see Fig. 1.7).

Since the donor star orbits around the centre of mass of the binary system, the projected orbital velocity along the line of sight (radial velocity hereafter) will change from maximum (when moving away from the observer) to minimum (when moving towards the observer) values. Assuming a circular orbit (see Sec. 1.1), the velocity along the line of sight ( $v_{\text{orb}}$ ) at a certain instant is given by the expression:

$$v_{\text{orb}} = \gamma + K_2 \sin 2\pi(\phi - \phi_0); \quad \phi - \phi_0 = (t - t_0)/P_{\text{orb}}$$

where  $K_2$  is the radial velocity semi-amplitude of the companion star,  $\gamma$  is the systemic velocity (i.e. radial velocity of the binary system centre of mass) and  $\phi$  stands for the binary

Este documento incorpora firma electrónica, y es copia auténtica de un documento electrónico archivado por la ULL según la Ley 39/2015.  
Su autenticidad puede ser contrastada en la siguiente dirección <https://sede.ull.es/validacion/>

Identificador del documento: 970342

Código de verificación: pkuTTaUi

Firmado por: DANIEL MATA SÁNCHEZ  
UNIVERSIDAD DE LA LAGUNA

Fecha: 29/06/2017 10:41:42

JORGE CASARES VELAZQUEZ  
UNIVERSIDAD DE LA LAGUNA

29/06/2017 11:14:09

TEODORO MUÑOZ DARIAS  
UNIVERSIDAD DE LA LAGUNA

29/06/2017 12:50:38

ERNESTO PEREDA DE PABLO  
UNIVERSIDAD DE LA LAGUNA

04/07/2017 18:28:11

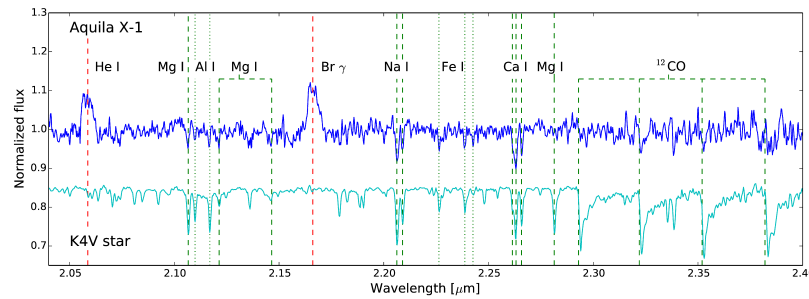


FIGURE 1.7— Top: quiescence spectrum in the near-infrared of the NS LMXB Aquila X-1 (Mata Sánchez et al. 2017a). It exhibits both absorption features from the donor star and broad emission lines arising from the disc (e.g. Br $\gamma$ , He I). For comparison, a template K4V star has been plotted (bottom).

orbital phase at a certain time  $t$ . By convention, orbital phase  $\phi = 0$  is defined at the time when the donor star is between the observer and the compact object, while the opposite situation (compact object between the donor and the observer) defines  $\phi = 0.5$ . At both phases the radial velocity is just the systemic velocity of the binary (see Fig. 1.8).

When analysing the donor star absorption features in an LMXB quiescent spectrum, different effects must be taken into account.

- Orbital smearing: if a single spectrum of an LMXB is obtained using an exposure time which spans a significant fraction of  $P_{\text{orb}}$ , the observed absorption lines arising from the companion star will be broadened. To avoid this, several short exposure-time spectra must be obtained with  $t_{\text{exp}} < P_{\text{orb}} \Delta v / (2\pi K_2)$ , being  $\Delta v$  the spectral resolution.
- Rotational broadening: LMXBs are long-lived binaries, and their orbits are not only circular but also tidally locked. This typically results in significantly high donor star rotational velocities, compared to isolated field stars of similar spectral type. This effectively broadens the absorption lines due to the different projected velocities at the stellar photosphere (see Sec. 1.4).
- Veiling: the amount of flux from the accretion flow (e.g. accretion disc) contributing to the continuum light in the Opt-NIR depends on several factors, such as the epoch (different activity levels have been observed within quiescence in several systems, see e.g. Cantrell et al. 2008) and the wavelength range (lower veiling is typically present in the near-infrared, see Fig. 1.3). The effect of the veiling on the donor star absorption features is to dilute their equivalent width (EWs), sometimes making them undetectable.

Este documento incorpora firma electrónica, y es copia auténtica de un documento electrónico archivado por la ULL según la Ley 39/2015.  
Su autenticidad puede ser contrastada en la siguiente dirección <https://sede.ull.es/validacion/>

Identificador del documento: 970342

Código de verificación: pkuTTaUi

Fecha: 29/06/2017 10:41:42

Firmado por: DANIEL MATA SÁNCHEZ  
UNIVERSIDAD DE LA LAGUNA

JORGE CASARES VELAZQUEZ  
UNIVERSIDAD DE LA LAGUNA

TEODORO MUÑOZ DARIAS  
UNIVERSIDAD DE LA LAGUNA

ERNESTO PEREDA DE PABLO  
UNIVERSIDAD DE LA LAGUNA

29/06/2017 11:14:09

29/06/2017 12:50:38

04/07/2017 18:28:11

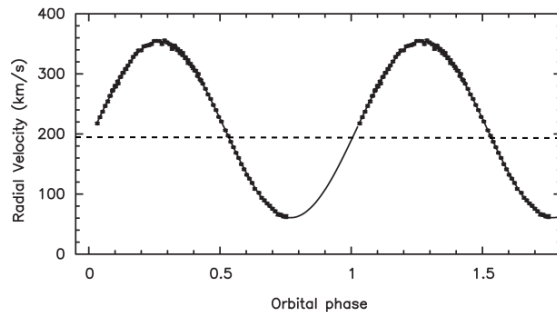


FIGURE 1.8— Donor star radial velocity curve of the NS LMXB Cen X-4. The systemic velocity (shown as a horizontal dashed line) is  $\gamma = 194.5 \pm 0.2 \text{ km s}^{-1}$ , while the radial velocity semi-amplitude of the donor is  $K_2 = 147.3 \pm 0.3 \text{ km s}^{-1}$ . Adapted from Shahbaz, Watson & Dhillon (2014).

#### Accretion disc

Aperiodic variability (flickering) in the optical light curves has been observed during the quiescent state of several XRTs (Zurita, Casares & Shahbaz 2003). The origin of this flickering is still uncertain and different models have been proposed to explain it (e.g. mass transfer instabilities, magnetic reconnection events). This effectively results in a variable contribution of non-stellar emission to the Opt-NIR spectra. Given the typically blue SED of the disc (see Fig. 1.3), this effect is expected to be less critical in the near-infrared than in the optical (see Sec. 4).

Apart from the thermal continuum contribution, the main spectral features associated with the accretion disc are broad emission lines of hydrogen and helium (see Fig. 1.9). These arise from the cooler, outer regions of the disc, where hydrogen (or helium, respectively) recombines ( $< 10^3 \text{ K}$  for hydrogen and  $< 3 \times 10^3 \text{ K}$  for helium).

The width and shape (e.g. either single-peaked or double-peaked) of the emission lines are due to the Doppler effect. Let us consider a Keplerian velocity distribution for the accretion disc as well as an observer whose line of sight subtends a certain angle ( $i$ , the orbital inclination) with respect to the orbital axis (see Fig. 1.10). Those regions with the same projected velocity from the observer's point of view will contribute to the same Doppler-shifted emission (Fig. 1.10). Since the emission from the outer parts of the disc is the main contributor to the emission line flux, the line profile will peak at the projected velocities of the outer disc rim. Note that a face-on system ( $i = 0^\circ$ ) would produce a narrow emission line at the rest frame velocity of the binary, while an edge-on system ( $i = 90^\circ$ ) would generate the maximum double-peak separation and the broadest emission line wings.

In the context of this thesis, it is important to note that high-inclination CVs of the dwarf-nova type have shown broad emission lines with narrow, absorption cores, sometimes dipping below the continuum level. These are thought to be produced by self-absorption of neutral hydrogen above the plane of the disc in the outer rings, which produces an absorption of the

Este documento incorpora firma electrónica, y es copia auténtica de un documento electrónico archivado por la ULL según la Ley 39/2015.  
Su autenticidad puede ser contrastada en la siguiente dirección <https://sede.ull.es/validacion/>

Identificador del documento: 970342

Código de verificación: pkuTTaUi

Fecha: 29/06/2017 10:41:42

Firmado por: DANIEL MATA SÁNCHEZ  
UNIVERSIDAD DE LA LAGUNA

JORGE CASARES VELAZQUEZ  
UNIVERSIDAD DE LA LAGUNA

TEODORO MUÑOZ DARIAS  
UNIVERSIDAD DE LA LAGUNA

ERNESTO PEREDA DE PABLO  
UNIVERSIDAD DE LA LAGUNA

29/06/2017 11:14:09

29/06/2017 12:50:38

04/07/2017 18:28:11

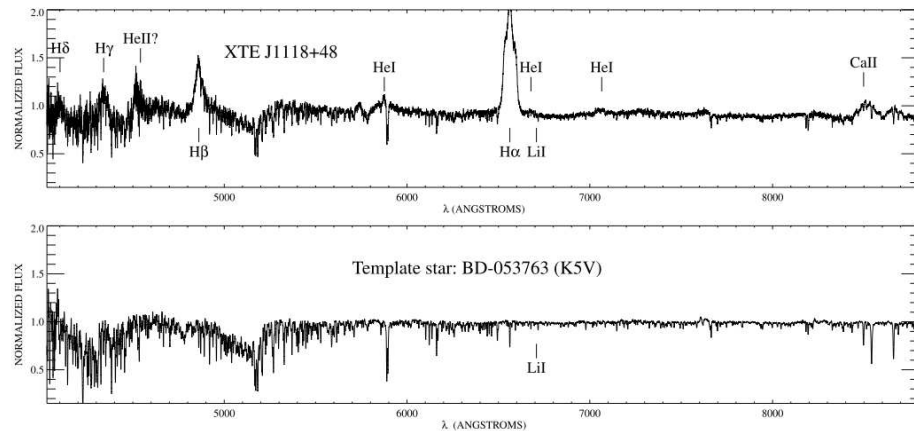


FIGURE 1.9— Top: quiescence optical spectrum of the BH XRT XTE J1118+480 (González Hernández et al. 2008). It exhibits broad emission lines arising from the disc (e.g.  $H\alpha$ , He I), as well as absorption lines from the donor. This spectrum is the average of many individual spectra, which have been corrected for the motion of the companion star. Bottom: a K5V template star spectra is included for comparison.

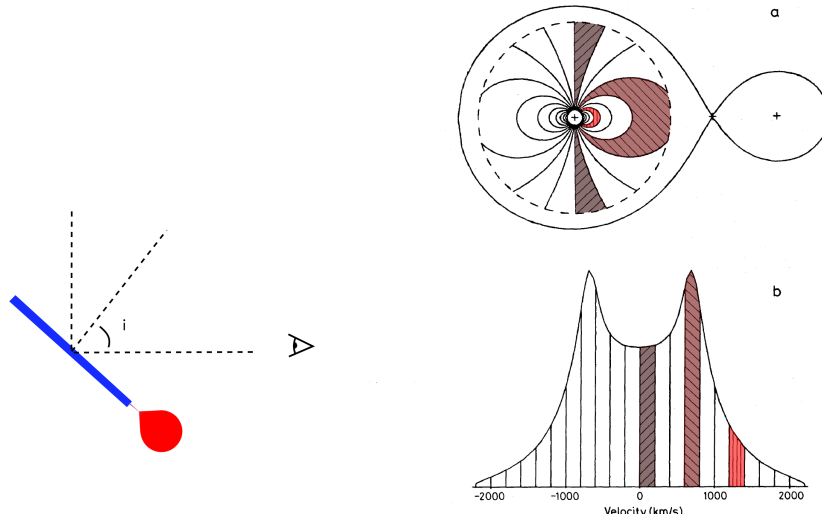


FIGURE 1.10— Left panel: observing diagram of an LMXB. The accretion disc is shown in blue, the companion star in red. The eye defines the observer's position. Right panel: (a) sketch of the accretion disc regions with the same projected velocity (considering the observational configuration of left panel) and their corresponding contribution to the emission line profile (b). Adapted from Horne & Marsh (1986).

Este documento incorpora firma electrónica, y es copia auténtica de un documento electrónico archivado por la ULL según la Ley 39/2015.  
Su autenticidad puede ser contrastada en la siguiente dirección <https://sede.ull.es/validacion/>

Identificador del documento: 970342

Código de verificación: pkuTTaUi

Firmado por: DANIEL MATA SÁNCHEZ  
UNIVERSIDAD DE LA LAGUNA

Fecha: 29/06/2017 10:41:42

JORGE CASARES VELAZQUEZ  
UNIVERSIDAD DE LA LAGUNA

29/06/2017 11:14:09

TEODORO MUÑOZ DARIAS  
UNIVERSIDAD DE LA LAGUNA

29/06/2017 12:50:38

ERNESTO PEREDA DE PABLO  
UNIVERSIDAD DE LA LAGUNA

04/07/2017 18:28:11

continuum light at null Doppler shift only in high-inclination systems (e.g. Marsh, Horne & Shipman 1987). In Mata Sánchez et al. (2015b), we found similar narrow cores in the quiescent spectra of the BH LMXB Swift J1357.2-0933, which suggests that this effect is not restricted to CVs but is also observed in high-inclination LMXBs (see Sec. 3).

### 1.3.2 Outburst

#### *Accretion disc*

The outburst spectra are dominated by the emission from a hot accretion disc, making the thermal continuum bluer than in quiescence. Broad emission lines from the accretion disc are also observed in outburst. However, these become narrower than in quiescence, as the disc expands and gets hotter. Thus, neutral hydrogen recombination is produced at larger radii (and then, lower velocities). It is also observed that a new lower-velocity contribution fills the double peak during the outburst. The origin of this contribution remains unclear, but some authors suggest that it is due to a nebula formed by ejected material during the outburst surrounding the binary (see e.g. Matthews et al. 2015).

#### *Outflows*

Outflows from LMXBs are observed during the outburst in the form of jets (mainly in the hard state) and hot X-ray winds (in the soft state, see Sec. 1.2). Our recent discovery of ejecta-related features in the optical band (Muñoz-Darias et al. 2016) during the latest outburst of V404 Cygni (BH LMXB, see Sec. 6) revealed the key influence of outflows on the outburst evolution.

#### *Donor star*

Fluorescence lines are generated when the X-ray/UV radiation produced in the innermost regions of the disc are reprocessed and re-emitted as optical light. The irradiated inner face of the donor star is also affected and therefore produces similar fluorescence lines. This is the basis of the so-called Bowen technique (see Sec. 1.4).

Este documento incorpora firma electrónica, y es copia auténtica de un documento electrónico archivado por la ULL según la Ley 39/2015.  
Su autenticidad puede ser contrastada en la siguiente dirección <https://sede.ull.es/validacion/>

Identificador del documento: 970342

Código de verificación: pkUTTaaUi

Fecha: 29/06/2017 10:41:42

Firmado por: DANIEL MATA SÁNCHEZ  
UNIVERSIDAD DE LA LAGUNA

JORGE CASARES VELAZQUEZ  
UNIVERSIDAD DE LA LAGUNA

TEODORO MUÑOZ DARIAS  
UNIVERSIDAD DE LA LAGUNA

ERNESTO PEREDA DE PABLO  
UNIVERSIDAD DE LA LAGUNA

29/06/2017 11:14:09

29/06/2017 12:50:38

04/07/2017 18:28:11

### 1.4 Dynamical studies

The vast majority of astrophysical events are only accessible to us through the emitted light detected by our instruments. LMXBs are no exception (apart from gravitational wave emission, e.g. Abadie et al. 2011), and their study depends on analysing every piece of information obtained from multiwavelength observations.

Dynamical studies of LMXBs allow us to obtain their fundamental parameters, such as  $P_{\text{orb}}$ ,  $i$ , the radial velocities of the components and, in the best case scenario, their masses. From Kepler's third law, we can define the mass function of an LMXB:

$$f(M_1) = \frac{K_2^3 P_{\text{orb}}}{2\pi G} = \frac{M_1 \sin^3 i}{(1+q)^2}; \quad q = \frac{K_1}{K_2} = \frac{M_2}{M_1}$$

where  $M_1$  and  $K_1$  are the compact object mass and its radial velocity semi-amplitude, respectively;  $M_2$  and  $K_2$  are the equivalent parameters for the donor star and  $G$  the gravitational constant. Given that the mass ratio ( $q$ ) is always positive, the mass function is a strict lower limit to the compact object mass. In LMXBs, as  $q$  is smaller than unity ( $M_1 > M_2$ ), the mass function sets more restrictive constraints than in HMXBs.

Below, we detail the different techniques we used along this work to determine fundamental parameters of LMXBs.

#### 1.4.1 Orbital period and inclination

$P_{\text{orb}}$  is arguably the most fundamental binary parameter, as it gives information about the scale of the system. In Fig. 1.11, the longest  $P_{\text{orb}}$  BH LMXBs [GRS 1915+105 and GS 2023+338 (V404 Cygni), with  $P_{\text{orb}} = 33.85 \pm 0.16$  d and  $P_{\text{orb}} = 6.4714 \pm 0.0001$  d, respectively; Steeghs et al. 2013; Casares & Charles 1994] have the larger orbital separations, companions and accretion discs. This is an expected result, as the Roche lobe size depends on  $P_{\text{orb}}$  (Paczyński 1971). Indeed, by measuring  $P_{\text{orb}}$ , the donor star mean density ( $\rho_2$ ) can be obtained (Faulkner, Flannery & Warner 1972):

$$P_{\text{orb}} = 3.83 \cdot 10^4 \langle \rho_2 \rangle^{-1/2}$$

where  $\rho_2$  is measured in g cm<sup>-3</sup>, and  $P_{\text{orb}}$  in seconds.

Combining this value with tabulated stellar parameters (e.g. Cox 2000), it is possible to infer the spectral type of the donor star, previous assumption of its evolutionary stage (see Sec. 3).

Edge-on systems exhibit eclipses in their outburst X-ray light curves, which are produced when the companion star crosses the line-of-sight between the observer and the accretion disc. This occurs once per orbital cycle, therefore defining  $P_{\text{orb}}$ . Other systems with high inclination, but not high enough to produce eclipses, may show dips in the X-ray light curve. These dips have been typically interpreted as the occultation of the central X-ray source by neutral/low ionised outer disc material (White & Mason 1985). The presence of dips is widely accepted as a solid indicator of high orbital inclinations ( $i \gtrsim 60^\circ$ , see Fig. 1.12), and, since they are produced once per orbit  $P_{\text{orb}}$  can be measured.

Este documento incorpora firma electrónica, y es copia auténtica de un documento electrónico archivado por la ULL según la Ley 39/2015.  
Su autenticidad puede ser contrastada en la siguiente dirección <https://sede.ull.es/validacion/>

Identificador del documento: 970342

Código de verificación: pkuTTaUi

Fecha: 29/06/2017 10:41:42

Firmado por: DANIEL MATA SÁNCHEZ UNIVERSIDAD DE LA LAGUNA	29/06/2017 11:14:09
JORGE CASARES VELAZQUEZ UNIVERSIDAD DE LA LAGUNA	29/06/2017 12:50:38
TEODORO MUÑOZ DARIAS UNIVERSIDAD DE LA LAGUNA	04/07/2017 18:28:11
ERNESTO PEREDA DE PABLO UNIVERSIDAD DE LA LAGUNA	

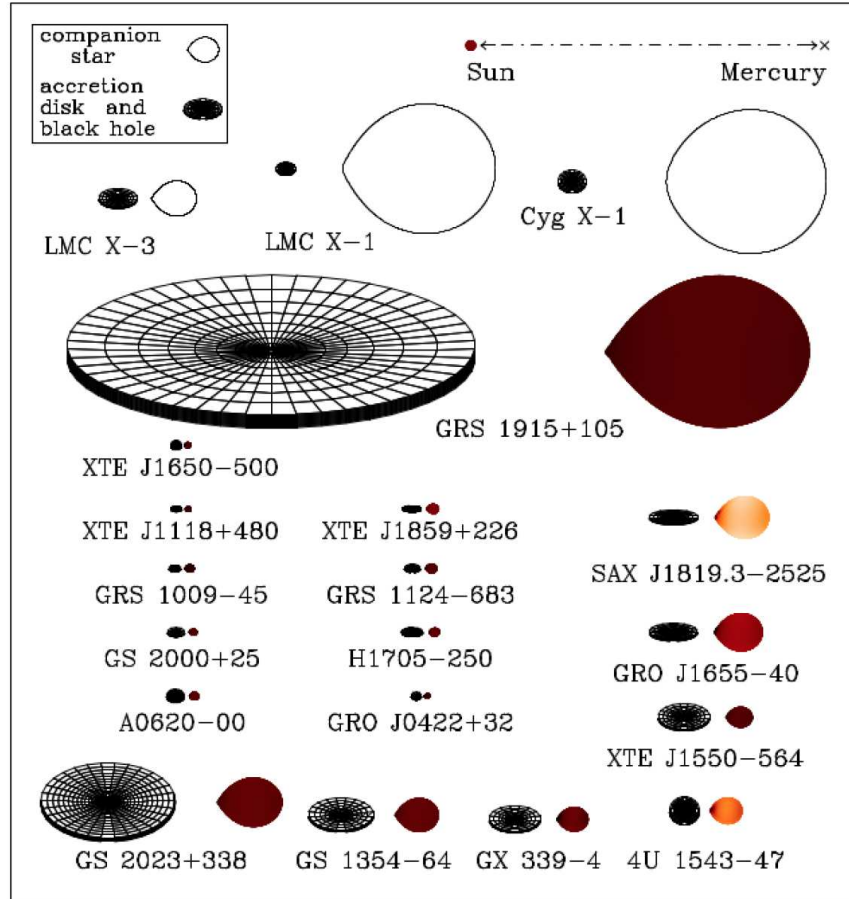


FIGURE 1.11— Twenty BH X-ray binaries scaled to the Sun-Mercury distance. We note that the three upper systems (LMC X-1, LMC X-3 and Cyg X-1) are HMXBs. Credit: Jerry Orosz.

Este documento incorpora firma electrónica, y es copia auténtica de un documento electrónico archivado por la ULL según la Ley 39/2015.  
Su autenticidad puede ser contrastada en la siguiente dirección <https://sede.ull.es/validacion/>

Identificador del documento: 970342

Código de verificación: pkuTTaUi

Firmado por: DANIEL MATA SÁNCHEZ  
UNIVERSIDAD DE LA LAGUNA

Fecha: 29/06/2017 10:41:42

JORGE CASARES VELAZQUEZ  
UNIVERSIDAD DE LA LAGUNA

29/06/2017 11:14:09

TEODORO MUÑOZ DARIAS  
UNIVERSIDAD DE LA LAGUNA

29/06/2017 12:50:38

ERNESTO PEREDA DE PABLO  
UNIVERSIDAD DE LA LAGUNA

04/07/2017 18:28:11

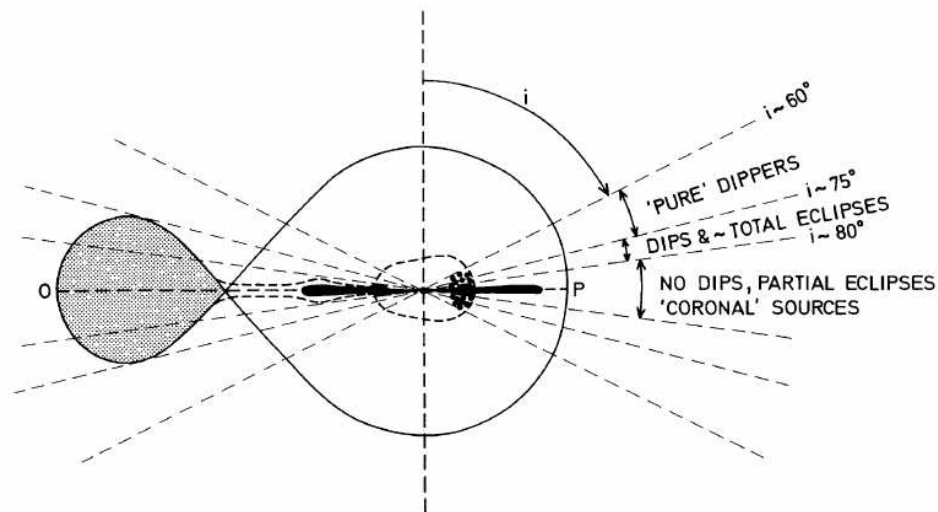


FIGURE 1.12— Diagram with the different dipping phenomenology found in X-ray light curves depending on the orbital inclination of the system. From Frank, King & Lasota (1987).

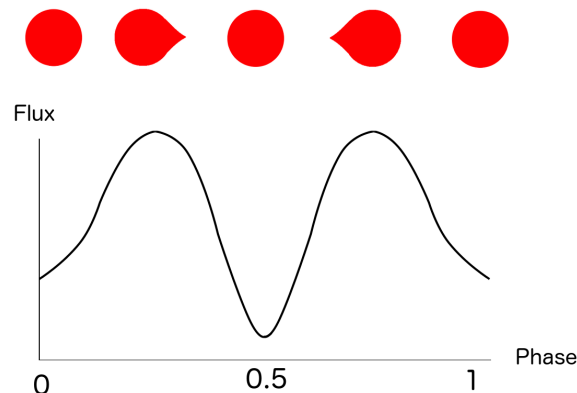


FIGURE 1.13— Ellipsoidal modulation produced by the changing projected area of the donor star with orbital phase. The difference in brightness of the two minima depends on system parameters such as the orbital inclination, limb darkening and gravity darkening (due to the companion distorted shape).

Este documento incorpora firma electrónica, y es copia auténtica de un documento electrónico archivado por la ULL según la Ley 39/2015.  
Su autenticidad puede ser contrastada en la siguiente dirección <https://sede.ull.es/validacion/>

Identificador del documento: 970342

Código de verificación: pkuTTaUi

Fecha: 29/06/2017 10:41:42

Firmado por: DANIEL MATA SÁNCHEZ  
UNIVERSIDAD DE LA LAGUNA

29/06/2017 11:14:09

JORGE CASARES VELAZQUEZ  
UNIVERSIDAD DE LA LAGUNA

29/06/2017 12:50:38

TEODORO MUÑOZ DARIAS  
UNIVERSIDAD DE LA LAGUNA

04/07/2017 18:28:11

ERNESTO PEREDA DE PABLO  
UNIVERSIDAD DE LA LAGUNA

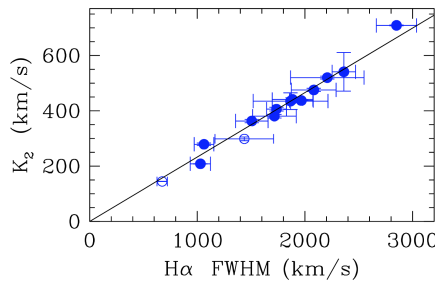


FIGURE 1.14— FWHM –  $K_2$  correlation for XRTs, including the best linear fit. Blue solid circles indicate BHs while NSs are marked by open circles. From Casares (2015).

For non-eclipsing LMXBs, the  $P_{\text{orb}}$  determination relies on the study of optical modulations. Opt-NIR light curves during quiescence are usually dominated by an ellipsoidal modulation, produced by the deformation of the donor star within its Roche lobe (Fig. 1.13). The donor star variable contribution can be modelled in order to obtain other parameters of the system such as  $i$ . Nevertheless, this ideal scenario is not always met in quiescence, as the accretion disc contributes to the optical emission and produces flickering that can sometimes veil completely this modulation (e.g. see Zurita et al. 2003, Shahbaz et al. 2013).

During outburst, modulations, if present, typically amount to a small percentage of the total flux, and are usually associated to the hot, inner face of the companion, which is being irradiated by the central X-ray source. However, orbital modulations obtained during outburst must be treated with caution. In some systems, the precession of the disc is able to produce a beat period (called superhump) with the true  $P_{\text{orb}}$ , which can dominate the light curves (e.g. O'Donoghue & Charles 1996). In some other cases, photometric modulations unrelated to  $P_{\text{orb}}$  and of unknown origin have been detected (e.g. Leibowitz et al. 1991, Udalski & Kaluzny 1991).

When photometric modulations are absent, an indirect estimation of  $P_{\text{orb}}$  is still possible through the observed correlation between  $P_{\text{orb}}$  and the  $V$ -band photometric amplitude from outburst to quiescence (see Shahbaz & Kuulkers 1998).

#### 1.4.2 Donor star radial velocity

The classical approach to measure the donor star radial velocity curve requires the observation of the system during quiescence. If the donor star photospheric absorption lines are visible in the Opt-NIR spectra, time-resolved spectroscopy can provide its radial velocity curve through cross-correlation with spectral templates. This radial velocity curve follows a sinusoidal pattern (given that the orbit is circular, see Fig. 1.8) characterised by its semi-amplitude  $K_2$ .

However, the accretion disc of some LMXBs is luminous enough to completely outshine the donor star features, even in quiescence (see Sec. 3). The only known method to obtain  $K_2$  from quiescent spectra in these systems is to apply the recently presented correlation (see Fig. 1.14, Casares 2015) between  $K_2$  and the full-width-at-half-maximum (FWHM) of the H $\alpha$  emission line:  $K_2 = 0.233(13)\text{FWHM}$ .

Because the (disc) H $\alpha$  line is much stronger than the weak photospheric lines from the donor, this technique is also very useful to study faint quiescent XRTs (e.g. Zurita, Corral-Santana & Casares 2015).

#### *The Bowen technique: observing the companion during outburst*

Opt-NIR outburst spectra are characterised by the companion star contribution being typically swamped by the reprocessed light from the accretion flow. The high X-ray radiation produced in the disc inner regions is able to power the ionisation of helium atoms. The ultraviolet photons associated with their Lyman  $\alpha$  decay produce a cascade of transitions, which ultimately generate fluorescence lines when reprocessed in colder regions (McClintock, Canizares & Tarter 1975, Schachter, Filippenko & Kahn 1989). These emission lines typically arise from the irradiated, external regions of the disc, producing both broad (if generated in wide regions) and narrow (if produced at a particular spot in the disc, e.g. the hot spot) high-excitation lines (e.g. NIII, CIII and OII).

However, Steeghs & Casares (2002) found through high-resolution spectroscopy a new set of narrow, fluorescence emission lines (most prominent within the so-called Bowen blend) in the persistent LMXB Sco X-1. When tracing their radial velocities, they found them to be in anti-phase with disc lines that trace the motion of the compact star (e.g. He II 4686 Å). This behaviour is only explained if they originate through fluorescence not in the accretion disc, but on the irradiated inner face of the donor star. Based on the detection of the donor emission lines, they developed the so-called Bowen technique, given that the Bowen blend (4640 – 4650 Å, with lines of CIII, NIII and OII) has proven to be the best spectral region for its application.

The Bowen technique allowed, for the first time, to measure the donor star radial velocity curve in the persistent LMXB Sco X-1 and to constrain its semi-amplitude. However, the velocities inferred from these emission lines correspond to those of the inner face of the companion; and hence they only represent a lower limit to the true velocity of the donor star's centre of mass.

In order to correct for this effect, numerical solutions have been obtained (Muñoz-Darias, Casares & Martínez-Pais 2005). The so-called K-correction depends on  $q$ ,  $i$  and also on the accretion disc aperture angle ( $\alpha$ , see Fig. 1.16). The shadow projected on the inner face of the companion star by the outer regions of the accretion disc with higher vertical extension will determine the irradiation pattern on the donor's surface, and therefore will change the centre of mass of the emitted light (see Fig. 1.16). The Bowen technique has been successfully applied to a dozen LMXBs (see e.g. Cornelisse et al. 2008; Muñoz-Darias 2009), providing their first dynamical solutions.

#### 1.4.3 Donor star rotational velocity

The donor star is assumed to be tidally locked with the binary orbit since LMXBs are typically  $\gtrsim 10^7$  years old (Witte & Savonije 2001). Consequently, the relation between the projected rotational velocity of the donor ( $v_{\text{rot}} \sin i$ ),  $K_2$  and  $q$  follows the expression (Wade & Horne 1988):

Este documento incorpora firma electrónica, y es copia auténtica de un documento electrónico archivado por la ULL según la Ley 39/2015.  
Su autenticidad puede ser contrastada en la siguiente dirección <https://sede.ull.es/validacion/>

Identificador del documento: 970342

Código de verificación: pkuTTaUi

Fecha: 29/06/2017 10:41:42

Firmado por: DANIEL MATA SÁNCHEZ  
UNIVERSIDAD DE LA LAGUNA

JORGE CASARES VELAZQUEZ  
UNIVERSIDAD DE LA LAGUNA

TEODORO MUÑOZ DARIAS  
UNIVERSIDAD DE LA LAGUNA

ERNESTO PEREDA DE PABLO  
UNIVERSIDAD DE LA LAGUNA

29/06/2017 11:14:09

29/06/2017 12:50:38

04/07/2017 18:28:11

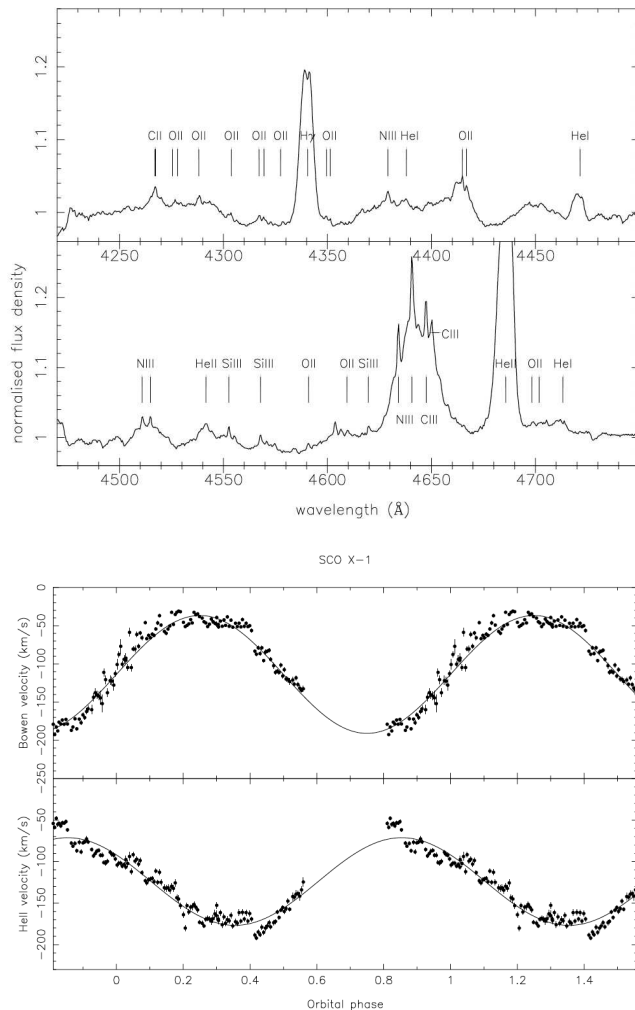


FIGURE 1.15—Top: narrow emission lines observed in the persistent LMXB Sco X-1, including the Bowen blend. Bottom: radial velocity curve of both the Bowen blend narrow components and the He II 4686 Å wings (tracing the movement of the compact object), in antiphase. From Steeghs & Casares (2002).

Este documento incorpora firma electrónica, y es copia auténtica de un documento electrónico archivado por la ULL según la Ley 39/2015.  
Su autenticidad puede ser contrastada en la siguiente dirección <https://sede.ull.es/validacion/>

Identificador del documento: 970342

Código de verificación: pkuTTaUi

Firmado por: DANIEL MATA SÁNCHEZ  
UNIVERSIDAD DE LA LAGUNA

Fecha: 29/06/2017 10:41:42

JORGE CASARES VELAZQUEZ  
UNIVERSIDAD DE LA LAGUNA

29/06/2017 11:14:09

TEODORO MUÑOZ DARIAS  
UNIVERSIDAD DE LA LAGUNA

29/06/2017 12:50:38

ERNESTO PEREDA DE PABLO  
UNIVERSIDAD DE LA LAGUNA

04/07/2017 18:28:11

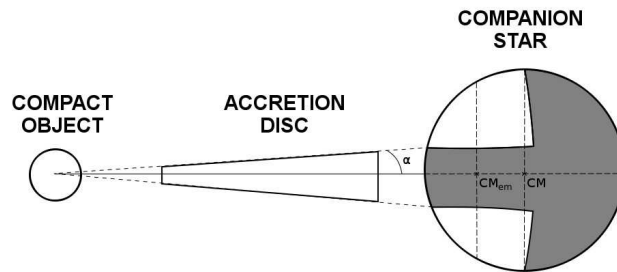


FIGURE 1.16— Diagram of an LMXB, where the irradiation of the companion star by the innermost regions of the accretion disc is shadowed by the outer disc rim. The accretion disc aperture angle is  $\alpha$ . The centre of mass of the emission-line forming region ( $CM_{em}$ ) as well as the true centre of mass of the companion (CM) are marked.

$$v_{\text{rot}} \sin i = 0.462 K_2 q^{1/3} (1 + q)^{2/3}$$

The rotational velocity can be measured from the broadening of the absorption lines in the averaged quiescent spectrum (see Fig. 1.17), which combined with an independent measurement of  $K_2$  allows to determine  $q$ . Note that the Doppler shifts caused by the orbital motion of the star have to be properly corrected when combining the phase-resolved spectra. In particular, the exposure time of each individual spectrum is limited by the orbital smearing (see Sec. 1.3).

#### 1.4.4 Compact object orbital velocity

The best technique to derive precise measurements of the compact object orbital movement is only feasible for those LMXBs harbouring pulsars. Since X-ray pulses arise from the surface of the NS, the evolution of the pulse delay over an orbit can be used to derive highly precise values of  $K_1$  (e.g. Jonker, van der Klis & Groot 2003, Papitto et al. 2007).

On the other hand, the broad emission lines of hydrogen and helium observed in the Opt-NIR spectra are known to be formed in the accretion disc. As the disc follows the compact object, the radial velocity curves of disc lines contain information on  $K_1$ . However, extracting  $K_1$  from the broad, complex disc emission line profiles is not straightforward. In the first place, asymmetries in the lines are not uncommon. Furthermore, the contribution to the broad line comes from different regions of the accretion disc, rotating at different velocities (see Sec. 1.3). One of the most exploited techniques to solve this situation requires fitting only the emission line wings, as they are formed at the disc regions with highest velocity, which corresponds to

Este documento incorpora firma electrónica, y es copia auténtica de un documento electrónico archivado por la ULL según la Ley 39/2015.  
Su autenticidad puede ser contrastada en la siguiente dirección <https://sede.ull.es/validacion/>

Identificador del documento: 970342

Código de verificación: pkuTTaUi

Firmado por: DANIEL MATA SÁNCHEZ  
UNIVERSIDAD DE LA LAGUNA

Fecha: 29/06/2017 10:41:42

JORGE CASARES VELAZQUEZ  
UNIVERSIDAD DE LA LAGUNA

29/06/2017 11:14:09

TEODORO MUÑOZ DARIAS  
UNIVERSIDAD DE LA LAGUNA

29/06/2017 12:50:38

ERNESTO PEREDA DE PABLO  
UNIVERSIDAD DE LA LAGUNA

04/07/2017 18:28:11

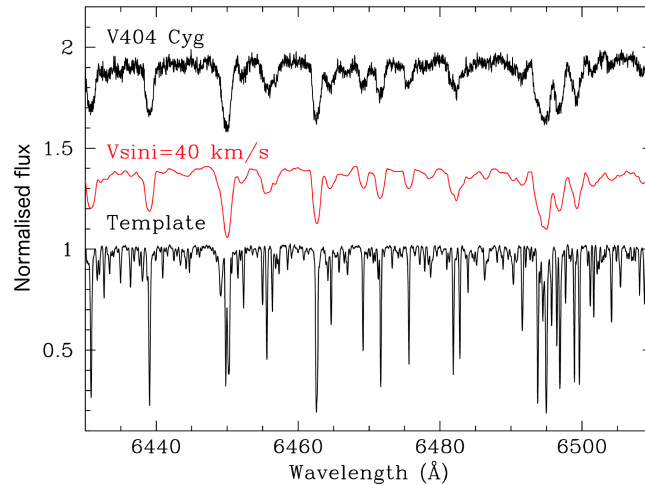


FIGURE 1.17— Top: normalised optical spectrum of V404 Cyg (BH XRT) during quiescence. This has been computed by averaging 20 individual spectra obtained at different orbital phases after removing the orbital motion of the companion star. Bottom: the template K0IV star. Middle: the same template spectrum after applying the optimal rotational broadening that best fits the spectrum of V404 Cyg. An offset has been applied for displaying purposes. From Casares & Jonker (2014).

Este documento incorpora firma electrónica, y es copia auténtica de un documento electrónico archivado por la ULL según la Ley 39/2015.  
Su autenticidad puede ser contrastada en la siguiente dirección <https://sede.ull.es/validacion/>

Identificador del documento: 970342

Código de verificación: pkuTTaUi

Firmado por: DANIEL MATA SÁNCHEZ  
UNIVERSIDAD DE LA LAGUNA

Fecha: 29/06/2017 10:41:42

JORGE CASARES VELAZQUEZ  
UNIVERSIDAD DE LA LAGUNA

29/06/2017 11:14:09

TEODORO MUÑOZ DARIAS  
UNIVERSIDAD DE LA LAGUNA

29/06/2017 12:50:38

ERNESTO PEREDA DE PABLO  
UNIVERSIDAD DE LA LAGUNA

04/07/2017 18:28:11

the inner parts of the disc and hence they better trace the compact object motion (e.g. Marsh 1988).

#### 1.4.5 Measuring masses: state of the art

The most robust method to measure the binary masses is through dynamical studies (detailed earlier). However, the measurement of these masses is not always straightforward. A knowledge of  $q$  and, most importantly, a reliable measurement of  $i$  are critical to derive accurate masses. The latter has the largest impact on the final masses because of its cubic dependence in the mass function equation.

If the mass function is large enough ( $f(M_1) > 3 M_\odot$ ), it implies that the compact object is more massive than the theoretical mass limit for a NS ( $M_1 > 3 M_\odot$ , see Rhoades & Ruffini 1974, Kalogera & Baym 1996). Therefore, it must be a BH.

Unfortunately, the current distribution of compact object masses in LMXBs is limited by the low number of dynamically confirmed masses. A clear, narrow peak in the NS mass distribution centred at  $\sim 1.4 M_\odot$  defines the classical mass of this compact object. NS masses span the range  $1.2 M_\odot$  (e.g. Kiziltan et al. 2013) to  $\sim 2.0 M_\odot$  (e.g. Demorest et al. 2010).

On the other hand, BHs are spread within  $\sim 5 - 16 M_\odot$  (see Fig. 1.18, left panel). The most remarkable feature in the distribution is the presence of an apparent mass gap  $\sim 2 - 5 M_\odot$ , as seen in Fig. 1.18 (e.g. Özel et al. 2010, Kreidberg et al. 2012). If this gap is indeed linked to the physics of supernova explosions (as suggested by different authors), it could be used to favour certain supernova (SN) models (e.g. Belczynski et al. 2012, Ugliano et al. 2012). Alternatively, the gap could be an observational bias (e.g. neglected flickering in ellipsoidal modelling leads to systematically lower inclinations and hence larger BH masses, see Kreidberg et al. 2012) or caused by selection effects (it has been proposed that low-mass BHs could be disrupted by SN explosions or perhaps are X-ray persistent).

More observational work is necessary to increase the sample of BH X-ray binaries, as well as to better characterise those already found. This will allow us to confirm or exclude the dearth of remnants between  $2 - 5 M_\odot$ .

In this thesis, we present the analysis of five different LMXBs, providing new constraints on their fundamental parameters, as well as unveiling new phenomena occurring during the outburst phases, including the discovery of a new type of disc wind in the canonical BH LMXB V404 Cyg (Sec. 6).

Este documento incorpora firma electrónica, y es copia auténtica de un documento electrónico archivado por la ULL según la Ley 39/2015.  
Su autenticidad puede ser contrastada en la siguiente dirección <https://sede.ull.es/validacion/>

Identificador del documento: 970342

Código de verificación: pkuTTaUi

Fecha: 29/06/2017 10:41:42

Firmado por: DANIEL MATA SÁNCHEZ UNIVERSIDAD DE LA LAGUNA	29/06/2017 11:14:09
JORGE CASARES VELAZQUEZ UNIVERSIDAD DE LA LAGUNA	29/06/2017 12:50:38
TEODORO MUÑOZ DARIAS UNIVERSIDAD DE LA LAGUNA	04/07/2017 18:28:11
ERNESTO PEREDA DE PABLO UNIVERSIDAD DE LA LAGUNA	

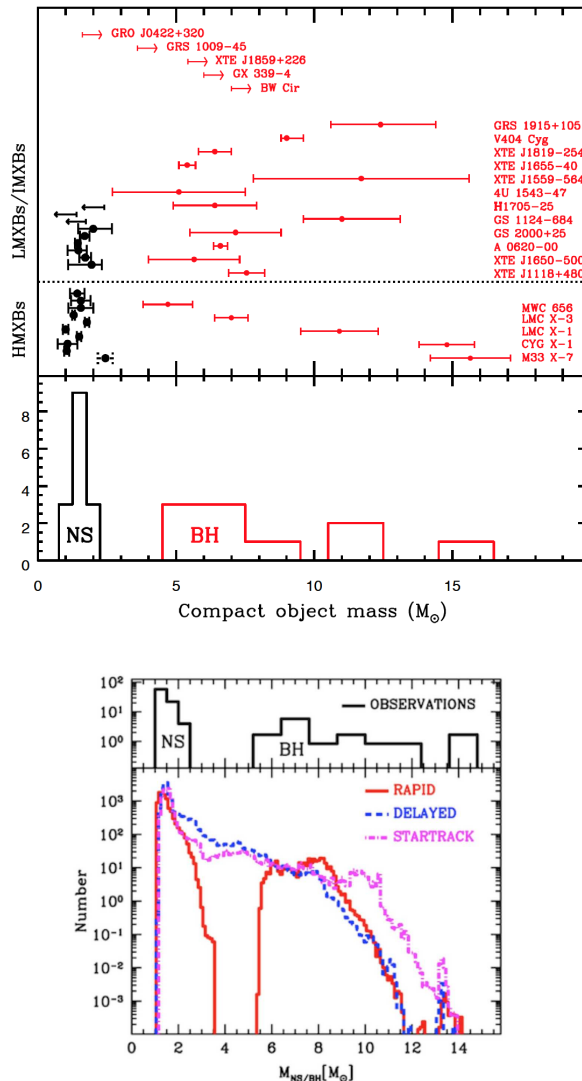


FIGURE 1.18— Top: in the top panel, dynamical masses of compact objects in X-ray binaries are shown, where NSs are indicated in black and BHs in red, respectively. Note that one particular point, 4U 1700-37, is plotted in dotted-line style because the nature of the compact star is uncertain. The horizontal dotted line separates LMXBs from HMXBs. In the bottom panel, the distribution of compact object masses is depicted. From Casares, Jonker & Israelian (2017). Bottom figure: the observed distribution of NSs and black hole masses, including every measured NS mass (not only those dynamically confirmed) is shown in the top panel. Bottom panel presents theoretical mass distributions of compact objects in X-ray binaries computed for different supernova models. From Belczynski et al. (2012).

Este documento incorpora firma electrónica, y es copia auténtica de un documento electrónico archivado por la ULL según la Ley 39/2015.  
Su autenticidad puede ser contrastada en la siguiente dirección <https://sede.ull.es/validacion/>

Identificador del documento: 970342

Código de verificación: pkuTTaUi

Firmado por: DANIEL MATA SÁNCHEZ  
UNIVERSIDAD DE LA LAGUNA

Fecha: 29/06/2017 10:41:42

JORGE CASARES VELAZQUEZ  
UNIVERSIDAD DE LA LAGUNA

29/06/2017 11:14:09

TEODORO MUÑOZ DARIAS  
UNIVERSIDAD DE LA LAGUNA

29/06/2017 12:50:38

ERNESTO PEREDA DE PABLO  
UNIVERSIDAD DE LA LAGUNA

04/07/2017 18:28:11

# 2

## Multiple outbursts of MAXI J1957+032

SEVERAL classes of object exhibit transient X-ray emission that can be detected through X-ray monitoring campaigns (CVs, LMXBs, HMXBs and even active stars). Many of them are found in the Galactic plane, as well as in the Galactic bulge. This implies that these are placed in crowded and large-extinction regions, where optical observations are not always feasible. Therefore, X-ray transient sources found outside the Galactic plane, where these limitations are less important, offer a great opportunity to obtain detailed multiwavelength observations. In particular, the population of high-latitude LMXBs is especially promising as they can constrain LMXB formation models (e.g. Nelemans, Tauris & van den Heuvel 1999).

Discovering the nature of a particular X-ray transient is not an easy task, as several observations at different wavelengths and over several epochs are mandatory. We present the recent detection of a new high-latitude X-ray transient, MAXI J1957+032, as well as the first optical follow-up of this system, performed by our team. We became interested in this system due to its particularly short outburst duration (< 5 days) and high recurrence time (4 outbursts in less than 16 months). We analyse X-ray light curves and X-ray spectra (Swift/XRT), optical to ultraviolet photometry (Swift/UVOT) and optical spectroscopy (Southern African Large Telescope) obtained during the different outbursts of this source. We compare our results with other known X-ray transient systems in order to infer the nature of this object and sketch its properties (Mata Sánchez et al. 2017b).

The work presented in this chapter was published under the title “*Swift and SALT observations of the multiple outbursts of MAXI J1957+032*” in Monthly Notices of the Royal Astronomical Society, Volume 468, pages 564-569, in 2017.



## Swift and SALT observations of the multiple outbursts of MAXI J1957+032

D. Mata Sánchez,<sup>1,2\*</sup> P. A. Charles,<sup>1,3</sup> M. Armas Padilla,<sup>1,2</sup> D. A. H. Buckley,<sup>4</sup>  
G. L. Israel,<sup>5</sup> M. Linares<sup>1,2</sup> and T. Muñoz-Darias<sup>1,2</sup>

<sup>1</sup>Instituto de Astrofísica de Canarias (IAC), E-38205 La Laguna, Tenerife, Spain

<sup>2</sup>Departamento de astrofísica, Universidad de La Laguna, E-38206 La Laguna, Tenerife, Spain

<sup>3</sup>Department of Physics and Astronomy, University of Southampton, Southampton SO17 1BJ, UK

<sup>4</sup>South African Astronomical Observatory, PO Box 9, 7935 Observatory, Cape Town, South Africa

<sup>5</sup>INAF – Osservatorio Astronomico di Roma, via Frascati 33, I-00040 Monteporzio Catone, Italy

Accepted 2017 February 21. Received 2017 February 20; in original form 2017 January 12

### ABSTRACT

The new recurrent X-ray transient MAXI J1957+032 has had four X-ray outbursts within 16 months, all very briefly detected (lasting <5 d). During the most recent event (2016 September/October), we obtained with the Southern African Large Telescope the first optical spectrum of the transient counterpart, showing the classic blue continuum of an X-ray irradiated disc in an LMXB and no other features. At high Galactic latitude below the plane ( $-13^\circ$ ) reddening is low but there is no quiescent counterpart visible on any of the existing sky surveys, nor any other known X-ray source in the region. *Swift* monitoring of three of the four events is presented, showing rapidly fading X-ray outbursts together with significant UVOT detections in the *UV* (*W1,M2,W2*), *U* and *B* bands. The optical properties are most like those of the short-period LMXBs, which, combined with the softening witnessed during the decay to quiescence would place the system at  $d < 13$  kpc. The short duration and short recurrence time of the outbursts are reminiscent of the accreting millisecond X-ray pulsars, which exhibit peak luminosities of  $\sim 1$  per cent  $L_{\text{Edd}}$ . Assuming this peak luminosity would place MAXI J1957+032 at a distance of  $d \sim 5\text{--}6$  kpc.

**Key words:** accretion, accretion discs – X-rays: binaries.

### 1 INTRODUCTION

The highly variable X-ray sky is populated with X-ray transients (XRTs). These are usually classified as objects typically in quiescence with X-ray luminosities well below  $10^{33}$  erg s $^{-1}$ , which increase by several orders of magnitude during outbursts. Within our Galaxy, luminous XRT behaviour is demonstrated by both high-mass and low-mass X-ray binaries (HMXBs and LMXBs, respectively), where the former are predominantly BeX systems involving neutron stars (NSs) in long (tens of days or more) eccentric orbits around a rapidly rotating Be star (e.g. Reig 2011). As we will show, the properties of J1957 are consistent with that of LMXB transients, which contain either a black hole (BH) or NS in a close (typically  $P_{\text{orb}} \sim$  hours) circular orbit with a low-mass, evolved donor (Remillard & McClintock 2006; Liu, van Paradijs & van den Heuvel 2007).

Since the demise of the *RXTE* all-sky monitor (ASM) in 2012, the X-ray sky monitoring task has been shared between the *INTEGRAL*,

*GRAL*, *Swift* and *MAXI* missions. Thanks to their wide field and all-sky monitoring programs (Kuulkers et al. 2007; Krimm et al. 2013 and Matsuoka et al. 2009, respectively), the last decade has seen the emergence of a number of new XRTs (*Swift* J1753.5–0127, MAXI J1659–152, *Swift* J1357.2–093313, MAXI J1305–704) at high Galactic latitude and subsequently found to have short periods ( $<5$  h). Combined with the already well-known XRTs, GRO J0422+32 and XTE J1118+480, this suggested the existence of a possible sub-group of LMXB XRTs, whose high latitude (and consequent low extinction) made them important targets for multiwavelength studies (see e.g. Shaw et al. 2013). Furthermore, since many of these XRTs are too faint in quiescence for current telescopes (especially the short period systems which tend to have the lowest mass donors), it is very important to undertake rapid follow-up optical spectroscopy while the X-ray outburst is underway, as it can then be possible to exploit the X-ray irradiation of the donor to provide constraints on the motion of the donor (see e.g. Cornelisse 2013).

The high-latitude XRT MAXI J1957+032 (hereafter ‘J1957’) was discovered in 2015, independently by both *MAXI* (Negoro et al. 2015) and *INTEGRAL* (Cherepashchuk et al. 2015, who designated the source IGR J19566+0326), and optically identified (Rau,

\* E-mail: dmata@iac.es

Yates & Greiner 2015) with a faint  $r' \sim 20$  star, there being no counterpart on sky-survey images (Chakrabarty, Jonker & Markwardt 2016). However, that and the subsequent two outbursts over the next year (Sugimoto et al. 2015; Tanaka et al. 2016<sup>1</sup>), decayed rapidly (within a matter of days), making extensive follow-up study almost impossible. Nevertheless, Marchesini et al. (2015) described a low-resolution ( $\sim 17$  Å) optical spectrum of J1957 taken during the 2015 October outburst (where Guver et al. 2015 had reported  $R = 18.3$  four days after the start of the outburst), which contained only absorption features consistent with an F-/G-type star, and no emission lines. This was surprising, as virtually all LMXB XRTs in outburst have optical spectra that are dominated entirely by the X-ray irradiated accretion disc, producing a strong blue continuum on which is usually superposed strong Balmer, HeII and Bowen emission features (see e.g. Charles & Coe 2006).

Furthermore, to have three X-ray outbursts within a year is unusual amongst the class of LMXB XRTs; so, when a new, brighter X-ray outburst of MAXI J1957+032 was reported in 2016 September (Negoro et al. 2016), we immediately initiated our SALT Transients ToO program (Buckley et al. 2016) in order to obtain further optical spectra of this intriguing object. Those data, together with the associated *Swift* monitoring of J1957, are the subject of this paper.

## 2 OBSERVATIONS

Due to the short duration and faintness of J1957 outbursts, both *MAXI/GSC* (2–20 keV) and *Swift/BAT* (15–50 keV) light curves do not exhibit any remarkable feature (e.g. rebrightening) other than the reported starting times of the four events. These correspond to 57153.58 (2015-05-11, epoch 1), 57301.52 (2015-10-06, epoch 2), 57394.35 (2016-01-07, epoch 3) and 57660.35 (2016-09-29, epoch 4); three of them marked in Fig. 1.

### 2.1 Swift/XRT

#### 2.1.1 Spectral analysis

Following the outburst alerts, the X-ray Telescope (hereafter Swift/XRT; Burrows et al. 2005) on board *Swift* (Gehrels et al. 2004) covered three of the four reported events. A total of 28 observations [two in window timing (WT) mode and the rest in photon counting (PC) mode] were performed, but due to the outburst rapid decline, J1957 is detected in only 10 of these observations. We processed the data making use of the HEASOFT v.6.18 software. The data reduction was carried out running the XRT PIPELINE task in which standard event grades of 0–12 and 0–2 were selected for the PC and WT mode observations, respectively. For each observation, the 0.5–10 keV spectrum, light curve and image were obtained using XSELECT. We used a circular region of  $\sim 40$ -arcsec radius centred at the source position (the inner 10 arcsec were excluded for 00033770019 observation, 57662.75, affected by pile-up). For the PC observations, three circular regions of similar size and shape, positioned on an empty sky region, were used for the background. On the other hand, an annulus centred on the source with  $\sim 82$  pixels for the inner radius and  $\sim 118$  pixels for the outer radius was used for the background of the WT observations. We created exposure maps and ancillary response files following the standard *Swift* analysis threads,<sup>2</sup> and we

<sup>1</sup> Note that the 2–20 keV fluxes quoted for January 7 and 8 are incorrect. They should have been 0.066 and 0.071 ph cm $^{-2}$  s $^{-1}$ , respectively.

<sup>2</sup> <http://www.swift.ac.uk/analysis/xrt/>

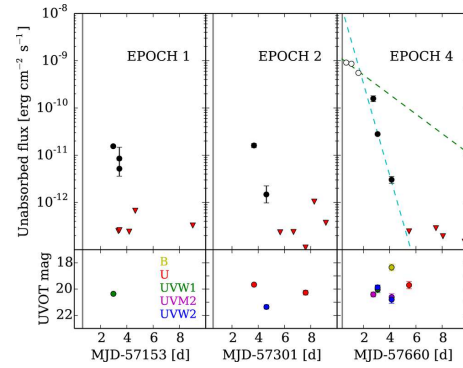


**Figure 1.** Upper panel: Detailed *Swift*/XRT (0.5–10 keV) monitoring of J1957 events 1, 2 and 4. The most detailed coverage is of event 4, where we also plot exponential decays of  $e$ -folding time-scales  $2.1 \pm 0.9$  and  $0.44 \pm 0.15$  d to the slow and fast declines, respectively. Empty circles refer to WT mode and filled circles to PC mode observations. The start times of the covered outbursts are marked by vertical dashed lines. Lower panel: *Swift*/UVOT (B, U, UVW1, UVM2 and UW2 filters) follow-up pointings are shown.

acquired the last version of the response matrix files from the High Energy Astrophysics Science Archive Research Center (HEASARC) calibration data base (CALDB). Finally, we grouped the spectra to have a minimum of 20 photons per bin to be able to consistently use the  $\chi^2$ . However, due to the low number of counts collected during various observations, we fitted these data using both C statistic and  $\chi^2$  but grouped them with a minimum of five photons per bin (see Table 1). The results using both methods were consistent with each other (e.g. Wijnands & Wang 2002; Armas Padilla et al. 2013). We fitted the spectra using XSPEC (v12.9, Arnaud 1996). All observations were well fitted with a simple power law (PL) plus absorbing column (PHABS in XSPEC) assuming the cross-sections of Verner et al. (1996) and the abundances of Wilms, Allen & McCray (2000). We assumed a constant hydrogen equivalent column density of  $N_H = 1.7 \times 10^{21}$  cm $^{-2}$ , inferred from our highest signal-to-noise spectrum (Fig. 2) and consistent with the low reddening expected for that direction (see next section). The photon-index of each spectrum's fit varies from  $1.90 \pm 0.02$  to  $2.34_{-0.25}^{+0.27}$  (from highest to lowest luminosity). The unabsorbed fluxes are reported in Fig. 1. We note that observation 00033770018 (57661.09) consists of two  $\sim 350$  s-long groups of detections  $\sim 13$  h apart (similar to the gap between the first group and the previous observation,  $\sim 14$  h), so we decided to plot two independent points in the light curve.

For the observations where J1957 is not detected, we determined the 95 per cent confidence upper-limit count rates using the prescription given by Gehrels (1986). We estimated the corresponding unabsorbed flux upper limits using the WEBPIMM (HEASARC tool). We co-added 10 *Swift*/XRT (PC mode) observations (11.7 ksec) in order to constrain the quiescent luminosity of MAXI J1957+032. We can thereby place a 95 per cent confidence upper limit on the 0.5–10 keV quiescent unabsorbed flux of  $(1\text{--}3) \times 10^{-13}$  erg cm $^{-2}$  s $^{-1}$  (assuming  $N_H = 1.7 \times 10^{21}$  cm $^{-2}$  and a PL photon index in the 1–3 range). Comparing with the epoch 4 detection at a flux of  $\sim 10^{-9}$  erg cm $^{-2}$  s $^{-1}$ , this reveals that the X-ray luminosity dropped by at least four orders of magnitude in just about a week.

**Table 1.** *Swift* observations log and spectral results for J1957 using a PHABS\*PO model. We assumed a constant  $N_{\text{H}}$  of  $1.7 \times 10^{21} \text{ cm}^{-2}$ , inferred from the highest signal-to-noise spectrum (00033770017).

ID	MJD	Mode	Exposure (ks)	$\Gamma$	$unabs, F_x (0.5\text{--}10 \text{ keV})$ ( $\text{erg cm}^{-2} \text{s}^{-1}$ )	$\chi^2_v (\text{dof})$
00033770001	57155.96	PC	2.9	$2.13 \pm 0.07$	$(1.55 \pm 0.08) \times 10^{-11}$	0.97 (167)
00033776001	57156.42	PC	0.44	$1.5 \pm 0.6$	$(8.5 \pm 6.7) \times 10^{-12}$	0.36 (5)
00033777001	57156.43	PC	0.45	$2.5 \pm 0.8$	$(5.2 \pm 2.6) \times 10^{-12}$	0.91 (6)
00033770009	57304.67	PC	0.96	$2.0 \pm 0.1$	$(1.61 \pm 0.16) \times 10^{-11}$	1.11 (67)
00033770010	57305.61	PC	0.98	$2.6 \pm 0.9$	$(1.5 \pm 0.5) \times 10^{-12}$	1.54 (5)
00033770017	57660.69	WT	0.97	$1.90 \pm 0.02$	$(9.13 \pm 0.13) \times 10^{-10}$	1.02 (364) <sup>b</sup>
00033770018 <sup>a</sup>	57661.09	WT	0.77	$1.92 \pm 0.02$	$(7.09 \pm 0.12) \times 10^{-10}$	1.04 (304) <sup>b</sup>
00033770018-1 <sup>a</sup>	57661.09	WT	0.45	$1.92 \pm 0.03$	$(8.65 \pm 0.18) \times 10^{-10}$	1.18 (252) <sup>b</sup>
00033770018-2 <sup>a</sup>	57661.62	WT	0.33	$1.93 \pm 0.04$	$(5.53 \pm 0.18) \times 10^{-10}$	0.89 (153) <sup>b</sup>
00033770019	57662.75	PC	0.37	$1.89 \pm 0.2$	$(1.58 \pm 0.22) \times 10^{-10}$	0.84 (80)
00033770020	57663.08	PC	1.7	$1.94 \pm 0.07$	$(2.80 \pm 0.17) \times 10^{-11}$	1.22 (164)
00033770021	57664.14	PC	1.7	$2.3 \pm 0.3$	$(3.03 \pm 0.49) \times 10^{-12}$	0.97 (27)

Notes. <sup>a</sup>Observation 00033770018 was divided in two sub-events of detections  $\sim$ 13 h apart (see Section 2.1.1).

<sup>b</sup>Spectra with a minimum of 20 photons per bin. The rest are grouped with a minimum of 5 photons per bin (see Section 2.1.1).

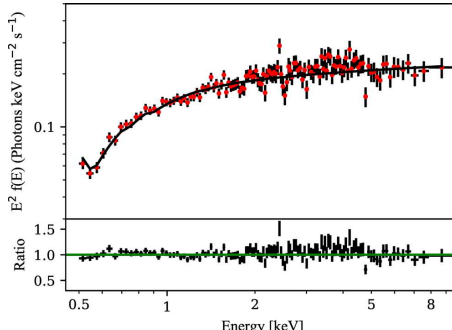


**Figure 2.** Unfolded spectra of observation 00033770017 (57660.69, 2016-09-29). The solid line represents the best fit using a PHABS\*POWERLAW model. The sub-panel shows the data-to-model ratio. Data have been re-binned in XSPEC for clarity.

### 2.1.2 Timing Analysis

We searched for pulsations and quasi-periodic oscillations in the three *Swift*/XRT observations with WT mode data (1.78 ms time resolution). These were taken on 57160 (2015-05-18, 1.3-ksec exposure), 57660 (2016-09-29, 1 ksec) and 57661 (2016-09-30, 0.8 ksec). We used 30- and 120-s-long Fast Fourier Transforms (FFTs), including energies between 1 and 10 keV, keeping the original time resolution and inspecting individual FFTs as well as observation averages. We detect neither coherent pulsations nor aperiodic variability in the 0.1–281 Hz frequency range. The most constraining upper limits come from the 57660 observation, when the average 1–10 keV count rate was  $\sim$ 16.5 count s $^{-1}$ . Following Vaughan et al. (1994), we estimate upper limits on the pulsed fraction of a sinusoidal signal. We find upper limits on the 0.1–281 Hz pulsed fraction between 2.2 per cent and 5.4 per cent (95 per cent confidence level), depending on the FFT length and exact frequency range. We note that, considering the pulsed fractions and spin frequencies of the accreting millisecond X-ray pulsars (AMXPs) (e.g. Patruno & Watts 2012, and references therein), this result does not exclude the presence of similar pulsations in J1957.

## 2.2 Swift/UVOT

There were also optical/UV observations of J1957 associated with many of the Swift/XRT pointings, and these were accessed from the Swift online archive. We used the UVOTSOURCE software (released as part of the HEASOFT package) to extract fluxes for J1957 using a 5-arcsec aperture centred at the position reported in Rau et al. (2015). J1957 was not detected in the V band, our best constraint being  $V < 17.85$  (MJD 57665.5). At different times it was seen in all other bands, with the brightest detections being  $B = 18.5 \pm 0.3$  (MJD 57664.1),  $U = 18.7 \pm 0.3$  (MJD 57665.5),  $UVW1 = 18.5 \pm 0.3$ ,  $UVM2 = 18.3 \pm 0.2$  and  $UVW2 = 18.1 \pm 0.2$  (MJD 57663.1). All values are Vega magnitude and were obtained during epoch 4. Using the relation  $N_{\text{H}} = 2.0 \pm 0.5 \times 10^{21} \text{ cm}^{-2}$ ,  $A_V$  (Watson 2011) and the Galactic hydrogen column density  $N_{\text{H}} = 0.95 \times 10^{21} \text{ cm}^{-2}$  [which yields  $E(B-V) = 0.14$ , Willingale et al. 2013], we obtain  $A_V \sim 0.5$  and  $A_B \sim 0.6$ . This implies that the brightest  $B$ -band detection corresponds to an intrinsic value of  $B = 17.9 \pm 0.3$ . We note that using a 5-arcsec aperture includes star ‘1’ (see Fig. 3), classified as an A-F star ( $R = 18.3$ ). It makes a small contribution in the  $B$  band ( $B > 19$ ), has no effect in the  $UV$  bands, but affects  $V$ -band observations, which will be disregarded.

## 2.3 SALT imaging and spectroscopy

We obtained optical imaging of J1957 with the Southern African Large Telescope (SALT, Buckley, Swart & Meiring 2006) on 57662.76 (2016-10-01, epoch 4), 2.4 d after the initial X-ray outburst report (Negoro et al. 2016). We used SALTICAM (O’Donoghue et al. 2006) to obtain a 60 s  $r'$ -band image (Fig. 3), which showed the previously identified optical counterpart (Guver et al. 2015; Marchesini et al. 2015) to be at  $r' = 18.5 \pm 0.15$ , similar to the  $R = 18.27$  reported 4.2 d after the 2015 October outburst (Guver et al. 2015), and brighter than the  $r' = 20.03$  measured 3.7 after the 2015 May outburst (Rau et al. 2015).

With this clear indication of renewed optical activity, we then immediately followed this with a 1000 s exposure spectrum using the SALT Robert Stobie Spectrograph (RSS). This was taken with the 300 l mm $^{-1}$  grating (mean resolving power of 320) covering 360–770 nm and through a 1.5 arcsec slit [the PSF was 1.3 arcsec full width at half-maximum (FWHM)], oriented as shown in Fig. 3 so as to exclude light from the nearby star ‘1’ (2.0 arcsec to the

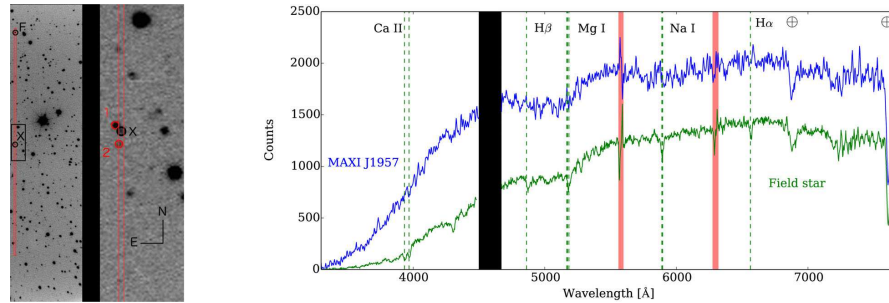


**Figure 3.** Left-hand panel: part of the SALTICAM  $r'$ -band image (left) of the region of J1957 (marked with ‘X’ and a black circle) showing the orientation of the RSS long slit (red box) and the field star ‘F’ that was included. The black box is blown up (right) so as to show the location of J1957 and its nearby stars marked ‘1’ and ‘2’, circled in red. Right-hand panel: RSS low-resolution spectra of J1957 (upper) and the simultaneously observed brighter field star (‘F’) whose flux has been reduced by  $\times 7$  to facilitate comparison. ‘F’ is a late-G star in the USNO catalogue (see text) and the key spectral features are marked as green-dashed lines. Telluric features are marked with the symbol  $\oplus$  and sky-subtraction residuals as red-shadowed bands. There are no cosmic features in J1957, but it is noticeably bluer than ‘F’. Colour figures are available in the online version.

NE of J1957). These data, together with associated arcs and bias frames were processed and reduced with the standard SALT pipeline (Crawford et al. 2010), followed by cosmic ray removal using the  $\text{IRAF}^3$  task ‘L.A. Cosmic’ (van Dokkum 2001) on the 2D image. We then extracted the spectrum of J1957 and other stars within the slit using standard  $\text{IRAF}$  routines. Wavelength calibration was performed using arc spectra with the MOLLY routines `arc` and `acal`, and the results are in Fig. 3.

The spectrum of J1957 is essentially featureless (apart from telluric lines), notably so in comparison with field star ‘F’, which was simultaneously in the slit. This star is USNO-B.1.0 0935-0543890, of observed spectral type G5-K0 and with  $B = 18.3$ ,  $B-R = 1.2$ , which we have used with our spectra to estimate  $B-V = 0.3$  for J1957 (significantly bluer than ‘F’ in our spectrum for which we obtain  $B-V = 0.7$ ). X-ray active LMXBs have optical spectra dominated by the X-ray irradiated disc, and often have strong Balmer and HeII lines in their spectra. However, the more compact systems, especially those seen at high inclination, have much weaker emission lines, often almost completely undetectable (e.g. Baglio et al. 2016). Indeed, ultracompact systems accretion discs should be depleted of hydrogen, as the companion star is itself degenerate (see Nelemans & Jonker 2010). We constrain the equivalent width of the  $H\alpha$  line to be lower than  $3\text{\AA}$  at  $3\sigma$  confidence level (assuming a conservative FWHM  $< 4400\text{\AA}$  determined by the widest  $H\alpha$  profile measured so far in a LMXB, see Mata Sánchez et al. 2015).

As already reported (Buckley et al. 2016), our spectrum contrasts with the A-F star absorption features reported by Marchesini et al. (2015) using the Nordic Optical Telescope (and ALFOSC) at a similar resolution 8.2 d after the epoch 2 outburst (2015 October). We re-analysed the ALFOSC data of this epoch, and from a 250 s image taken immediately after the spectrum, obtained  $R = 21.4 \pm 0.2$  for J1957. This led to the realization that the reported Nordic Optical Telescope (NOT) spectrum was not of J1957, but rather of star ‘1’, 2.0 arcsec NE of J1957. We measured star ‘1’ to have  $r' = 18.0 \pm 0.15$  and  $R = 18.3 \pm 0.1$ , respectively, from the SALTICAM and ALFOSC images taken a year apart, and is

consistent with the fluxes measured in the NOT spectrum. All of the photometry reported here used the same reference star, USNO B.1.0 0934-0560330.

### 3 DISCUSSION

Having resolved the question of the spectroscopic identification of J1957, and demonstrated that its optical spectrum is consistent with other LMXB XRTs in their active phase, the *Swift*/XRT light curve highlighted the extremely rapid decay of the outburst (and which Fig. 1 shows was likely the case for all the outbursts). The essential properties of this object are straightforward to summarize: (i) outburst light curves that increase rapidly (within a *MAXI* orbit we change from non-detection to the peak luminosity) and decay steeply, lasting  $< 5$  d in total; (ii) no detected rapid variability or type I X-ray bursts during their bright phase; (iii) have an associated optical brightening from quiescence of  $\geq 3$  mags; and (iv) hard X-ray spectrum (not that of a disc blackbody). With these properties at hand, we can rule out the following classifications for J1957:

(i) HMXB/BeX system: The outbursts of J1957 have already been noted to be non-periodic (Tanaka et al. 2016), and the large range of optical variability (combined with our SALT spectrum) from quiescence rules out the possibility of an early-type donor;

(ii) Superburster: The longest ‘superburst’ is  $\sim 0.3$  d (in ‘t Zand 2011), much less than the 5 d of each J1957 outburst, and there would be enormous theoretical difficulties in producing sufficient nuclear fuel for such a superburst.

#### 3.1 LMXB/XRT: comparison with Galactic Centre Region X-ray Transients

In spite of the extensive *RXTE*/ASM data base of XRT light curves (see e.g. Yan & Yu 2015), there are no BH LMXB/XRTs that display properties comparable to those of J1957. Within that same data base, only the NS system MXB 1730–335 (better known as the ‘Rapid Burster’) has a long-term light curve similar to that of J1957. Indeed, in the latter phases of the *RXTE* mission, MXB 1730–335 underwent six outbursts in barely 2 yr, each of which had a bright phase of usually  $< 10$  d. However, in its bright phase, this object

<sup>3</sup>IRAF is distributed by National Optical Astronomy Observatories, operated by the Association of Universities for Research in Astronomy, Inc., under contract with the National Science Foundation.

Este documento incorpora firma electrónica, y es copia auténtica de un documento electrónico archivado por la ULL según la Ley 39/2015. Su autenticidad puede ser contrastada en la siguiente dirección <a href="https://sede.ull.es/validacion/">https://sede.ull.es/validacion/</a>			
Identificador del documento: 970342		Código de verificación: pkuTTaUi	Fecha: 29/06/2017 10:41:42
Firmado por: DANIEL MATA SÁNCHEZ UNIVERSIDAD DE LA LAGUNA			29/06/2017 11:14:09
JORGE CASARES VELAZQUEZ UNIVERSIDAD DE LA LAGUNA			29/06/2017 12:50:38
TEODORO MUÑOZ DARIAS UNIVERSIDAD DE LA LAGUNA			04/07/2017 18:28:11
ERNESTO PEREDA DE PABLO UNIVERSIDAD DE LA LAGUNA			

emits most of its flux in the form of very rapid, type II X-ray bursts (e.g. Mahasena et al. 2003), which last only for 10 s or so. J1957 exhibits no such variations.

More recently, Degenaar et al. (2015) reported a 9 yr *Swift* X-ray monitoring of the Galactic Centre. During this campaign, various short outbursts ( $\sim 15$  d long) were detected peaking at  $L_X \sim 10^{35}$  erg s $^{-1}$ , both from very faint as well as brighter LMXBs. However, none of these have a recurrence time as short as J1957.

Perhaps the most comprehensive monitoring campaign on Galactic X-ray transients took place in the period 1996–2000 when the *BeppoSAX* Wide Field Cameras (WFC, which had a 40° field of view) observed the Galactic Centre region nine times for a total exposure of  $\sim 4$  Ms. As summarized by int’ Zand (2001), the combination of the *BeppoSAX* WFC observations and the *RXTE/ASM* data base led to the discovery of 31 LMXB XRTs that were active during this time interval. From this study (see their Table 2), there are four XRTs whose duration and peak X-ray flux are comparable to J1957. These are KS 1741–293, SAX J1748.9–2021, SAX J1750.8–2900 and SAX J1810.8–2609, all of whose outbursts lasted less than 10 d. However, subsequent *INTEGRAL* observations of the former (De Cesare et al. 2007) showed more extended periods of activity, and the latter two (Natalucci et al. 1999, 2000) both displayed Type I X-ray bursts with close to Eddington-limited properties. Despite J1957 not exhibiting any of those features, we note that either we could have missed the ignition of a hypothetical burst or maybe its outbursts are too short to trigger it. The remaining system SAX J1748.9–2021 is an AMXP spinning at 442 Hz in an 8.8-hr binary, and while it has recurrence times of order a year, the duration (of 8 d) was so similar in time-scale and light curve to J1957 that we decided to conduct a closer comparison with such objects.

### 3.2 Is J1957 an AMXP?

The most extensive review of AMXPs is that of Patruno & Watts (2012), in which we found N6440 X–2 to be very similar to J1957 both in recurrence time ( $\sim 1$  month, the shortest recurrence time of any known XRT) and duration (3–5 d) of its outbursts (Heinke et al. 2010). The peak luminosities of the AMXPs are typically around 1 per cent  $L_{\text{Edd}}$  ( $\sim 10^{36}$  erg s $^{-1}$  for a  $1.4M_{\odot}$  NS), which would place J1957 at  $d \sim 6$  kpc. Indeed, comparing directly with N6440 X–2 places J1957 at  $d \sim 5$  kpc. Another key similarity here is the light-curve shape of at least two AMXP (SAX J1808.4–3658 and IGR J00291+5934) during their (short, 1–2 weeks) periods of activity (see Fig. 1). They are characterized by an initial slow decay from the peak luminosity that ends with a sharp drop (see Hartman et al. 2008; Hartman, Galloway & Chakrabarty 2011). The knee of the light curve at a critical flux has been interpreted either as centrifugal inhibition of accretion or as the propagation of a cooling wave in the disc (Gilfanov et al. 1998). Assuming that these phenomena take place at the same luminosity level, we infer a distance to J1957 of  $d \sim 5$ –6 kpc (using  $d = 3.5$  kpc for SAX J1808.4–3658 and  $d = 4$  kpc for IGR J00291+5934).

There are three ultracompact AMXPs ( $P_{\text{orb}} < 1.3$  h) known to have exhibited short (below 2 weeks) outbursts: N6440 X–2 (Altamirano et al. 2010), XTE J1751–305 (Grebenev, Molkov & Sunyaev 2005; Patruno & Watts 2012) and Swift J1756.9–2508 (Patruno, Altamirano & Messenger 2010); which favours the association of short outbursts with short orbital period LMXBs. Nevertheless, we note that at least three other AMXPs with longer periods that have exhibited similarly short outbursts: IGR J00291+5934 (Hartman et al. 2011;  $P_{\text{orb}} = 2.5$  h reported by

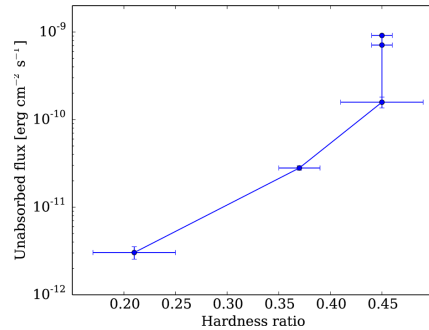


Figure 4. Hardness ratio for the Swift/XRT detections in the last outburst, defined as the ratio between (2–10 keV) and (0.5–2 keV) fluxes. The largest error point corresponds to the observation affected by pile-up (see Section 2).

Markwardt et al. 2004), Swift J1749.4–2807 ( $P_{\text{orb}} = 8.82$  h, see Wijnands et al. 2009 and Altamirano et al. 2011) and SAX J1748.9–2921 ( $P_{\text{orb}} = 8.77$  h, Patruno et al. 2009). On the other hand, there are short period AMXPs like XTE J0929–314 (Remillard, Swank & Strohmayer 2002) and XTE J1807–294 (Markwardt, Juda & Swank 2003) which exhibited outbursts lasting several months. Despite the fact that these examples highlight the inexactness of the correlation between short outbursts and short orbital periods, we propose J1957 as a short period LMXB due to the combination of short duration outbursts, high recurrence time and featureless optical spectrum.

Finally, assuming that the optical emission during active periods is dominated by an X-ray irradiated accretion disc, then we can use the X-ray/optical correlation equation of van Paradijs & McClintock (1994):  $M_V = 1.57 - 2.27 \log \Sigma$ , where  $\Sigma = (L_X/L_{\text{Edd}})^{1/2}/(P_{\text{orb}}[h])^{2/3}$  to derive an  $M_V$  for J1957 of 3.4, assuming a 2-h period. With our brightest  $B$  magnitude (see Section 2), this would imply a distance of about  $\sim 7$ –9 kpc, somewhat closer if the period were shorter.

### 3.3 The X-ray spectrum

Hysteresis patterns between Compton-dominated and thermal-dominated states have been observed in both BH and NS LMXBs (e.g. Belloni, Motta & Muñoz-Darias 2011; Muñoz-Darias et al. 2014). These hysteresis phases, which are not witnessed in J1957, are observed at luminosities larger than  $\sim 2$  per cent  $L_{\text{Edd}}$  (see also Maccarone 2003). On the other hand, a softening phase during the decay towards quiescence is detected at lower luminosities (Plotkin, Gallo & Jonker 2013; Wijnands et al. 2015). In J1957, we do observe a softening in the hardness ratio as the luminosity decreases by, at least, a factor of  $\sim 50$  (see Fig. 4).

Indeed, if the softening of the source begins at  $1.6 \times 10^{-10}$  erg cm $^{-2}$  s $^{-1}$ , given that Wijnands et al. (2015) found this event always below  $3 \times 10^{36}$  erg s $^{-1}$ , which would place J1957 at  $d < 13$  kpc. On the other hand, the non-detection in quiescence of J1957 in the USNO-B catalogue (Monet et al. 2003), whose limiting magnitude in  $V$  is  $\sim 21$ , implies a drop in luminosity of more than three magnitudes in the optical. If the donor is a dwarf star at a distance  $d < 13$  kpc, its absolute magnitude is constrained to  $M_V > 5.4$ . Using Cox (2000) tabulated values, this results in a spectral type later than G7 (K6 if  $d \sim 5$  kpc).

## Multiple outbursts of MAXI J1957+032 569

## 4 CONCLUSIONS

Our X-ray and optical analysis suggests that MAXI J1957+032 is a short period LMXB, given the short duration and frequent recurrence of its outbursts, as well as the featureless optical spectrum. The spectral analysis leads us to place the system at  $d < 13$  kpc, which combined with the non-detection of the quiescence counterpart results in a donor star spectral type later than G8. After comparing with the properties of other known XRTs, we find similarities with those of the AMXP class, which would place J1957 at  $d \sim 5$  kpc. Further multiwavelength observations are encouraged especially taking into account the short recurrence times this system has exhibited in the past  $\sim 1.5$  yr.

## ACKNOWLEDGEMENTS

DMS acknowledges Fundación La Caixa for the financial support received in the form of a PhD contract. PAC is grateful for the support of a Severo Ochoa Visiting Research Fellowship and the hospitality of the Instituto de Astrofísica de Canarias, where the work reported here was undertaken. We also acknowledge support by the Spanish Ministerio de Economía y Competitividad (MINECO) under grant AYA2013-42627. TMD acknowledges support via a Ramón y Cajal Fellowship (RYC-2015-18148). DAHB acknowledges support by the National Research Foundation and also thanks M. Kotze for supporting the SALT observations. MOLLY software developed by T. R. Marsh is gratefully acknowledged. This research has made use of *MAXI* data provided by RIKEN, JAXA and the *MAXI* team. We also acknowledge the use of public data from the *Swift* data archive. Some of the observations reported in this paper were obtained with the Southern African Large Telescope (SALT).

## REFERENCES

- Altamirano D. et al., 2010, ApJ, 712, L58  
 Altamirano D. et al., 2011, ApJ, 727, L18  
 Armas Padilla M., Degenaar N., Russell D. M., Wijnands R., 2013, MNRAS, 428, 3083  
 Arnaud K., 1996, in Jacoby G., Barnes J., eds, ASP Conf. Ser. Vol. 101, Astronomical Data Analysis Software and Systems V. Astron. Soc. Pac., San Francisco, p. 17  
 Baglio M. C., D'Avanzo P., Campana S., Goldoni P., Masetti N., Muñoz-Darias T., Patiño-Alvarez V., Chavushyan V., 2016, A&A, 587, A102  
 Belloni T. M., Motta S. E., Muñoz-Darias T., 2011, Bull. Astron. Soc. India, 39, 409  
 Buckley D. A. H., Swart G. P., Meiring J. G., 2006, in Stepp L. M., ed, Proc. SPIE Conf. Ser. Ground-based and Airborne Telescopes. SPIE, Bellingham, p. 62670Z  
 Buckley D. A. H., Kotze M. M., Charles P. A., Sanchez D. M., Muñoz-Darias T., Israel G., Masetti E. J. M. N., Jonker P., 2016, Astron. Telegram, 9649  
 Burrows D. N. et al., 2005, Space Sci. Rev., 120, 165  
 Chakrabarty D., Jonker P. G., Markwardt C. B., 2016, Astron. Telegram, 9591  
 Charles P. A., Coe M. J., 2006, in Lewin W. H. G., van der Klis M., eds, Compact Stellar X-Ray Sources. Cambridge Univ. Press, Cambridge, p. 215  
 Cherepashchuk A. M., Molkov S. V., Lutovinov A. A., Postnov K. A., 2015, Astron. Telegram, 7506  
 Cornelisse R., 2013, in Pugliese G., de Koter A., Wijburg M., eds, ASP Conf. Ser. Vol. 470, 370 Years of Astronomy in Utrecht. Astron. Soc. Pac., San Francisco, p. 263  
 Cox A. N., 2000, Allen's Astrophysical Quantities. AIP Press, New York  
 Crawford S. M. et al., 2010, Proc. SPIE Conf. Ser. Vol. 7737, Observatory Operations: Strategies, Processes, and Systems III. SPIE, Bellingham, p. 773725  
 Del Cesare G., Bazzano A., Martínez Núñez S., Stratta G., Tarana A., Del Santo M., Ubertini P., 2007, MNRAS, 380, 615  
 Degenaar N., Wijnands R., Miller J. M., Reynolds M. T., Kennea J., Gehrels N., 2015, J. High Energy Astrophys., 7, 137  
 Gehrels N. et al., 2004, ApJ, 611, 1005  
 Gilfanov M., Revnivtsev M., Sunyaev R., Churazov E., 1998, A&A, 338, L83  
 Grebenev S. A., Molkov S. V., Sunyaev R. A., 2005, Astron. Telegram, 446  
 Guver T. et al., 2015, Astron. Telegram, 8149  
 Hartman J. M. et al., 2008, ApJ, 675, 1468  
 Heinke C. O. et al., 2010, ApJ, 714, 894  
 't Zand J., 2011, preprint (arXiv:1102.3345)  
 't Zand J., 2001, in Giménez A., Reglero V., Winkler C., eds, ESA SP-459: Exploring the Gamma-Ray Universe. ESA, Noordwijk, p. 463  
 Krimm H. A. et al., 2013, ApJS, 209, 14  
 Kuulkers E. et al., 2007, A&A, 466, 595  
 Liu Q. Z., van Paradijs J., van den Heuvel E. P. J., 2007, A&A, 469, 807  
 Maccarone T. J., 2003, A&A, 409, 697  
 Mahasen P., Inoue H., Asai K., Dotani T., 2003, Publ. Astron. Soc. Japan, 55, 827  
 Marchesini E. J., Israel G. L., Masetti N., Rodriguez G., 2015, Astron. Telegram, 8197  
 Markwardt C. B., Juda M., Swank J. H., 2003, IAU Circ., 8095  
 Markwardt C. B., Galloway D. K., Chakrabarty D., Morgan E. H., Strohmayer T. E., 2004, Astron. Telegram, 360  
 Mata Sánchez D., Muñoz-Darias T., Casares J., Corral-Santana J. M., Shahbaz T., 2015, MNRAS, 454, 2199  
 Matsuo Ma. et al., 2009, PASJ, 61, 999  
 Monet D. G. et al., 2003, AJ, 125, 984  
 Muñoz-Darias T., Fender R. P., Motta S. E., Belloni T. M., 2014, MNRAS, 443, 3270  
 Natalucci L., Cornelisse R., Bazzano A., Cocchi M., Ubertini P., Heise J., 't Zand J. M., Smith M. J. S., 2000, ApJ, 536, 891  
 Negoro H. et al., 2015, Astron. Telegram, 7504  
 Negoro H. et al., 2016, Astron. Telegram, 9565  
 Nelemans G., Jonker P. G., 2010, New Astron. Rev., 54, 87  
 O'Donoghue D. et al., 2006, MNRAS, 372, 151  
 Patruno A., Watts A. L., 2012, preprint (arXiv:1206.2727)  
 Patruno A., Altamirano D., Hessels J. W. T., Casella P., Wijnands R., van der Klis M., 2009, ApJ, 690, 1856  
 Patruno A., Altamirano D., Messenger C., 2010, MNRAS, 403, 1426  
 Plotkin R. M., Galle E., Jonker P. G., 2013, ApJ, 773, 59  
 Rau A., Yates R., Greiner J., 2015, Astron. Telegram, 7524  
 Reig P., 2011, Ap&SS, 332, 1  
 Remillard R. A., McClintock J. E., 2006, ARA&A, 44, 49  
 Remillard R. A., Swank J., Strohmayer T., 2002, IAU Circ., 7893  
 Shaw A. W. et al., 2013, MNRAS, 433, 740  
 Sugimoto Y. et al., 2015, Astron. Telegram, 8143  
 Tanaka K. et al., 2016, Astron. Telegram, 8529  
 van Dokkum P. G., 2001, PASP, 113, 1420  
 van Paradijs J., McClintock J. E., 1994, A&A, 290, 133  
 Vaughan B. A. et al., 1994, ApJ, 435, 362  
 Verner D., Ferland G., Korista K., Yakovlev D., 1996, ApJ, 465, 487  
 Watson D., 2011, A&A, 533, A16  
 Wijnands R., Wang Q. D., 2002, ApJ, 568, L93  
 Wijnands R., Rol E., Cackett E., Starling R. L. C., Remillard R. A., 2009, MNRAS, 393, 126  
 Wijnands R., Degenaar N., Armas Padilla M., Altamirano D., Cavecchi Y., Linares M., Bahramian A., Heinke C. O., 2015, MNRAS, 454, 1371  
 Willingale R., Starling R. L. C., Beardmore A. P., Tanvir N. R., O'Brien P. T., 2013, MNRAS, 431, 394  
 Wilms J., Allen A., McCray R., 2000, ApJ, 542, 914  
 Yan Z., Yu W., 2015, ApJ, 805, 87

This paper has been typeset from a Te<sub>X</sub>/L<sub>A</sub>T<sub>E</sub>X file prepared by the author.

MNRAS 468, 564–569 (2017)

Este documento incorpora firma electrónica, y es copia auténtica de un documento electrónico archivado por la ULL según la Ley 39/2015.  
*Su autenticidad puede ser contrastada en la siguiente dirección https://sede.ull.es/validacion/*

Identificador del documento: 970342

Código de verificación: pkuTTaUi

Fecha: 29/06/2017 10:41:42

Firmado por: DANIEL MATA SÁNCHEZ  
 UNIVERSIDAD DE LA LAGUNA

29/06/2017 11:14:09

JORGE CASARES VELAZQUEZ  
 UNIVERSIDAD DE LA LAGUNA

29/06/2017 12:50:38

TEODORO MUÑOZ DARIAS  
 UNIVERSIDAD DE LA LAGUNA

04/07/2017 18:28:11

ERNESTO PEREDA DE PABLO  
 UNIVERSIDAD DE LA LAGUNA

Este documento incorpora firma electrónica, y es copia auténtica de un documento electrónico archivado por la ULL según la Ley 39/2015.  
*Su autenticidad puede ser contrastada en la siguiente dirección <https://sede.ull.es/validacion/>*

Identificador del documento: 970342

Código de verificación: pkuTTaUi

Firmado por: DANIEL MATA SÁNCHEZ UNIVERSIDAD DE LA LAGUNA	Fecha: 29/06/2017 10:41:42
JORGE CASARES VELAZQUEZ UNIVERSIDAD DE LA LAGUNA	29/06/2017 11:14:09
TEODORO MUÑOZ DARIAS UNIVERSIDAD DE LA LAGUNA	29/06/2017 12:50:38
ERNESTO PEREDA DE PABLO UNIVERSIDAD DE LA LAGUNA	04/07/2017 18:28:11

# 3

## The quiescence of the black hole transient Swift J1357.2-0933

THE decay to quiescence of an LMXB opens a new set of possible techniques to determine its fundamental parameters (see Sec. 1.4). Swift J1357.2-0933 is an X-ray transient detected in 2011 (Krimm et al. 2011), which shows very remarkable properties. On the basis of spectroscopic evidence, Corral-Santana et al. (2013) proposed that this system may contain a black hole. If that is the case, the  $P_{\text{orb}}$  measured during the outburst would be the second shortest in a black-hole LMXB. Its high Galactic latitude also makes it a candidate member of the black-hole transient population discovered outside the Galactic plane. Finally, the detection of optical dips advocates for a high orbital inclination ( $> 80^\circ$ ), being the first black hole of this class.

When Swift J1357.2-0933 settled into quiescence after its discovery outburst, we performed a spectroscopic campaign with the Gran Telescopio Canarias aimed at detecting the donor star spectral features and characterise its fundamental parameters.

The work presented in this chapter was published under the title “**Swift J1357.2-0933: a massive black hole in the Galactic thick disc**” in Monthly Notices of the Royal Astronomical Society, Volume 454, pages 2199-2204, in 2015 (Mata Sánchez et al. 2015b).



## Swift J1357.2–0933: a massive black hole in the Galactic thick disc

D. Mata Sánchez,<sup>1,2\*</sup> T. Muñoz-Darias,<sup>1,2</sup> J. Casares,<sup>1,2</sup> J. M. Corral-Santana<sup>3</sup>  
and T. Shahbaz<sup>1,2</sup>

<sup>1</sup>Instituto de Astrofísica de Canarias, E-38205 La Laguna, Tenerife, Spain

<sup>2</sup>Departamento de astrofísica, Univ. de La Laguna, E-38206 La Laguna, Tenerife, Spain

<sup>3</sup>Instituto de Astrofísica, Pontificia Universidad Católica de Chile, 7820436 Casilla 306, Santiago 22, Chile

Accepted 2015 September 8. Received 2015 September 7; in original form 2015 August 3

### ABSTRACT

Swift J1357.2–0933 is one of the shortest orbital period black hole X-ray transients. It exhibited deep optical dips together with an extremely broad H $\alpha$  line during outburst. We present 10.4-m Gran Telescopio Canarias (GTC) time-resolved spectroscopy during quiescence searching for donor star absorption features. The large contribution of the accretion flow to the total luminosity prevents the direct detection of the companion. Nevertheless, we constrain the non-stellar contribution to be larger than  $\sim$ 80 per cent of the total optical light, which sets new lower limits to the distance ( $d > 2.29$  kpc) and the height over the Galactic plane ( $z > 1.75$  kpc). This places the system in the Galactic thick disc. We measure a modulation in the centroid of the H $\alpha$  line with a period of  $P = 0.11 \pm 0.04$  d which, combined with the recently presented full width at half-maximum– $K_2$  correlation, results in a massive black hole ( $M_1 > 9.3 M_\odot$ ) and an  $\sim$ M2V companion star ( $M_2 \sim 0.4 M_\odot$ ). We also present further evidence supporting a very high orbital inclination ( $i \gtrsim 80^\circ$ ).

**Key words:** accretion, accretion discs – stars: black holes – X-rays: binaries.

### 1 INTRODUCTION

Galactic X-ray binaries offer the best opportunity to detect stellar mass black holes (BHs) through the accretion luminosity produced by material from the companion star falling into its gravitational well. The vast majority of BHs are detected in transient low-mass X-ray binaries (LMXBs), which spend most part of their lives in a faint, quiescent state (about  $10^{30–34}$  erg s $^{-1}$ ; see e.g. Armas Padilla et al. 2014b). They are discovered during occasional outburst, where their X-ray luminosity increases above  $\sim$ 10 per cent of the Eddington limit. There are only 17 dynamically confirmed black hole X-ray transients (BHTs), as well as  $\sim$ 33 candidates (see Casares & Jonker 2014; Corral-Santana et al. 2015).

Swift J1357.2–0933 (hereafter J1357) is an LMXB X-ray transient with Galactic coordinates  $l = 328.702$  and  $b = +50.004$  (Krimm et al. 2011), whose peak X-ray luminosity place it in the very faint regime (see Armas Padilla et al. 2013 for an X-ray analysis during outburst). The detection of optical dips both in outburst (Corral-Santana et al. 2013, hereafter CS13) and quiescence (Shahbaz et al. 2013) suggests J1357 is a very high inclination system. The orbital period is among the shortest of its class ( $P = 2.8$  h, CS13) and the mass function is constrained to be  $f(M_1) > 3.0 M_\odot$ , where the radial velocity of the donor ( $K_2$ ) was estimated from the double-peak separation of the H $\alpha$  profile (Orosz et al. 1994; Orosz & Bailyn 1995). This strongly advocates for the presence

of a BH. Rau, Greiner & Filgas (2011) proposed a tentative distance to the system of  $d \sim 1.5$  kpc considering the donor star to be the dominant source of quiescent light in the optical and near-infrared regime. However, the quiescent spectral energy distribution (SED) is best described by a single power-law model, which suggests little, if any, thermal contribution from the secondary star (Shahbaz et al. 2013). This implies that only lower limits to the distance can be obtained unless the donor star contribution is properly characterized.

### 2 OBSERVATIONS

J1357 was observed with the Optical System for Imaging and low-Intermediate-Resolution Integrated Spectroscopy (OSIRIS) located in the Nasmyth-B focus of the 10.4-m Gran Telescopio Canarias (GTC), in La Palma (Spain). We used the R500R optical grism combined with a 1.0 arcsec slit ( $R = 352, 4.88 \text{ \AA pixel}^{-1}$ ), covering the spectral range 4800–10 000  $\text{\AA}$ . Observations were obtained in four different nights within 2014 April to June.

11 consecutive spectra per night were acquired at airmasses in the range  $\sim$ 1.3–1.7, with individual exposure times of 875 s ( $\sim$ 3 h per night) sampling the proposed 2.8 h orbital period. We used IRAF<sup>1</sup> standard routines for bias and flat-field corrections. The slit

<sup>1</sup> IRAF is distributed by National Optical Astronomy Observatories, operated by the Association of Universities for Research in Astronomy, Inc., under contract with the National Science Foundation.

\* E-mail: dmata@iac.es

© 2015 The Authors

Published by Oxford University Press on behalf of the Royal Astronomical Society

Este documento incorpora firma electrónica, y es copia auténtica de un documento electrónico archivado por la ULL según la Ley 39/2015.  
Su autenticidad puede ser contrastada en la siguiente dirección <https://sede.ull.es/validacion/>

Identificador del documento: 970342

Código de verificación: pkuTTaUi

Fecha: 29/06/2017 10:41:42

Firmado por: DANIEL MATA SÁNCHEZ  
UNIVERSIDAD DE LA LAGUNA

29/06/2017 11:14:09

JORGE CASARES VELAZQUEZ  
UNIVERSIDAD DE LA LAGUNA

29/06/2017 12:50:38

TEODORO MUÑOZ DARIAS  
UNIVERSIDAD DE LA LAGUNA

04/07/2017 18:28:11

ERNESTO PEREDA DE PABLO  
UNIVERSIDAD DE LA LAGUNA

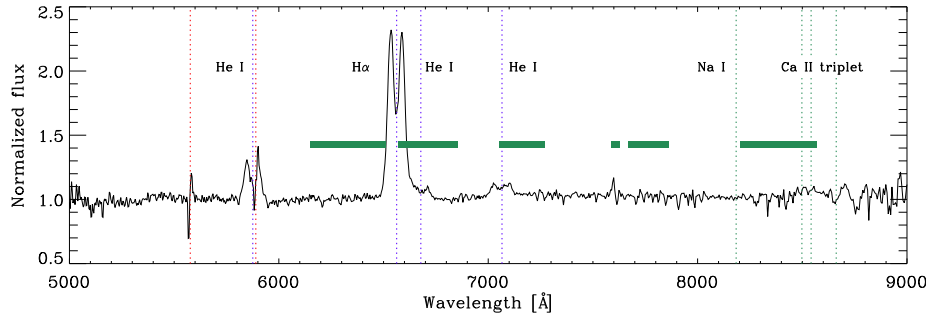


**Figure 1.** Averaged spectrum of J1357. Accretion disc emission features ( $H\alpha$  and He I) are marked with blue, dotted vertical lines. Regions contaminated by sky subtraction residuals are plotted as red, dotted vertical lines. The expected M-type donor star absorption features are shown as green bands (TiO molecular bands) and green, dotted vertical lines (Na I and Ca II triplet).

was rotated to PA =  $-53^\circ 16'$  in order to allow for simultaneous observations of the object and a nearby early-type dwarf star located at 2.06 arcmin NE of the target. The wavelength calibration was obtained from observations of calibration arcs and instrumental flexure was calculated from the drift of the [O I] 5577 Å sky line and subsequently corrected in every individual spectrum.

The spectrum of the calibration star is classified as an F8V after comparison with templates from the *MILES* spectral library (Sánchez-Blázquez et al. 2006, Falcón-Barroso et al. 2011) using  $\chi^2$  minimization routines within *MOLLY* (e.g. Casares et al. 1996). In order to maximize the chances of detecting donor star absorption features in J1357, we produced a set of telluric spectra by removing the F8V spectral lines, which were subsequently subtracted from the target to produce spectra free of telluric features (e.g. Beekman et al. 2000).

The above strategy yielded four sets of 11 spectra. Points deviating more than  $3\sigma$  above or below the continuum, probably caused by bad pixels or residuals from the sky subtraction, were interpolated. One spectrum was discarded on each of the two first nights due to very poor signal-to-noise ratio (S/N) caused by the presence of clouds. Absorption features from the donor star are not evident in any of the spectra, nor in the combined spectrum (see Fig. 1).

### 3 RESULTS

Using the 42 GTC spectra, we have determined the veiling factor, the orbital period and the main properties of the  $H\alpha$  line in quiescence.

#### 3.1 Search for companion star features: skew-mapping

The skew-mapping technique has been applied in cataclysmic variables to detect weak companion star features (e.g. Vande Putte et al. 2003, Smith et al. 2005). Our analysis compares a template M3V star spectrum with different Doppler-corrected averaged spectra created from our data base. Each averaged spectrum is produced by considering a specific zero phase in the range 0–1 (we inspect all values with a 0.05 step) and velocity of the companion star between  $K_2 = 0$ – $2000 \text{ km s}^{-1}$ , in  $100 \text{ km s}^{-1}$  steps. Individual spectra are shifted and co-added assuming the orbital period of CS13. The cross-correlation with the M3 template star is expected to reveal a significant peak above noise at the correct parameters for the companion star motion. This technique did not reveal any preferred

value in the  $K_2 - \text{zero phase}$  parameter space, not even after considering several different periods around the one proposed in CS13 ( $0.09$ – $0.15 \text{ d}^{-1}$ , steps of  $0.001 \text{ d}^{-1}$ ). Therefore, we conclude that no companion star features are present in our spectra.

#### 3.2 Veiling factor

Magnitudes in the OSIRIS  $r'$  filter were obtained from the acquisition images of each night:  $r'_1 = 21.71 \pm 0.08$ ;  $r'_2 = 21.45 \pm 0.06$ ;  $r'_3 = 20.84 \pm 0.08$ ;  $r'_4 = 21.00 \pm 0.11$ . The first two values (April 29th and 30th) are similar to those reported in Shahbaz et al. (2013,  $r' = 21.54 \pm 0.35$ ). On the other hand, the latest two nights (June 2nd and 28th) reveal a somehow brighter system (but still in quiescence). We note that although this might be caused by known strong short-term variability displayed by the system (Shahbaz et al. 2013), the spectra of the first two nights are clearly noisier under similar sky conditions, reflecting a true drop in brightness.

The absence of companion star features imposes a minimum constraint to the veiling factor ( $X$ ), defined as the fractional contribution of the accretion related luminosity ( $L'_{\text{acc}}$ ) to the total flux ( $L'_{\text{acc}} + L'_2$ , where  $L'_2$  is the donor star luminosity) in the OSIRIS  $r'$  filter wavelength range (5500–7400 Å). On the other hand, by considering the relation between the orbital period and the mean density presented in Faulkner, Flannery & Warner (1972), and tabulated values for main-sequence stars (Cox 2000), the spectral type of the companion star is constrained to be M2V or later. We compared our spectrum with templates of main-sequence stars from the *MILES* Spectral Library. For each spectral type, we measured the normalized flux of the deepest photospheric absorption line present in the template spectrum. The veiling necessary to make these features shallower than the noise level ( $3\sigma$ ) within the corresponding spectral region of the J1357 spectrum is a lower limit to the veiling factor (see Mata Sánchez et al. 2015 for a similar analysis of NIR spectra).

In particular, we find that the required veiling factor for an M2V star to be swamped by the accretion flux is  $X > 0.81$ . This limit is also valid if the donor is evolved and its spectral type is later than M2V (we have explored spectral types as late as M6V). This result is obtained using the averaged quiescent spectrum of the first two nights where the system is fainter, and therefore, a higher contribution of the companion star is expected.

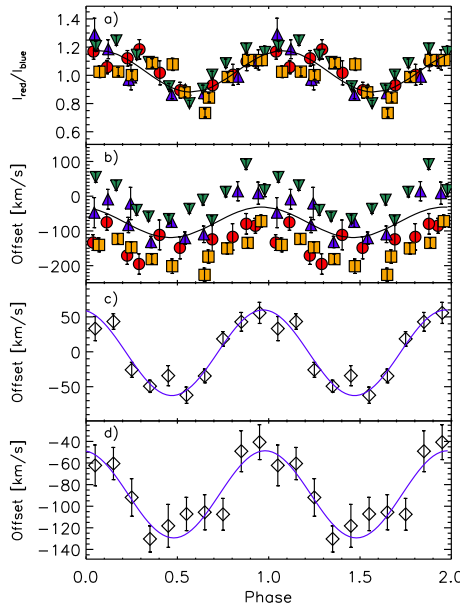


**Figure 2.** Orbital evolution of several  $H\alpha$  parameters obtained from our two-Gaussian model fit (three top panels) and from a diagnostic diagram (bottom panel) folded with the best-fitting period obtained from periodogram analysis. Panel (a) intensity ratio between red and blue peak. Best fit is represented as a black, solid line. Panel (b) radial velocities of the non-detrended centroid as measured by the two-Gaussian model. In both panels, each night is represented by different symbols and colours as follows: red circles (April 29th), blue triangles (April 30th), green upside-down triangles (June 2nd) and orange squares (June 28th). The best sinusoidal fit to the non-detrended data is also shown. Panel (c) radial velocities of the line centroid obtained from 10 phase bin averaged spectra after de-trending. The best sinusoidal fit is shown as a blue, solid line. Panel (d) same as previous panel but using radial velocity curves from the diagnostic diagram (Gaussian separation of  $a = 4500 \text{ km s}^{-1}$ ). Data are plotted over two phase cycles for clarity.

We have explored spectral types as late as M6V, obtaining similar results than for M2V. We note that using slightly different tabulated values for dwarf star mean densities (e.g. Carroll & Ostlie 2006), does not affect our results.

### 3.3 Orbital period from a two-Gaussian model fit

We fit the  $H\alpha$  double-peaked emission profile with a model consisting of two Gaussians with equal FWHM. The height of the Gaussians and offset with respect to the  $H\alpha$  rest wavelength ( $6562.78 \text{ \AA}$ ) are left as free parameters.

#### $H\alpha$ centroid velocity

The mean of the Gaussians offsets is expected to trace the motion of the accretion disc around the centre of mass of the system. We note that the mean offset value for each night was significantly

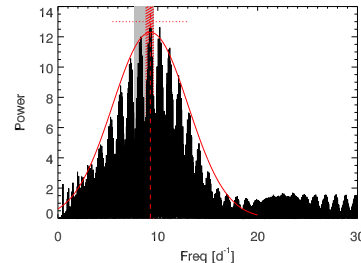


**Figure 3.** Periodogram obtained with the Lomb-Scargle method. Red, solid line shows a Gaussian fit to the highest group of peaks. The red, dotted horizontal line represents the  $1\sigma$  uncertainty ( $P = 0.11 \pm 0.04 \text{ d}$ ). We inspected frequencies up to  $60 \text{ d}^{-1}$ , but the power spectrum for frequencies over  $30 \text{ d}^{-1}$  is nearly flat. The red, dashed vertical line refers to the strongest peak consistent with the outburst period proposed by CS13. Grey band depicts the constraint to the period ( $P = 0.117 \pm 0.013 \text{ d}$ ) from outburst data (CS13). The red, striped band refers to the standard deviation obtained from a Gaussian fit to the family of peaks inside the grey band ( $P = 0.109 \pm 0.005 \text{ d}$ ).

different (see Fig. 2b). This behaviour has been reported in other BHTs, for example in XTE J1118+480 it is explained as a result of disc precession (Torres et al. 2002). Recently, Torres et al. (2015) detected variations in the systemic velocity of J1357. They did not consider this result to support the precessing disc scenario, but interpreted as systematic effects. However, our longer data base suggests that instead this is a consequence of a physical process taking place in the system. In order to fit the whole sample, we then decided to de-trend the mean nightly offsets.

We performed a Lomb-Scargle normalized periodogram of the (de-trended) mean offset variations and the result is presented in Fig. 3. We used the *period* time series analysis package (Dhillon, Privet & Duffey 2001). A Gaussian fit to the broad peak with the highest power yields a period of  $P = 0.11 \pm 0.04 \text{ d}$  ( $1\sigma$ ). This is consistent with the one measured by CS13 using a longer data base with higher S/N during outburst ( $P = 0.117 \pm 0.013 \text{ d}$ ). We find two families of peaks consistent with the outburst period. Gaussian fits result in  $P = 0.109 \pm 0.005 \text{ d}$  and  $P = 0.121 \pm 0.006 \text{ d}$ , respectively. The former is favoured by its highest amplitude (depicted as a red, striped band in Fig. 3). Nevertheless, further observations are necessary to confirm this result. We note that comparable results are obtained by performing sinusoidal fits and minimize chi-square.

The data were folded on the previously obtained period and are shown in Fig. 2b, where different colours and symbols are used to mark different systemic velocities observed on each night. We subsequently performed a non-linear least squares fit to the data using the following sinusoidal function:

$$V = \gamma + K_1 \sin(2\pi(\phi - \phi_0)).$$

We obtained  $K_1 = 44 \pm 3 \text{ km s}^{-1}$ ,  $\gamma = 75 \pm 2 \text{ km s}^{-1}$  and  $\phi_0 = 0.71 \pm 0.01$ . Even if it might be qualitatively acceptable, the high reduced chi-square value ( $\chi^2_r = 17.26$ ) shows that the non-de-trended data does not properly fit to a sinusoid, and de-trending is necessary for an optimal analysis. Subsequently, the original spectra were combined into 10 phase bins after removing each night's mean value. The fit results in  $\phi_0 = 0.720 \pm 0.009$  and  $K_1 = 61 \pm 4 \text{ km s}^{-1}$  for  $\chi^2_r = 1.30$  (see Fig. 2c).

*Intensity ratio and double peak separation*

The intensity ratio of the peaks of the H $\alpha$  profile (defined as  $I_{\text{red}}/I_{\text{blue}}$ ) exhibits a periodicity similar to that observed in the centroid offsets. Folding these data on to the previously obtained period and fitting a sinusoidal result in  $\chi^2_r = 5.12$  (see Fig. 2a). Torres et al. (2015) reported asymmetric H $\alpha$  profiles, but no recurrent variability was observed. The detection of this periodic evolution of the profile along four different nights suggest a scenario with an asymmetric outer disc structure, perhaps a hotspot on a tidal arm. This would also explain the deviation observed from a perfect fit, since other processes affecting the intensity ratio might be at play.

The double-peak separation does not show significant variability, and it is consistent with a constant value. The weighted average of the double-peak separation is  $D_p = 2430 \pm 50 \text{ km s}^{-1}$ , significantly larger than the one measured in outburst by CS13 ( $D_p = 1790 \pm 67 \text{ km s}^{-1}$ ). This implies that the outer disc velocity ( $v_d = 1215 \pm 25 \text{ km s}^{-1}$ ) is higher in quiescence, which is an expected behaviour since the disc expands during outburst, reaching areas with lower velocities. The reported value is consistent within  $2\sigma$  with that reported by Torres et al. (2015,  $D_p = 2340 \pm 20 \text{ km s}^{-1}$ ).

**3.4 The diagnostic diagram**

The broad wings of the H $\alpha$  profile are supposed to trace the motion of the compact object. We apply the diagnostic diagram (aka double Gaussian technique Shafter, Szkody & Thorstensen 1986), aiming at constraining radial velocity variations of the H $\alpha$  wings. We inspected several Gaussian separations ( $a = 2500\text{--}5000 \text{ km s}^{-1}$ ) to perform a diagnostic diagram analogous to that presented in CS13. Unfortunately, our limited data base and the lower S/N ratio prevents us from obtaining conclusive determinations for the  $K_1$  and  $\gamma$  values. A wide plateau on the evolution of the fitted parameters from  $a = 4000 \text{ km s}^{-1}$ , combined with the inspection of the individual radial velocity curves, suggests  $a = 4500 \text{ km s}^{-1}$  as the preferred value (see the folded, radial velocity curve for this separation in Fig. 2d).

Mean values of the compact object orbital velocity ( $K_1 = 40 \pm 12 \text{ km s}^{-1}$ ) and systematic velocity of the system ( $\gamma = -79 \pm 13 \text{ km s}^{-1}$ ) are obtained from sinusoidal fits to radial velocity curves in the range  $a = 4000\text{--}5000 \text{ km s}^{-1}$  (uncertainties refer to standard deviations). This result is consistent with previous determinations of the systemic velocity in quiescence ( $\gamma = -130 \pm 50 \text{ km s}^{-1}$ ; Torres et al. 2015) and the compact object's velocity reported in outburst ( $K_1 = 43 \pm 2 \text{ km s}^{-1}$ ; CS13). However, the systemic velocity value obtained from the outburst periodogram ( $\gamma \sim -150 \text{ km s}^{-1}$ ; CS13) does not seem to be in agreement with our results.

We note that, in contrast to the two-Gaussian profile modelling (see Section 3.3), nightly de-trending is not necessary for the radial velocity curves obtained with the double Gaussian technique. This can be explained by considering that the two-Gaussian modelling traces the core of the H $\alpha$  double peak profile, and therefore, outer parts of the disc where disc precession effects might be important. However, the diagnostic diagram is sensitive to the emission line wings, which traces inner parts of the disc less affected by companion star tidal forces.

**3.5 H-alpha full width at half-maximum**

We have measured the full width at half-maximum (FWHM) of the H $\alpha$  emission profile in each individual spectrum. After subtracting quadratically the instrumental resolution, the average value

is FWHM =  $4152 \pm 209 \text{ km s}^{-1}$ , where the uncertainty reflects the standard deviation of the 42 measures. This value is larger than the one measured in outburst (FWHM  $\sim 3300 \text{ km s}^{-1}$ , CS13) and consistent with the quiescence value reported in Torres et al. (2015) and Casares (2015), i.e. FWHM =  $4025 \pm 110 \text{ km s}^{-1}$  and FWHM =  $4085 \pm 328 \text{ km s}^{-1}$ , respectively. The previously reported broadest FWHM corresponds to XTE J1118+480 (FWHM  $\sim 2500 \text{ km s}^{-1}$ ; Torres et al. 2004).

**4 DISCUSSION**

Observations taken during the outburst decay have sometimes resulted in wrong orbital period determinations (e.g. V404 Cygni; Casares, Charles & Naylor 1992). However, in our case, the orbital period measured from quiescent spectra is fully consistent with the outburst results, supporting CS13 conclusions. Casares (2015) has recently presented a correlation between the FWHM of H $\alpha$  and the orbital velocity of the companion star  $K_2 \simeq 0.233(13)$  FWHM. For the case of J1357 this results in a donor star velocity of  $K_2 = 967 \pm 49 \text{ km s}^{-1}$ . Note that this value is consistent with the independent empirical relation derived for quiescent BHT between the outer disc velocity ( $v_d$ ) and  $K_2$  (Orosz et al. 1994; Orosz & Bailyn 1995), which results in  $K_2 > 806 \text{ km s}^{-1}$  (see also Torres et al. 2015). This, combined with CS13 orbital period (fully consistent with our results) yields  $f(M_1) = 11.0 \pm 2.1 \text{ M}_\odot$  (i.e.  $M_{\text{BH}} > 8.3 \text{ M}_\odot$  at 90 per cent confidence). If we include the BH orbital velocity estimated in CS13 ( $K_1 = 43 \pm 2 \text{ km s}^{-1}$ ), the obtained mass ratio ( $q = M_2/M_1 \sim 0.04$ ) provides more restrictive limits to both  $M_{\text{BH}}$  and  $M_2$ . We find  $M_{\text{BH}} \geq 9.3 \text{ M}_\odot$  and  $M_2 \geq 0.4 \text{ M}_\odot$ . Here, we use the limit value for the orbital inclination  $i = 90^\circ$ . This conservative result places the system as the most massive LMXB BH together with GRS 1915+105 ( $10.1 \pm 0.6 \text{ M}_\odot$ ; Steeghs et al. 2013). Only Cyg X-1, a high-mass X-ray binary, exceeds the BH mass presented here ( $\sim 15 \text{ M}_\odot$ ; Orosz et al. 2011). The donor star mass is consistent with the constraint on the spectral type (later than M2V; see Section 3.2), which requires  $M_2 \lesssim 0.4 \text{ M}_\odot$ .

**4.1 Distance and height over the Galactic plane**

The constraint on the veiling factor, combined with the spectral type (mass) of the donor star, imposes a more restrictive lower limit on the distance to the system. Photometric values were obtained from acquisition images (one per night) in the  $r'$ -band. We use the relation between  $r'$ ,  $B$  and  $V$  magnitudes described in Fukugita et al. (1996), combined with  $M_V$  and  $B - V$  tabulated values of main-sequence stars (Cox 2000) to obtain absolute magnitudes,  $M_{r'}$ . If we consider the latest spectral type for the donor star proposed by CS13 ( $M_{r'} = 11.61$ ), we obtain a conservative lower limit to the distance of the system. This assumes a somewhat evolved donor from the Smith & Dhillon (1998) empirical relation, instead of a main-sequence star. We measure  $r' = 21.6 \pm 0.2$  from the two nights when the system is faintest, which combined with  $X > 0.81$  results in a conservative constraint to the distance of  $d > 2.29 \text{ kpc}$ . If we consider the companion star spectral type obtained in the previous section ( $M_{r'} = 9.28$ ), the system is required to be further than  $d > 6.7 \text{ kpc}$ , a value which is close to the upper limit reported in Shahbaz et al. (2013).

The above constraint to the distance sets new lower limits to the X-ray luminosity during both outburst and quiescence. Armas Padilla et al. (2013, 2014b) obtained  $L_{\text{quies}} = 8 \times 10^{39} \text{ erg s}^{-1}$  and  $L_{\text{peak}} = 10^{35} \text{ erg s}^{-1}$  considering a distance of  $d = 1.5 \text{ kpc}$ . Our constraint implies:  $L_{\text{quies}} > 1.9 \times 10^{30} \text{ erg s}^{-1}$  and

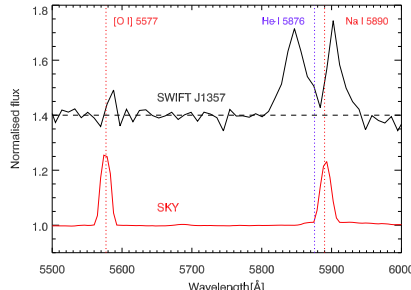


**Figure 4.** Spectra centred on the He I (5876 Å) emission line. Upper spectrum: normalized, averaged J1357 spectrum of the two brightest nights after sky subtraction. Lower spectrum: averaged spectrum of the sky multiplied by a constant factor in order to compare with the upper spectrum.

$L_{\text{peak}} > 2.33 \times 10^{35} \text{ erg s}^{-1}$ . These values are still consistent with J1357 being a very faint X-ray transient and perhaps the faintest stellar mass BH known in quiescence (see Armas Padilla et al. 2014b for a discussion on the topic).

The lower limit to the distance, combined with the high Galactic latitude ( $b = 50.004$ ), places the system at  $z > 1.75$  kpc above the Galactic plane. Other BHT that might be members of the Galactic thick disc population ( $z \gtrsim 1$  kpc; Gilmore & Reid 1983) are: SWIFT J1357.2-0933 (this work and CS13), MAXI J1659-152 (BH candidate; Kuulkers et al. 2013), XTE J1118+480 (Uemura et al. 2000; Gelino et al. 2006), XTE J1859+226 (Corral-Santana et al. 2011), H1705-250 (Remillard et al. 1996; Jonker & Nelemans 2004), GS 1354-64 (Casares et al. 2004, 2009) and SWIFT J1753.5-0127 (BH candidate; Zurita et al. 2008); see Corral-Santana et al. (2015).

#### 4.2 On the orbital inclination

The He I 5876 Å emission line exhibits a particular profile with a sharp, deep absorption core, even reaching 0.95 the continuum value in some spectra. This has to be treated with caution since the Na I 5890 Å sky line is placed close to the core of the double-peaked He I profile, and therefore a deficient sky subtraction could affect the profile. In order to minimize this effect, we combined the data of the two nights where the object was brighter, because this allows for a better correction. The final extracted spectrum (see Fig. 4) still exhibits a sharp core profile, reaching  $\sim 1.05$  times the continuum level. The residual sky subtraction of the nearest and equally intense sky line [O I] 5577 Å is reduced to almost noise level. This result suggests that the deep absorption core is a real feature.

Deep He I line absorption cores have only been previously observed in eclipsing, high inclination ( $i \gtrsim 75^\circ$ ; Schoembs & Hartmann 1983) cataclysmic variables in quiescence e.g. Z Cha, (Marsh, Horne & Shipman 1987), which has  $i = 81^\circ$ . Obscuring material above the plane of the accretion disc has been proposed as the origin of the deep, central absorption observed in He I and Balmer hydrogen lines (see Rayne & Whelan 1981). Therefore, it should not be surprising to find similar behaviour in high inclination BHTs. However, only systems with inclinations up to  $i \sim 70^\circ$  have been discovered and detected in quiescence so far (e.g. XTE J1118+480; Gelino et al. 2006). None of them shows such deep absorption cores. Torres et al. (2015) already noticed depth variations in the core of

H  $\alpha$  profile. We also observe variations in the normalized flux of the H  $\alpha$  core in the range 1.3–2.1 times the continuum value.

It has been suggested by Armas Padilla et al. (2014a) and Torres et al. (2015) that the X-ray properties of the source (e.g. absence of emission/absorption lines) and the low extinction, comparable to that expected from interstellar material in the line of sight, argue against the very high inclination ( $i \gtrsim 80^\circ$ ) scenario proposed by CS13. Given the lack of eclipsing BHs, the closest comparison can be made with high-inclination neutron star systems. These only show absorption lines during thermal soft states (Ponti, Muñoz-Darias & Fender 2014; Ponti et al. 2015). However, it should be noted that J1357 never abandoned the hard state (see Muñoz-Darias et al. 2014 for a direct comparison between neutron star and BH states). On the other hand, the two eclipsing accretion disc corona sources X1822-371 and 2S 0921-63, show extinction values consistent with an interstellar origin (i.e. no intrinsic extinction) when fitted with standard hard state spectral models (Laria et al. 2001; Kallman et al. 2003). This suggests that X-ray photons emitted in the direction of the outer disc rim do not reach the observer, and only those radiated above/below the rim do it, solely interacting with the interstellar material in the line of sight. Therefore, we still consider  $i \geq 80^\circ$  as the most plausible value. The detection of He I line cores and the already large BH mass (for  $i = 90^\circ$ ) presented here further support this conclusion.

#### 5 CONCLUSIONS

We have used 10.4-m GTC optical spectra of Swift J1357 to constrain the accretion related contribution to the optical emission in quiescence. This yields more restrictive lower limits to the distance ( $d > 2.29$  kpc) and height over the Galactic plane ( $z > 1.75$  kpc), placing the system in the Galactic thick disc. We detect variability in the H  $\alpha$  profile modulated with a period  $P = 0.11 \pm 0.04$  d, confirming the period detected in outburst. Using the recently presented FWHM– $K_2$  correlation, new constraints to the fundamental parameters are derived. In particular, we obtain  $M_{\text{BH}} > 9.3 M_\odot$ . We also favour  $q \sim 0.04$  and  $M_2 \sim 0.4 M_\odot$ . This indicates that Swift J1357 harbours one of the most massive BHs known in our Galaxy.

#### ACKNOWLEDGEMENTS

We are thankful to Gabriele Ponti for useful discussion on the X-ray properties of the source. DMS acknowledges Fundación La Caixa for the financial support received in the form of a PhD contract. JMC-S acknowledge financial support to CONICYT through the FONDECYT project no. 3140310. We also acknowledge support by the Spanish Ministerio de Economía y competitividad (MINECO) under grant AYA2013-42627. MOLLY software developed by T. R. Marsh is gratefully acknowledged.

#### REFERENCES

- Armas Padilla M., Degenaar N., Russell D. M., Wijnands R., 2013, MNRAS, 428, 3083
- Armas Padilla M., Wijnands R., Altamirano D., Méndez M., Miller J. M., Degenaar N., 2014a, MNRAS, 439, 3908
- Armas Padilla M., Wijnands R., Degenaar N., Muñoz-Darias T., Casares J., Fender R. P., 2014b, MNRAS, 444, 902
- Beckman G., Somers M., Naylor T., Hellier C., 2000, MNRAS, 318, 9
- Carroll B. W., Ostlie D. A., 2006, An Introduction to Modern Astrophysics and Cosmology, Pearson, San Francisco

MNRAS **454**, 2199–2204 (2015)

Este documento incorpora firma electrónica, y es copia auténtica de un documento electrónico archivado por la ULL según la Ley 39/2015.  
Su autenticidad puede ser contrastada en la siguiente dirección <https://sede.ull.es/validacion/>

Identificador del documento: 970342

Código de verificación: pkuTTaUi

Fecha: 29/06/2017 10:41:42

Firmado por: DANIEL MATA SÁNCHEZ  
UNIVERSIDAD DE LA LAGUNA

29/06/2017 11:14:09

JORGE CASARES VELAZQUEZ  
UNIVERSIDAD DE LA LAGUNA

29/06/2017 12:50:38

TEODORO MUÑOZ DARIAS  
UNIVERSIDAD DE LA LAGUNA

04/07/2017 18:28:11

ERNESTO PEREDA DE PABLO  
UNIVERSIDAD DE LA LAGUNA

- Casares J., 2015, ApJ, 808, 80
- Casares J., Jonker P. G., 2014, Space Sci. Rev., 183, 223
- Casares J., Charles P. A., Naylor T., 1992, Nature, 355, 614
- Casares J., Mouchet M., Martínez-Pais I. G., Harlaftis E. T., 1996, MNRAS, 282, 182
- Casares J., Zurita C., Shahbaz T., Charles P. A., Fender R. P., 2004, ApJ, 613, L133
- Casares J. et al., 2009, ApJS, 181, 238
- Corral-Santana J. M., Casares J., Shahbaz T., Zurita C., Martínez-Pais I. G., Rodríguez-Gil P., 2011, MNRAS, 413, L15
- Corral-Santana J. M., Casares J., Muñoz-Darias T., Rodríguez-Gil P., Shahbaz T., Torres M. A. P., Zurita C., Tyndall A. A., 2013, Science, 339, 1048 (CS13)
- Corral-Santana J. M., Casares J., Muñoz-Darias T., Bauer F. E., Russell D. M., 2015, A&A, submitted
- Cox A. N., 2000, Allen's Astrophysical Quantities. AIP Press, New York
- Dhillon V. S., Privett G. J., Duffey K. P., 2001, Starlink User Note, 167
- Falcón-Barroso J. J., Sánchez-Blázquez P., Vazdekis A., Ricciardelli E., Cardiel N., Cenarro A. J., Gorgas J., Peletier R. F., 2011, A&A, 532, A95
- Faulkner J., Flannery B. P., Warner B., 1972, ApJ, 175, L79
- Fukugita M., Ichikawa T., Gunn J. E., Doi M., Shimasaku K., Schneider D. P., 1996, AJ, 111, 1748
- Gelino D. M., Balman Ş., Kızılıoğlu Ü., Yılmaz A., Kalemci E., Tomsick J. A., 2006, ApJ, 642, 438
- Gilmore G., Reid N., 1983, MNRAS, 202, 1025
- Iaria R., Di Salvo T., Burderi L., Robba N. R., 2001, ApJ, 557, 24
- Jonker P. G., Nelemans G., 2004, MNRAS, 354, 355
- Kallman T. R., Angelini L., Boroson B., Cottam J., 2003, ApJ, 583, 861
- Krimm H. A. et al., 2011, Astron. Telegram, 3138, 1
- Kuulkers E. et al., 2013, A&A, 552, A32
- Marsh T. R., Horne K., Shipman H. L., 1987, MNRAS, 225, 551
- Mata Sánchez D., Muñoz-Darias T., Casares J., Steeghs D., Ramos Almeida C., Acosta Pulido J. A., 2015, MNRAS, 449, L1
- Muñoz-Darias T., Fender R. P., Motta S. E., Belloni T. M., 2014, MNRAS, 443, 3270
- Orosz J. A., Bailyn C. D., 1995, ApJ, 446, L59
- Orosz J. A., Bailyn C. D., Remillard R. A., McClintock J. E., Foltz C. B., 1994, ApJ, 436, 848
- Orosz J. A., McClintock J. E., Aufdenberg J. P., Remillard R. A., Reid M. J., Narayan R., Gou L., 2011, ApJ, 742, 84
- Ponti G., Muñoz-Darias T., Fender R. P., 2014, MNRAS, 444, 1829
- Ponti G. et al., 2015, MNRAS, 446, 1536
- Rau A., Greiner J., Filgas R., 2011, The Astron. Telegram, 3140, 1
- Rayne M. W., Whelan J. A. J., 1981, MNRAS, 196, 73
- Remillard R. A., Orosz J. A., McClintock J. E., Bailyn C. D., 1996, ApJ, 459, 226
- Sánchez-Blázquez P. et al., 2006, MNRAS, 371, 703
- Schoenber R., Hartmann K., 1983, A&A, 128, 37
- Shafter A. W., Szkody P., Thorstensen J. R., 1986, ApJ, 308, 765
- Shahbaz T., Russell D. M., Zurita C., Casares J., Corral-Santana J. M., Dhillon V. S., Marsh T. R., 2013, MNRAS, 434, 2696
- Smith D. A., Dhillon V. S., 1998, MNRAS, 301, 767
- Smith R. C., Mehes O., Vande Putte D., Hawkins N. A., 2005, MNRAS, 360, 364
- Steeghs D., McClintock J. E., Parsons S. G., Reid M. J., Littlefair S., Dhillon V. S., 2013, ApJ, 768, 185
- Torres M. A. P. et al., 2002, ApJ, 569, 423
- Torres M. A. P., Callanan P. J., García M. R., Zhao P., Laycock S., Kong A. H., 2004, ApJ, 612, 1026
- Torres M. A. P., Jonker P. G., Miller-Jones J. C. A., Steeghs D., Repetto S., Wu J., 2015, MNRAS, 450, 4292
- Uemura M. et al., 2000, PASJ, 52, L15
- Vande Putte D., Smith R. C., Hawkins N. A., Martin J. S., 2003, MNRAS, 342, 151
- Zurita C., Durant M., Torres M. A. P., Shahbaz T., Casares J., Steeghs D., 2008, ApJ, 681, 1458

This paper has been typeset from a TeX/LaTeX file prepared by the author.

Este documento incorpora firma electrónica, y es copia auténtica de un documento electrónico archivado por la ULL según la Ley 39/2015.  
*Su autenticidad puede ser contrastada en la siguiente dirección <https://sede.ull.es/validacion/>*

Identificador del documento: 970342

Código de verificación: pkuTTaUi

Firmado por: DANIEL MATA SÁNCHEZ UNIVERSIDAD DE LA LAGUNA	Fecha: 29/06/2017 10:41:42
JORGE CASARES VELAZQUEZ UNIVERSIDAD DE LA LAGUNA	29/06/2017 11:14:09
TEODORO MUÑOZ DARIAS UNIVERSIDAD DE LA LAGUNA	29/06/2017 12:50:38
ERNESTO PEREDA DE PABLO UNIVERSIDAD DE LA LAGUNA	04/07/2017 18:28:11

# 4

## Scorpius X-1: the canonical neutron-star LMXB

**S**CORPIUS X-1 (Sco X-1 hereafter) was the first extrasolar X-ray source discovered (Giacconi et al. 1962). It is also the brightest persistent X-ray source in the sky. Many works have been dedicated to this source, considered to be the canonical persistent LMXB. Indeed, Sco X-1 has even been proposed as a target for the search of persistent high-frequency gravitational waves (e.g. Abadie et al. 2011, Galloway et al. 2014).

Despite this intensive follow-up, several fundamental parameters of Sco X-1 remain unknown. In particular, the persistent emission veils completely the donor star in the optical, preventing dynamical studies. Taking advantage of the intrinsic lower emission of the disc in the NIR band (see 1.2), we performed a spectroscopic campaign in the K-band aimed at detecting the elusive donor star features. We managed to constrain the donor star and NS masses by combining the NIR analysis, Monte Carlo techniques and measurements collected from literature, including Bowen fluorescence studies.

The work presented in this chapter was published under the title “**Mass constraints to Sco X-1 from Bowen fluorescence and deep near-infrared spectroscopy**” in Monthly Notices of the Royal Astronomical Society Letters, Volume 449, pages L1-L5, in 2015 (Mata Sánchez et al. 2015a).



## Mass constraints to Sco X-1 from Bowen fluorescence and deep near-infrared spectroscopy

D. Mata Sánchez,<sup>1,2\*</sup> T. Muñoz-Darias,<sup>1,2,3</sup> J. Casares,<sup>1,2</sup> D. Steeghs,<sup>4</sup>  
C. Ramos Almeida<sup>1,2†</sup> and J. A. Acosta Pulido<sup>1,2</sup>

<sup>1</sup>Instituto de Astrofísica de Canarias, E-38205 La Laguna, Tenerife, Spain

<sup>2</sup>Departamento de astrofísica, Univ. de La Laguna, E-38206 La Laguna, Tenerife, Spain

<sup>3</sup>Department of Physics, Astrophysics, University of Oxford, Keble Road, Oxford OX1 3RH, UK

<sup>4</sup>Department of Physics, University of Warwick, Coventry CV4 7AL, UK

Accepted 2015 January 2. Received 2014 December 12

### ABSTRACT

More than 50 years after the dawn of X-ray astronomy, the dynamical parameters of the prototypical X-ray binary Sco X-1 are still unknown. We combine a Monte Carlo analysis, which includes all the previously known orbital parameters of the system, along with the  $K$ -correction to set dynamical constraints to the masses of the compact object ( $M_1 < 1.73 M_\odot$ ) and the companion star ( $0.28 M_\odot < M_2 < 0.70 M_\odot$ ). For the case of a canonical neutron star mass of  $M_1 \sim 1.4 M_\odot$ , the orbital inclination is found to be lower than  $40^\circ$ . We also present the best near-infrared spectrum of the source to date. There is no evidence of donor star features on it, but we are able to constrain the veiling factor as a function of the spectral type of the secondary star. The combination of both techniques restricts the spectral type of the donor to be later than K4 and luminosity class IV. It also constrains the contribution of the companion light to the infrared emission of Sco X-1 to be lower than 33 per cent. This implies that the accretion related luminosity of the system in the  $K$  band is larger than  $\sim 4 \times 10^{35}$  erg s $^{-1}$ .

**Key words:** accretion, accretion discs – gravitational waves – stars: neutron – infrared: stars – X-rays: binaries.

### 1 INTRODUCTION

Low-mass X-ray binaries (LMXBs) harbour a low-mass donor star which transfers matter on to a black hole or a neutron star (NS) via an accretion disc. They can be divided into two populations according to their long-term behaviour. *Transient* systems spend most part of their lives in a faint, quiescent state, but show occasional outburst, where their X-ray luminosity increases above  $\sim 10$  per cent of the Eddington luminosity ( $L_{\text{Edd}}$ ). There is also a population of  $\sim 200$  sources that are always X-ray active, displaying luminosities above  $L_X \simeq 10^{36}$  erg s $^{-1}$  (but see Armas Padilla, Degenaar & Wijnands 2013). The so-called *persistent* sources mostly harbour NS accretors, whilst the vast majority of black holes are found in transient systems. Transient LMXBs have provided a number of dynamical NS and black hole mass measurements thanks to the detection of the donor star during the quiescent phase (e.g. Casares & Jonker 2014). This is not the case for the majority of the persistent population, where the companion spectrum is totally swamped by the reprocessed light from the accretion flow. Only for a few long or-

period systems a full orbital solution exists, since they harbour giant (i.e. bright), companion stars.

Due to the blue spectrum of the accretion discs, and the typically late spectral types of the donor stars, near-infrared (NIR) observations offer a good opportunity to detect the companion star spectral features (e.g. Bandyopadhyay et al. 1997) and obtain a full dynamical solution (see Steeghs et al. 2013 for a study purely based on NIR data).

Scorpius X-1 is the prototype LMXB and also the brightest persistent X-ray source in the sky, being the target of numerous studies since its discovery (Giacconi et al. 1962). Although the spectral classification of the companion star is unknown, its relatively long orbital period ( $P_{\text{orb}} = 18.9$  h; Gottlieb, Wright & Liller 1975) suggests an evolved, late-type star. Bradshaw, Fomalont & Geldzahler (1999) measured the trigonometric parallax of Sco X-1 using Very Long Baseline Array (VLBA) radio observations, and deduced a distance of  $2.8 \pm 0.3$  kpc. Further observations allowed the detection of twin radio lobes, leading to an inclination value of  $44^\circ \pm 6^\circ$ . This value assumes that the radio-jet is perpendicular to the orbital plane (Fomalont, Geldzahler & Bradshaw 2001). Even though the system does not show any of the NS identifying features (thermonuclear X-ray bursts or pulsations), a NS accretor is widely assumed based on its X-ray behaviour (see van der Klis 2006; Muñoz-Darias et al. 2014 for X-ray emission from NS in LMXBs).

\*E-mail: dmata@iac.es

†Marie Curie Fellow.

## L2 D. Mata Sánchez et al.

Steeghs & Casares (2002) presented an optical spectroscopic technique for measuring system parameters in persistent LMXBs. It is based on the discovery of narrow emission lines within the Bowen blend, arising from the irradiated face of the donor star in Sco X-1 and powered by fluorescence. This claim is based on the narrowness, Doppler velocities and phase of the lines. Also, timing studies of the fluorescence emission have shown a time lag with the irradiating X-ray flux which is consistent with the light time between the two components of the binary (Muñoz-Darias et al. 2007). Radial velocity studies of the Bowen lines (Bowen technique hereinafter) have been successfully applied to other dozen LMXBs (see Cornelisse et al. 2008; Muñoz-Darias 2009), providing the first dynamical solutions to some classical NS systems (e.g. Casares et al. 2006; Cornelisse et al. 2007) and the canonical black hole transient GX 339-4 (Hynes et al. 2003; Muñoz-Darias, Casares & Martínez-Pais 2008). The velocity inferred from these emission lines ( $K_{\text{em}}$ ) corresponds to that of the irradiated region of the companion; hence it only represents a lower limit to that of its centre of mass ( $K_2$ ). In order to correct  $K_{\text{em}}$  from this effect numerical solutions should be applied, such as those computed by Muñoz-Darias, Casares & Martínez-Pais (2005, see Section 2).

In this Letter, we aim at constraining the masses of the components in Sco X-1 by combining two different techniques: (i) a  $K$ -correction along with Monte Carlo analysis accounting for constraints on the orbital parameters from previous studies (Section 2) and (ii) NIR intermediate-resolution spectroscopy obtained around orbital phase zero, when the non-heated face of the donor star is oriented towards the Earth (Section 3). We note that Sco X-1, besides being the prototypical LMXB, is also an important object in the search for persistent gravitational waves, which also requires an accurate determination of its system parameters (e.g. Abadie et al. 2011; Galloway et al. 2014).

## 2 THE K-CORRECTION

The companion star of Sco X-1 has been solely detected through the Bowen technique described above. A  $K_{\text{em}}$  velocity was initially reported by Steeghs & Casares (2002), and very recently refined by Galloway et al. (2014, see Table 1). This velocity can be translated to that of the centre of mass of the donor by the so-called  $K$ -correction ( $K_c$ ). Muñoz-Darias et al. (2005) presented numerical solutions for  $K_c$ , which is parametrized by the following equation:

$$K_c = \frac{K_{\text{em}}}{K_2} \cong N_0 + N_1 q + N_2 q^2 + N_3 q^3 + N_4 q^4, \quad (1)$$

where  $q = \frac{M_2}{M_1}$  is the mass ratio ( $M_1$  and  $M_2$  are the masses of the compact object and the donor star, respectively). The  $N_i$  values are tabulated and depend on both the opening angle of the accretion disc that shades the companion ( $\alpha$ ), and the orbital inclination ( $i$ ). Therefore,  $K_c$  is always lower than 1, and approaches unity as  $\alpha$  increases and the regions of the companion with lower radial velocities become shaded. For the limit case in which the companion

**Table 1.** Observational measurements included in the Monte Carlo analysis.

$K_{\text{em}}(\text{km s}^{-1})$	$K_{1\text{min}}(\text{km s}^{-1})$	$K_{1\text{max}}(\text{km s}^{-1})$	$i(\text{deg})$
$74.9 \pm 0.5^{(a)}$	$40 \pm 5^{(b)}$	$53 \pm 1^{(b)}$	$44 \pm 6^{(c)}$

References: <sup>a</sup>Galloway et al. (2014); <sup>b</sup>Steeghs & Casares (2002); <sup>c</sup>Fomalont et al. (2001).

is fully shaded by the disc (i.e.  $\alpha = \alpha_M$ ),  $K_c$  is at maximum and can be approximated by the following expression:

$$K_c = 1 - f(q)(1+q) \quad f(q) \cong 1 - 0.213 \left( \frac{q}{1+q} \right)^{2/3}. \quad (2)$$

Therefore, for a given  $q$  and  $K_{\text{em}}$ , the true  $K_2$  velocity is in the range:

$$K_{\text{em}}/K_c(\alpha_M) < K_2 < K_{\text{em}}/K_c(\alpha_0), \quad (3)$$

where  $K_c(\alpha_0)$  represents the case in which the disc is not present and the inner face of the companion star is fully irradiated ( $\alpha = 0^\circ$ ). This gives the maximum  $K$ -correction and, therefore,  $K_c$  would be minimum.

### 2.1 Monte Carlo analysis

The mass of the compact object ( $M_1$ ) can be inferred using the mass function formula, which is directly derived from Kepler's laws:

$$M_1 = \frac{P_{\text{orb}}}{2\pi G} \frac{K_2^3(1+q)^2}{\sin^3 i}. \quad (4)$$

For the case of Sco X-1, some of the above system parameters are poorly constrained (e.g. orbital inclination) and for some others we just have extremal values (see also Section 4). This is the case of  $K_1$  and  $K_2$ , the radial velocities of the compact object and the donor star, respectively. To deal with this, we performed a Monte Carlo analysis in order to obtain reliable limits to the compact object mass. We simulated  $10^6$  random, normally-distributed values of  $i$  and  $K_{\text{em}}$ , and lower and upper limits to the radial velocity of the compact object ( $K_{1\text{min}}$  and  $K_{1\text{max}}$ , respectively) centred at the values reported in Table 1. We apply both  $K_c(\alpha_0)$  and  $K_c(\alpha_M)$  to each simulated  $K_{\text{em}}$  value. Finally, we solved equation (4) for  $10^2$  steps in  $q$  (from 0 to 0.8), using the previously defined distribution of  $i$  values, as well as the orbital period reported in Galloway et al. (2014). We obtained four  $M_1$  distributions: two lower limits corresponding to  $K_2(\alpha_M)$  and  $K_{1\text{min}}$ , and two upper limits from  $K_2(\alpha_0)$  and  $K_{1\text{max}}$ . These limits are represented by solid and dashed lines, respectively in Fig. 1 and are obtained by adopting the value of  $M_1$  above or below 90 per cent of the points (for upper and lower limits, respectively) in each distribution and for every sampled value of  $q$ .

### 2.2 The masses of the NS and the companion

The intersections of the solid lines in Fig. 1 provide absolute limits to  $M_1$  and  $q$ . They yield extremal values to the system parameters with, at least<sup>1</sup>, 90 per cent confidence level:

$$0.22 M_\odot < M_1 < 1.73 M_\odot$$

$$0.24 < q < 0.75$$

$$0.05 M_\odot < M_2 < 1.30 M_\odot.$$

Therefore, we obtain a robust upper limit of  $M_1 < 1.73 M_\odot$ , consistent with a NS accretor. The lower limit is, on the other hand, not very restrictive. Adopting instead  $M_{1\text{min}} = 1 M_\odot$  as a conservative minimum value for the mass of a NS (see e.g. Kiziltan et al. 2013), we further restrict the mass ratio to  $0.28 < q < 0.51$ , and hence  $0.28 M_\odot < M_2 < 0.70 M_\odot$ .

<sup>1</sup> The confidence level of these results is actually slightly higher since two 90 per cent limits (apart from that of the inclination) are simultaneously verified.

## Mass constraints to Sco X-1 L3

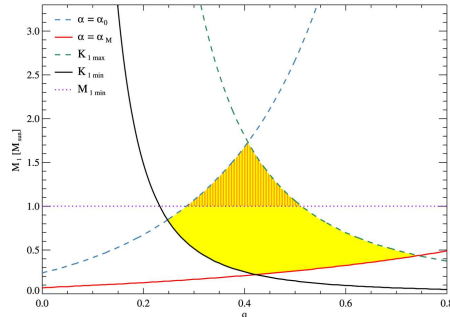


**Figure 1.**  $K$ -correction for Sco X-1 obtained through a Monte Carlo simulation ( $10^6$  events). We plot in solid and dashed, coloured lines the obtained limits to  $M_1$  as a function of  $q$ . The upper limits correspond to  $K_c(\alpha_0)$  (blue, dashed line) and  $K_{1\max}$  (green, dashed line). The lower limits are defined by  $K_c(\alpha_M)$  (red, solid line) and  $K_{1\min}$  (black, solid line). The yellow band represents the 90 per cent probability region delimited by the previous limits. The violet, dotted line corresponds to the imposed  $M_1 > 1 M_\odot$  constraint (see the text), which restrict the allowed parameter space to the orange striped triangle.

## 3 NIR SPECTROSCOPY

We observed Sco X-1 on 2008 June 28, using the Long-slit Intermediate Resolution Infrared Spectrograph (Acosta-Pulido, Dominguez-Tagle & Manchado 2003; Manchado et al. 2004) at the Cassegrain focus of the 4.2-m William Herschel Telescope (WHT), in La Palma (Spain). We used the  $K$ -band grism ( $R = 2500$ ,  $3.5 \text{ \AA pixel}^{-1}$  dispersion) combined with a  $0.75$  arcsec slit. The use of grisms as dispersers usually does not permit to vary the spectral range. In our case, the employed slit (10p75ext) consists of two slits which are offset along the dispersion axis by about 115 pixels in both senses. This allowed us to redshift the nominal spectral range to  $2.09$ – $2.45 \mu\text{m}$ , which includes the CO bandheads.

We performed seven nodding cycles of three positions each, with an exposure time of 900 s per cycle at airmasses in the range  $\sim 1.4$ – $1.5$ . We cover orbital phases,  $\varphi = 0.01$ – $0.13$  (using the ephemerides from Galloway et al. 2014) and the total exposure time was 1.75 h. For the data reduction process, we used `IRAF`<sup>2</sup>/`lirisdr` task package<sup>3</sup>, as well as a modified version of the package `xteileor_general` developed by Vacca, Cushing & Rayner (2003) to perform the telluric correction to the final spectra (see Ramos Almeida, Pérez García & Acosta-Pulido 2009; Ramos Almeida et al. 2013, for a more detailed description of the data reduction process).

This strategy yielded seven (nodding averaged) NIR spectra of Sco X-1. Absorption features from the donor star are not evident in any of them, which were combined to produce a higher signal-to-noise average spectrum. Points deviating more than  $3\sigma$  above or below the continuum, probably caused by bad pixels or residual from the sky subtraction, were interpolated. The combined, normalized spectrum is presented in Fig. 2. To our knowledge this is the best NIR spectrum of Sco X-1 available to date (see

<sup>2</sup> `IRAF` is distributed by National Optical Astronomy Observatories, operated by the Association of Universities for Research in Astronomy, Inc., under contract with the National Science Foundation.

<sup>3</sup> The `IRAF` `lirisdr` task package is supported by Jose Acosta.

Bandyopadhyay et al. 1997 for a previous example). No absorption lines from the companion star are detected. The most prominent feature in the spectrum is a strong Br  $\gamma$  emission line, whose full width at half-maximum, FWHM =  $480 \pm 20 \text{ km s}^{-1}$ , is consistent with that of H $\alpha$  (FWHM =  $440 \pm 20 \text{ km s}^{-1}$ ). This latter value was obtained from previous observations performed by our team with the Intermediate Dispersion Spectrograph at the Cassegrain focus of the 2.5-m Isaac Newton Telescope, in La Palma (Spain).

## 3.1 Veiling factor

Since no features from the companion are evident in our NIR spectrum, we investigated the amount of flux from the accretion flow required to veil the donor. This obviously depends on its spectral type. As a first step, we compared our spectrum with templates of G–M main-sequence stars from the *IRTF Spectral Library* (Rayner, Cushing & Vacca 2009). In Fig. 2, we present normalized spectra of G0V, K0V and M5V stars, which cover the same spectral region as that of Sco X-1. For each spectral type, we define  $F_{\text{depth}}$  as the normalized flux of the deepest photospheric absorption line present in the NIR spectrum. These correspond to Na I ( $2.206 \mu\text{m}$ ), Mg I ( $2.282 \mu\text{m}$ ) and  $^{12}\text{CO}$  ( $2.295 \mu\text{m}$ ), for M5V, G0V and K0V, respectively. Similarly, we define the veiling factor ( $X$ ) as the fractional contribution of the accretion related luminosity ( $L_{\text{acc}}^K$ ) to the total flux. The veiling necessary to make these features shallower than the noise level ( $3\sigma$ ) within the corresponding spectral region of the Sco X-1 spectrum is a lower limit to this factor. Therefore,

$$X \geq 1 - \frac{3\sigma}{F_{\text{depth}}} \quad X = \frac{L_{\text{acc}}^K}{L_{\text{acc}}^K + L_2^K}, \quad (5)$$

where  $L_2^K$  is the luminosity of the donor.  $X$  is always in the range  $0 \leq X < 1$  and depends on the spectral type of the companion. Our lower limits to the fractional contribution of the accretion luminosity of Sco X-1 NIR flux ( $X_{\min}$ ) are reported in the first column of Table 2. It varies from 0.09 to 0.78 for the cases of G0V and M5V, respectively.

## 4 DISCUSSION

The  $K$ -correction and Monte Carlo analysis (see Section 2) impose an upper limit to the compact object mass of  $M_1 < 1.73 M_\odot$ . This rules out a massive NS ( $\sim 2 M_\odot$ ) like e.g. that presented in Demorest et al. (2010). More accurate values of  $\alpha$ ,  $i$  and  $K_1$  are necessary to improve this constraint. de Jong, van Paradijs & Augusteijn (1996) proposed an average value of  $\alpha = 12^\circ$  for persistent LMXBs. Using this value, we can calculate  $K_2$  by applying the same methodology, which constrains the mass of the compact object to  $M_1 < 1.25 M_\odot$ . This value is lower than the canonical NS mass ( $M_1 \sim 1.4 M_\odot$ ). However, we note that NS masses down to  $M_1 \sim 1.2 M_\odot$  have been reported (e.g. Kiziltan et al. 2013). If we fix the NS mass to the canonical value, we obtain  $\alpha \leq 11^\circ$  and  $K_1 > 47 \text{ km s}^{-1}$ . All the above constraints require an inclination as low as  $i \sim 36^\circ$  (we are quoting 90 per cent confidence limits).

The upper limit to  $K_1$  used in this work was obtained by applying the double Gaussian method to the He II lines, while the lower limit comes from Doppler tomography analysis of H $\beta$  (Steeghs & Casares 2002). Our analysis rules out this lower limit for a NS mass higher than  $1 M_\odot$  (see Fig. 1), and suggest the upper limit to be close to the real value. Interestingly, the latter stands true for another NS system analysed using the double Gaussian technique, namely X 1822-371 (Muñoz-Darias et al., in preparation; see also Casares et al. 2003), in which the  $K_1$  velocity is accurately known (Jonker & van der Klis 2001). Fixing  $M_1 = 1.4 M_\odot$  and assuming

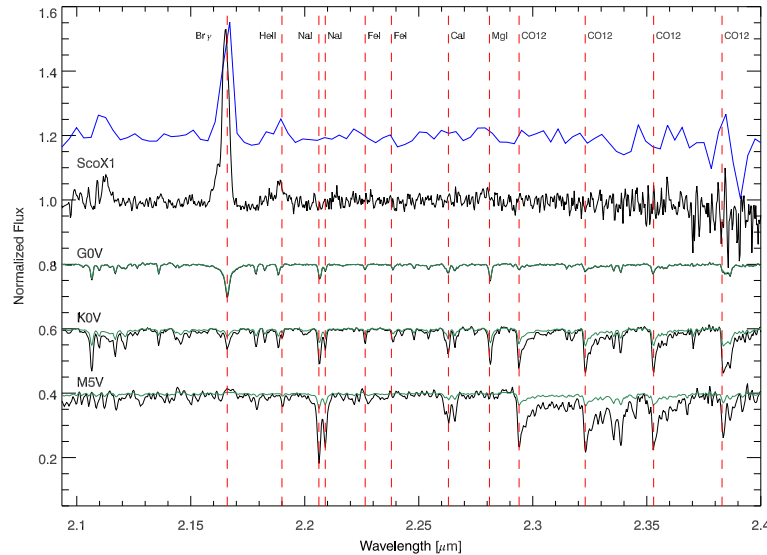


**Figure 2.** Normalized NIR spectrum of Sco X-1 obtained by averaging the seven nodding cycles (black solid line). For comparison we show (blue solid line; positive offset applied) the spectrum degraded to the resolution of the best NIR spectrum available so far (Bandyopadhyay et al. 1997). We also include the spectra of three template stars (negative offsets applied) from IRTF Spectral Library as black and green solid lines. The latter have been veiled by the limit values reported in Table 2 for its corresponding spectral type. Typical NIR spectral features are identified by vertical, red, dashed lines.

$K_1 = K_{\max}$ , we obtain an absolute upper limit of  $i \sim 40^\circ$ , which is only satisfied if  $\alpha = 0^\circ$  (i.e. applying  $K_c(\alpha_0)$ ). Larger values of the opening angle or lower values of  $K_1$  would result in even lower inclinations. We note that inclinations  $\gtrsim 50^\circ$  were favoured to better explain time lags between reprocessed light (Bowen emission) and X-rays observed in Sco X-1. This value was found when the time lags were compared with those predicted by numerical transfer functions with a maximum response. However, we note results consistent with those presented here are also obtained if a broader range of expected delays and/or more conservative solutions are considered (see Muñoz-Darias et al. 2007 for details).

Finally, since Sco X-1 is not eclipsing, we can use our constraints to the mass ratio ( $q$ ) and the Roche lobe radius (derived through the formulae in Paczyński 1971) to infer a maximum inclination purely based on this condition (i.e. absence of eclipses). This yields  $i < 70^\circ$ .

#### 4.1 The nature of the donor star

Although our observations were performed at the most favourable orbital phase, we fail to detect any companion star feature in the NIR spectrum of Sco X-1 (see Section 3). Nevertheless, we obtain a lower limit to the veiling factor as a function of the spectral type of the secondary, and this can be used to discuss its nature. We initially found  $0.05 M_\odot < M_2 < 1.30 M_\odot$ , and assuming an accretor heavier than  $1 M_\odot$ , we infer  $0.28 M_\odot < M_2 < 0.70 M_\odot$ . Faulkner, Flannery & Warner (1972) presented a direct relation between the mean density of the companion star and the orbital period in the Roche lobe filling binaries. For a main-sequence companion in an 18.9 h orbital period, this result in a spectral type A0 (Cox 2000). However, the features of an A0V donor would dominate the

**Table 2.** Minimum veiling factor ( $X_{\min}$ ) and implied minimum  $K$ -magnitude ( $M_{K\min}$ ) for the donor star.  $M_K^V$ ,  $M_K^{IV}$  and  $M_K^{III}$  refer  $K$ -magnitudes of dwarf-to-giant standard stars.

Sp. Type	$X_{\min}$	$M_{K\min}$	$M_K^V$	$M_K^{IV}$	$M_K^{III}$
G0	0.09	-1.04	3.18 <sup>(a,b)</sup>	3.05 <sup>(a,b,c)</sup>	-1.18 <sup>(a,b)</sup>
K0	0.61	-0.12	4.13 <sup>(a,b)</sup>	3.89 <sup>(a,b,c)</sup>	-1.65 <sup>(a,b)</sup>
M5	0.78	0.51	7.80 <sup>(a,b)</sup>	7.06 <sup>(a,b,c)</sup>	-6.50 <sup>(a,b)</sup>

References: <sup>a</sup>Cox (2000); <sup>b</sup>Koornneef (1983); <sup>c</sup>Paczyński (1971).

observed spectrum. Similarly, its mass ( $M_2 = 2.9 M_\odot$ ) is ruled out by our results. This implies that the donor star is not a regular dwarf star but a somewhat more evolved object. Our upper limit ( $M_2 < 0.70 M_\odot$ ) constrains the spectral type to be later than K4, since this value corresponds to a main-sequence donor. Using the same procedure as in Section 3 for a K4 donor, we obtain a lower limit to the veiling factor of  $X > 0.66$ .

We can independently test the allowed spectral types for the companion star by solely using the veiling factor constraints. In a first step, we use the absolute  $K$ -magnitude value of Sco X-1  $M_K^{VI} = -1.14$  (see Wachter et al. 2005 and references therein) to set a minimum value of the absolute  $K$ -magnitude of the donor star as a function of the spectral type (see Table 2). Then, we combine the values tabulated for  $M_V$  and  $(V - K)$  (see Cox 2000 and Koornneef 1983, respectively) to infer absolute  $K$ -magnitudes for different spectral types and luminosity classes. We conclude that all the inspected spectral types would be compatible with the veiling constraints if the companion were in the main sequence ( $M_K^V$ ). However, doing the same for giant stars ( $M_K^{III}$ ) we are able to rule out luminosity class III (and earlier) for the donor. On the

Mass constraints to *Sco X-1* L5

other hand, assuming that the companion star radius is at the Roche lobe (Paczynski 1971), we obtain subgiant  $K$ -magnitudes ( $M_K^{IV}$ ) compatible with our veiling constraints (see Table 2).

## 4.2 Accretion luminosity in the NIR

The above constraint to the veiling factor ( $X > 0.66$ ) implies that the accretion luminosity ( $L_{acc}^K$ ) accounts for more than 2/3 of the observed  $K$ -band flux. If we consider the  $K$ -band luminosity of Sco X-1 reported by Wachter et al. (2005), and propagate the errors on the interstellar extinction and the distance, we obtain  $8 \pm 2 \times 10^{35}$  erg s $^{-1}$ . As noted by these authors, the error is not dominated by uncertainties in the measurements but reflects real variability (~25 per cent) in the  $K$  band. According to the MAXI all sky monitor (Matsuoka et al. 2009), the day of our observations Sco X-1 flux was within 10 per cent of its long-term average. Since data were obtained when the donor contribution is at maximum, we can use the limit  $X > 0.66$  to constrain the accretion luminosity of Sco X-1 in the NIR, which is therefore in range  $4 \times 10^{35}$  erg s $^{-1} < L_{acc}^K < 10^{36}$  erg s $^{-1}$ .

## 5 CONCLUSIONS

We performed a Monte Carlo analysis along with the  $K$ -correction to constrain the dynamical parameters of the prototypical X-ray binary Scorpius X-1. We obtain the following constraints, at 90 per cent confidence level:

$$M_1 < 1.73 M_\odot; 0.28 < q < 0.51; 0.28 M_\odot < M_2 < 0.70 M_\odot.$$

Thus, the presence of a massive NS ( $\sim 2 M_\odot$ ) in this system is ruled out. If we consider standard values for LMXBs, a possible set of parameters would be a canonical NS of  $M_1 \sim 1.4 M_\odot$ , an orbital inclination of  $i \sim 36^\circ$  and a disc opening angle of  $\sim 11^\circ$ . Assuming  $M_1 = 1.4 M_\odot$  necessarily implies  $i \lesssim 40^\circ$ . Higher values of the inclination would only be possible if the NS is lighter than the canonical value or any of the measurements used in this work is not correct.

We also presented the best NIR spectrum of the source to date. Despite the non-detection of donor star features, our deep observations constrain the spectral type of the donor to be later than K4 and luminosity class IV. We obtain a lower limit to the veiling factor in the NIR of  $X > 0.66$ , implying that the accretion related luminosity in the  $K$  band is larger than a few times  $10^{35}$  erg s $^{-1}$ .

## ACKNOWLEDGEMENTS

DMS acknowledges Fundación La Caixa for the financial support received in the form of a PhD contract. TMD acknowledges funding via an EU Marie Curie Intra-European Fellowships under contract numbers 2011-301355. CRA is supported by a Marie Curie Intra European Fellowship within the 7th European Community Framework programme (PIEF-GA-2012-327934). The WHT is operated on the island of La Palma by the Isaac Newton Group in the Spanish Observatorio del Roque de los Muchachos of the Instituto de Astrofísica de Canarias. DMS and JC acknowledge the hospitality of the Department of Astrophysics of the Oxford University (UK) where part of this work was carried out. This Letter is supported by the Spanish Ministerio de Economía y Competitividad (MINECO) under grants AYA 2010-18080 and SEV-2011-0187.

## REFERENCES

- Abadie J. et al., 2011, Phys. Rev. Lett., 107, 271102  
 Acosta-Pulido J., Dominguez-Tagle C., Manchado A., 2003, in Iye M., Moorwood A. F. M., eds, Proc. SPIE Conf. Ser. Vol. 4841, Instrument Design and Performance for Optical/Infrared Ground-based Telescopes, SPIE, Bellingham, p. 437  
 Amas Padilla M., Degenaar N., Wijnands R., 2013, MNRAS, 434, 1586  
 Bandyopadhyay R., Shabaz T., Charles P. A., van Kerkwijk M. H., Naylor T., 1997, MNRAS, 285, 718  
 Bradshaw C. F., Fomalont E. B., Geldzahler B. J., 1999, ApJ, 512, L121  
 Casares J., Jonker P. G., 2014, Space Sci. Rev., 183, 223  
 Casares J., Steeghs D., Hynes R. I., Charles P. A., O'Brien K., 2003, ApJ, 590, 1041  
 Casares J., Cornelisse R., Steeghs D., Charles P. A., Hynes R. I., O'Brien K., Strohmayer T. E., 2006, MNRAS, 373, 1235  
 Cornelisse R., Casares J., Steeghs D., Barnes A. D., Charles P. A., Hynes R. I., O'Brien K., 2007, MNRAS, 375, 1463  
 Cornelisse R., Casares J., Muñoz-Darias T., Steeghs D., Charles P., Hynes R., O'Brien K., Barnes A., 2008, in Bandyopadhyay R. M., Wachter S., Geline D., Geline C. R., eds, AIP Conf. Proc. Vol. 1010, A Population Explosion: The Nature & Evolution of X-ray Binaries in Diverse Environments, Am. Inst. Phys., New York, p. 148  
 Cox A. N., 2000, Allen's Astrophysical Quantities, Springer-Verlag, Berlin  
 de Jong J. A., van Paradijs J., Augusteijn T., 1996, A&A, 314, 484  
 Demorest P. B., Pennucci T., Ransom S. M., Roberts M. S. E., Hessels J. W. T., 2010, Nature, 467, 1081  
 Faulkner J., Flannery B. P., Warner B., 1972, ApJ, 175, L79  
 Fomalont E. B., Geldzahler B. J., Bradshaw C. F., 2001, ApJ, 558, 283  
 Galloway D. K., Premachandra S., Steeghs D., Marsh T., Casares J., Cornelisse R., 2014, ApJ, 781, 14  
 Giacconi R., Gursky H., Paolini F. R., Rossi B. B., 1962, Phys. Rev. Lett., 9, 439  
 Gottlieb E. W., Wright E. L., Liller W., 1975, ApJ, 195, L33  
 Hynes R. I., Steeghs D., Casares J., Charles P. A., O'Brien K., 2003, ApJ, 583, L95  
 Jonker P. G., van der Klis M., 2001, ApJ, 553, L43  
 Kiziltan B., Kottas A., De Yoreo M., Thorsett S. E., 2013, ApJ, 778, 66  
 Koormeef J., 1983, A&A, 128, 84  
 Manchado A. et al., 2004, in Moorwood A. F. M., Iye M., eds, Proc. SPIE Conf. Ser. Vol. 5492, Ground-based Instrumentation for Astronomy, SPIE, Bellingham, p. 1094  
 Matsuoka M. et al., 2009, PASJ, 61, 999  
 Muñoz-Darias T., 2009, PASP, 121, 935  
 Muñoz-Darias T., Casares J., Martínez-Pais I. G., 2005, ApJ, 635, 502  
 Muñoz-Darias T., Martínez-Pais I. G., Casares J., Dhillon V. S., Marsh T. R., Cornelisse R., Steeghs D., Charles P. A., 2007, MNRAS, 379, 1637  
 Muñoz-Darias T., Casares J., Martínez-Pais I. G., 2008, MNRAS, 385, 2205  
 Muñoz-Darias T., Fender R. P., Motta S. E., Belloni T. M., 2014, MNRAS, 443, 3270  
 Paczyński B., 1971, ARA&A, 9, 183  
 Ramos Almeida C., Pérez García A. M., Acosta-Pulido J. A., 2009, ApJ, 694, 1379  
 Ramos Almeida C., Rodríguez Espinosa J. M., Acosta-Pulido J. A., Alonso-Herrero A., Pérez García A. M., Rodríguez-Eugenio N., 2013, MNRAS, 429, 3449  
 Rayner J. T., Cushing M. C., Vacca W. D., 2009, ApJS, 185, 289  
 Steeghs D., Casares J., 2002, ApJ, 568, 273  
 Steeghs D., McClintock J. E., Parsons S. G., Reid M. J., Littlefair S., Dhillon V. S., 2013, ApJ, 768, 185  
 Vacca W. D., Cushing M. C., Rayner J. T., 2003, PASP, 115, 389  
 van der Klis M., 2006, Compact Stellar X-ray Sources, Cambridge Univ. Press, Cambridge, p. 39  
 Wachter S., Wellhouse J. W., Patel S. K., Smale A. P., Alves J. F., Bouchet P., 2005, ApJ, 621, 393

This paper has been typeset from a TeX/LaTeX file prepared by the author.

MNRASL 449, L1–L5 (2015)

Este documento incorpora firma electrónica, y es copia auténtica de un documento electrónico archivado por la ULL según la Ley 39/2015.  
*Su autenticidad puede ser contrastada en la siguiente dirección <https://sede.ull.es/validacion/>*

Identificador del documento: 970342

Código de verificación: pkuTTaUi

Fecha: 29/06/2017 10:41:42

Firmado por: DANIEL MATA SÁNCHEZ  
 UNIVERSIDAD DE LA LAGUNA

29/06/2017 11:14:09

JORGE CASARES VELAZQUEZ  
 UNIVERSIDAD DE LA LAGUNA

29/06/2017 12:50:38

TEODORO MUÑOZ DARIAS  
 UNIVERSIDAD DE LA LAGUNA

04/07/2017 18:28:11

ERNESTO PEREDA DE PABLO  
 UNIVERSIDAD DE LA LAGUNA

# 5

## The donor of Aquila X-1 revealed

AQUILA X-1 (Aql X-1 hereafter) is the canonical neutron-star transient LMXB due to the brightness amplitude and frequency of its outbursts. Despite its relatively bright quiescent optical magnitude ( $V \sim 21.6$ , Chevalier et al. 1999) its donor star absorption features have never been detected. The reason is the presence of an interloper star only 0.4 arcsec away from the source, with similar spectral type and brighter in  $V$ -band than the suspected companion by 2 magnitudes.

Using the Very Large Telescope equipped with the Spectrograph for INtegral Field Observations in the Near Infrared and the Adaptive Optics module, we managed to not only resolve Aql X-1 from this interloper, but to obtain phase-resolved spectroscopy. This allowed us to determine, for the first time, the radial velocity curve and spectral type of the companion star, and therefore place new constraints on the neutron star mass and the orbital inclination.

The work presented in this chapter was published under the title “**The donor of Aquila X-1 revealed by high-angular resolution near-infrared spectroscopy**” in Monthly Notices of the Royal Astronomical Society Letters, Volume 464, pages L41-L45, in 2017 (Mata Sánchez et al. 2017a).



## The donor of Aquila X-1 revealed by high-angular resolution near-infrared spectroscopy

D. Mata Sánchez,<sup>1,2</sup> T. Muñoz-Darias,<sup>1,2</sup> J. Casares<sup>1,2,3</sup> and F. Jiménez-Ibarra<sup>1,2</sup>

<sup>1</sup>Instituto de Astrofísica de Canarias, E-38205 La Laguna, Tenerife, Spain

<sup>2</sup>Departamento de astrofísica, Univ. de La Laguna, E-38206 La Laguna, Tenerife, Spain

<sup>3</sup>Department of Physics, Astrophysics, University of Oxford, Denys Wilkinson Building, Keble Road, Oxford OX1 3RH, UK

Accepted 2016 August 27. Received 2016 August 26; in original form 2016 July 12

### ABSTRACT

The low-mass X-ray binary Aquila X-1 is one of the most active neutron star X-ray transients. Despite its relatively bright quiescent optical counterpart, the detection of its companion has been hampered by the presence of a nearby interloper star. Using the Spectrograph for INtegral Field Observations in the Near Infrared (SINFONI) on the Very Large Telescope-8.2m telescope, we unambiguously single out Aquila X-1 from the interloper. Phase-resolved near-infrared spectroscopy reveals absorption features from a K4 ± 2 companion star moving at a projected velocity of  $K_2 = 136 \pm 4 \text{ km s}^{-1}$ . We here present the first dynamical solution and associated fundamental parameters of Aquila X-1, imposing new constraints on the orbital inclination ( $36^\circ < i < 47^\circ$ ) and the distance ( $d = 6 \pm 2 \text{ kpc}$ ) to this prototypical neutron star transient.

**Key words:** accretion, accretion discs – stars: neutron – X-rays: binaries.

### 1 INTRODUCTION

Neutron star X-ray transients (NSXRTs) are a sub-type of low-mass X-ray binaries harbouring a low-mass star ( $\lesssim 1 M_\odot$ ) and a neutron star (NS). They spend most of their lives in a faint, quiescent state, but show occasional outbursts where their X-ray luminosity increases above  $\sim 10$  per cent of the Eddington luminosity. Observing NSXRTs in outburst, while convenient for accretion studies (e.g. Muñoz-Darias et al. 2014), implies that most of the system luminosity arises from non-stellar components, completely veiling the companion star spectral features and preventing a dynamical solution even in the infrared (e.g. Mata Sánchez et al. 2015). On the other hand, the study of NSXRTs in their fainter, quiescent state – where the relative contribution of the companion star to the total flux is larger – depends greatly on the distance to the source and the Galactic extinction.

Aquila X-1 (hereafter Aql X-1, discovered by Kunte et al. 1973) is a recurrent NSXRT which has exhibited both coherent millisecond X-ray pulsations at  $\sim 1.8$  ms (Casella et al. 2008) and thermonuclear bursts (e.g. Galloway et al. 2008). Despite showing recurrent outbursts and having a relatively accessible quiescent optical magnitude ( $V = 21.6$ ; Chevalier et al. 1999), a radial velocity study of the donor star is still missing. This has been prevented by the presence of an interloper star placed less than 0.5 arcsec apart from Aql X-1 (Chevalier et al. 1999). The interloper is  $\sim 2$  mag brighter than Aql X-1 in the  $V$  band but of comparable brightness at near-infrared (NIR) wavelengths. In this work, we exploit the

better spatial resolution inherent to the NIR observations as well as adaptive optics techniques to obtain phase-resolved, integral field spectroscopy (IFS), which allow us to clearly resolve Aql X-1 from the interloper star.

### 2 OBSERVATIONS

The Spectrograph for INtegral Field Observations in the Near Infrared (SINFONI) is fed by an adaptive optics module and currently installed at the Cassegrain focus of the 8.2 m Very Large Telescope at Cerro Paranal (Chile). We obtained IFS in  $K$  band (resolving power  $R \sim 4000$ ) with an adaptive optics module working under natural guide star mode and a spatial pixel scale of  $0.05 \text{ arcsec} \times 0.1 \text{ arcsec}$  (with a field of view of  $3 \text{ arcsec} \times 3 \text{ arcsec}$ ).

The campaign includes 24 observations performed across several nights and sampling different orbital phases (always during the quiescent state) from 2010 May 5 to 2011 September 29. Each observation consists of 3-nodding 300 s exposures that were combined to subtract the sky contribution for a total exposure time of 900 s per observation. The reduction of the spectroscopic cubes was performed using public SINFONI pipeline recipes. The final products are 24 cubes, where Aql X-1 and the interloper star are clearly resolved (see Fig. 1) with a typical full width at half-maximum (FWHM) of  $\sim 0.18 \text{ arcsec}$  (note that the  $K$ -band diffraction limit for an 8.2 m telescope is  $\sim 0.07 \text{ arcsec}$ ). Early-type standard stars were observed each night with the same instrumental configuration in order to carry out a telluric correction. Likewise, K0–M0 spectral type templates were obtained for radial velocity analysis and spectral classification.

\* E-mail: dmata@iac.es

© 2016 The Authors

Published by Oxford University Press on behalf of the Royal Astronomical Society

Este documento incorpora firma electrónica, y es copia auténtica de un documento electrónico archivado por la ULL según la Ley 39/2015.  
Su autenticidad puede ser contrastada en la siguiente dirección <https://sede.ull.es/validacion/>

Identificador del documento: 970342

Código de verificación: pkuTTaUi

Fecha: 29/06/2017 10:41:42

Firmado por: DANIEL MATA SÁNCHEZ  
UNIVERSIDAD DE LA LAGUNA

29/06/2017 11:14:09

JORGE CASARES VELAZQUEZ  
UNIVERSIDAD DE LA LAGUNA

29/06/2017 12:50:38

TEODORO MUÑOZ DARIAS  
UNIVERSIDAD DE LA LAGUNA

04/07/2017 18:28:11

ERNESTO PEREDA DE PABLO  
UNIVERSIDAD DE LA LAGUNA

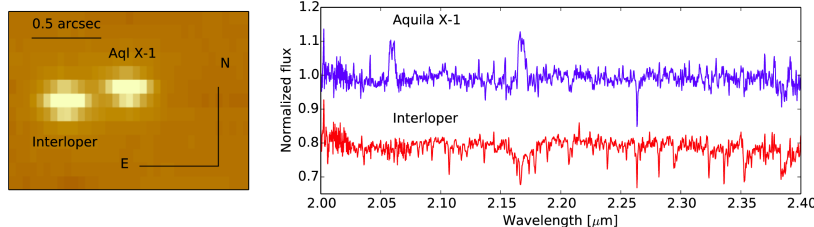


**Figure 1.** Left-hand panel: collapsed cube in the spectral dimension. Aql X-1 and the interloper are clearly resolved. Right-hand panel: averaged, normalized spectrum of Aql X-1 (blue, solid line) and the interloper star (red, solid line). A flux offset of 0.2 has been applied for display purposes.

We extracted the spectra using an aperture radius of 0.1 arcsec, which provided independent, non-contaminated spectra of both Aql X-1 and the interloper. Spectra were analysed with the MOLLY software. A telluric correction was applied using the atmospheric transmission profile derived from each standard star after masking their early-type spectral features. Since our study requires precise measurement of orbital velocities, a wavelength correction due to flexure effects was performed using the sky spectra. The spectra were re-calibrated using OH emission lines (Rousselot et al. 2000), which yielded corrections under  $<40\text{ km s}^{-1}$ . The final, averaged spectra are presented in Fig. 1.

### 3 RESULTS

The averaged spectrum of Aql X-1 (Fig. 1) shows both emission lines from the accretion disc and absorption features from the donor star. The individual spectra are noisier, but have enough quality [signal-to-noise ratio (SNR)  $\sim 11$ ] to perform a radial velocity study.

#### 3.1 Radial velocity curve of the donor star

Our SINFONI spectral templates have an SNR too low to be used in a radial velocity study. Instead, we compared our object spectra with F–M main-sequence stars templates from the *IRTF Spectral Library* (Cushing, Rayner & Vacca 2005; Rayner, Cushing & Vacca 2009) after degrading our data to their lower resolution ( $R \sim 2000$ ). We use the MOLLY *xcor* routine to perform the cross-correlation, obtaining the radial velocity shift of each individual spectrum. To carry out this task, we considered a spectral region free of both emission lines and residuals from the telluric correction, where prominent absorption features such as Na I doublet (2.206–2.208 μm) and Ca I triplet

(2.261–2.266 μm) are present (Fig. 2). For each spectrum, we computed the binary phase using the most accurate orbital elements available in the literature, i.e.  $P_{\text{orb}} = 0.789\,498 \pm 0.000\,010\text{ d}^{-1}$  (García et al. 1999) and  $T_0 = 2450\,282.220 \pm 0.003\text{ d}$  (Chevalier & Illyasky 1998). We note that the phase uncertainty, projected on to our last data point, amounts to  $\pm 0.10$ . The resultant radial velocity curve (Fig. 3) reveals a clear orbital modulation caused by the motion of the donor star (see Section 4). A sinusoidal fit to the data of the form:

$$V = V + K_2 \sin(2\pi(\phi - \phi_0)), \quad (1)$$

where  $V$  is the observed velocity,  $\gamma$  is the systemic velocity,  $\phi_0$  the phase offset and  $K_2$  the donor star orbital velocity, yields:  $K_2 = 136 \pm 4\text{ km s}^{-1}$ ;  $\gamma = 104 \pm 3\text{ km s}^{-1}$  and  $\phi_0 = 0.130 \pm 0.005$  ( $\chi^2_{\text{red}} = 0.86$ ). This is obtained from the cross-correlation with the K4V template, but we note that G–M templates return values consistent within  $1\sigma$ . Our data allow us to define a new  $T_0$  from the epoch with the maximum number of observations ( $T_0 = 2455\,810.387 \pm 0.005\text{ d}$ ). Using this new value, we refine the orbital period to  $P_{\text{orb}} = 0.789\,5126 \pm 0.000\,0010\text{ d}^{-1}$ .

#### 3.2 Spectral classification and veiling

Fig. 2 shows that both the donor star and the accretion flow contribute to the NIR emission of Aql X-1. Therefore, the actual spectrum of the companion is veiled by a factor  $X$ , defined as the fractional contribution of non-stellar sources to the total flux (e.g. the accretion disc contribution). In order to constrain  $X$  and the spectral type of the companion we produced a grid of spectra sampling the range  $0 < X < 1$  for each template, and compared them with the

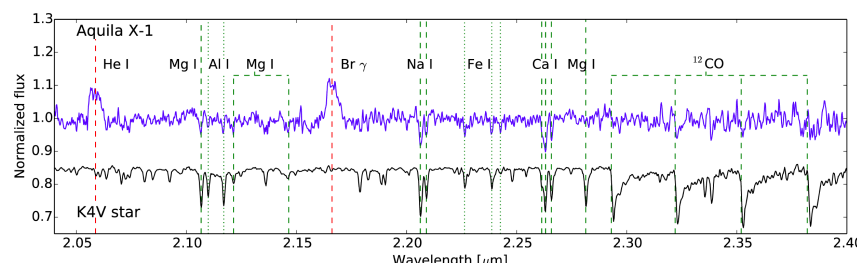


**Figure 2.** Averaged spectrum of Aquila X-1 in the rest frame of the companion star (top). Accretion disc emission features (Br  $\gamma$  and He I) are marked with red, dashed vertical lines. The expected K-type donor star absorption features are shown as green, dashed and dotted vertical lines, with the Na I doublet and the Ca II triplet being the most prominent. A template K4V spectrum is depicted for comparison (bottom).

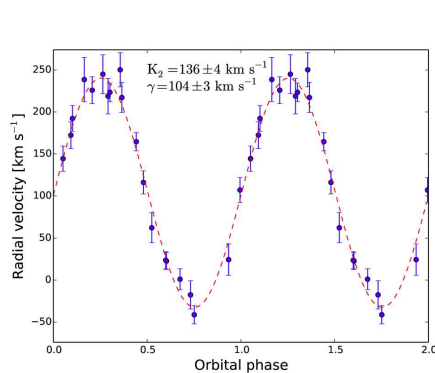


**Figure 3.** Radial velocity curve obtained using a K4V template. A sinusoidal fit is depicted as a dashed red line. Four spectra whose radial velocities deviate more than  $1.5\sigma$  from the fit due to their lower SNR (poor seeing) were discarded in order to produce a cleaner radial velocity curve. Two orbital phases are shown for clarity.

averaged spectrum of Aql X-1 in the donor star rest frame using a  $\chi^2$  minimization routine. The minimum of the  $\chi^2$  distribution constrains the donor star spectral type to be  $K4 \pm 2$  and the  $K$  band veiling to  $X = 0.36 \pm 0.10$ . The same analysis reveals a  $G9 \pm 2V$  spectral type for the interloper.

### 3.3 Diagnostic diagram: the radial velocity curve of the NS

In order to constrain the radial velocity of the NS, we analysed the evolution of the most prominent emission line present in the spectra, namely  $Br\gamma$  ( $2.166\mu m$ ). We constructed a diagnostic diagram (Shafter, Szkody & Thorstensen 1986) where we fit the emission line in each spectrum to a double Gaussian model with a fixed separation ( $a$ ). Large  $a$  values trace the movement of the wings of the line, which are expected to be formed in the inner parts of the accretion disc. For each  $a$  value, we apply a sinusoidal fit (similar to equation 1) to the obtained velocities. By averaging the results for separations in the range  $a = 600-800\text{ km s}^{-1}$ , where we found that the fit was acceptable (including visual inspection) and stable, we infer:  $K_1 = 56 \pm 11\text{ km s}^{-1}$ ;  $\gamma = 132 \pm 10\text{ km s}^{-1}$ ;  $\phi_0 = 0.63 \pm 0.03$ . We carried out the same analysis using the fainter  $He\alpha$  ( $2.059\mu m$ ) line and obtained consistent results.

The systemic velocity derived from this technique is consistent within  $2.2\sigma$  with the  $\gamma$  derived from the donor star radial velocity curve. Likewise, the zero phase  $\phi_0 \sim 0.5$  suggests that the wings of the lines are formed in the surrounding disc around the NS, tracing its movement. Therefore, we propose  $K_1 = 56 \pm 11\text{ km s}^{-1}$  as a good estimate of the radial velocity of the NS. We note that both  $K_1$  and  $\gamma$  derived from the diagnostic diagram are consistent with previous determinations using optical emission lines by García et al. (1999,  $K_1 = 70 \pm 20\text{ km s}^{-1}$ ,  $\gamma = 150 \pm 20\text{ km s}^{-1}$ ,  $He\alpha$ ) and Cornelisse et al. (2007,  $K_1 = 68 \pm 5\text{ km s}^{-1}$ ,  $\gamma = 130 \pm 20\text{ km s}^{-1}$ ,  $He\beta$ ).

### 3.4 Astrometry of Aql X-1 and light curves

The high angular resolution achieved by SINFONI allowed us to single out Aql X-1 from a nearby field star. Aiming at refining the object coordinates, we collapsed each individual cube along the spectral

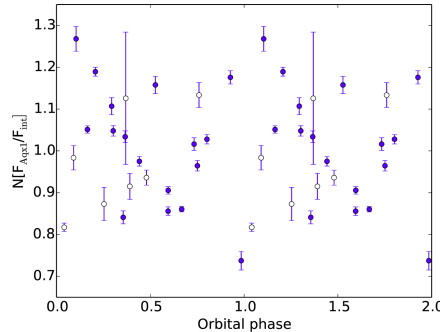


**Figure 4.**  $K$ -band flux variability of Aql X-1 (relative to the interloper) as a function of the orbital phase. Filled dots refer to observations with seeing better than  $<0.22$  arcsec, while empty dots depict those with poorer seeing (up to  $0.40$  arcsec). Two orbital cycles are shown for clarity.

dimension and fitted a bi-dimensional Gaussian to the resultant ‘photometric’ images. We derived a centroid position relative to the interloper of  $\Delta\alpha = -0.0295 \pm 0.0006\text{s}$ ;  $\Delta\delta = 0.083 \pm 0.011$  arcsec, which is consistent within  $1.5\sigma$  with that obtained from ultraviolet observations (Hynes & Robinson 2012), yielding a separation of  $0.450 \pm 0.014$  arcsec. The collapsed images can also be used to perform differential photometry against the interloper star, which is expected to remain constant during the observations. The obtained light curve from aperture photometry (see Fig. 4) shows variability at  $\sim 20$  per cent ( $\sim 0.3$  mag) level ( $\sigma = 0.13$ ), but there is no clear orbital modulation (see Section 4).

### 3.5 Rotational broadening

In an attempt to measure the rotational broadening of the companion star in Aql X-1, we compared the breadth of the absorption features – using the averaged spectrum in the companion star rest frame – with template stars observed with the same instrumental configuration. These cover spectral types K0IV, K3V, K7V and M0V and were co-added in order to produce a single ‘K-type’ template with sufficient SNR for this analysis. We then artificially broadened this grandsum template spectrum using a linear limb-darkening coefficient of 0.33 (Al-Naimiy 1978), and compared it with the Aql X-1 spectrum using *optsub* MOLLY routine to determine the best fit. Unfortunately, we were not able to resolve the minimum of the  $\chi^2$  distribution. This is not surprising given that our spectral resolution is  $\sim 75\text{ km s}^{-1}$  and we expect (using our  $K_2$  and  $K_1$  values; see Wade & Horne 1988) a rotational broadening of  $\sim 60\text{ km s}^{-1}$ .

## 4 DISCUSSION

We have determined the orbital velocities of the system components in Aql X-1 as well as the donor star spectral type. We can use these results to constrain other fundamental parameters of the system such as the inclination, the NS mass and the distance.

### 4.1 The distance to Aql X-1

$K$ -band photometry was carried out using the data cubes after collapsing in the spectral dimension. These were compared

with standard stars observed each night. The mean values for the interloper star and Aql X-1 are  $K_{\text{int}} = 16.3 \pm 0.3$  and  $K_{\text{Aql}} = 16.7 \pm 0.3$ , respectively, where the uncertainty refers to one standard deviation. The observed hydrogen equivalent column density  $N_{\text{H}} = (4.4 \pm 0.1) \times 10^{21} \text{ cm}^{-2}$  (Campana et al. 2014) and the relation  $N_{\text{H}} = (2.0 \pm 0.5) \times 10^{21} \text{ cm}^{-2} A_{\text{V}}$  (Watson 2011) yields  $A_{\text{V}} = 2.2 \pm 0.6$ . We apply the extinction relation provided by Cardelli, Clayton & Mathis (1989) to derive the extinction in the  $K$  band:  $A_K = 0.114 A_{\text{V}} = 0.25 \pm 0.06$ . If we consider the veiling factor from Section 2, the apparent magnitude of the donor star of Aql X-1 is  $K_{\text{donor}} = 16.9 \pm 0.4$ .

Cox (2000) provides absolute visual magnitudes and stellar parameters of dwarf and giant stars. Conversion to the  $K$  band can be achieved through the bolometric correction tables from Masama, Jordi & Ribas (2006). On the other hand, a  $K4 \pm 2$  dwarf star is not large enough to fill the Roche lobe of a 19h orbital period system, and therefore no accretion would be expected. The frequent outbursts observed in Aql X-1 require the donor star to be an evolved star which has expanded to the Roche Lobe radius  $R_L = 1.5 \pm 0.1 R_{\odot}$  (Eggleton 1983). Taking this into account, we predict an absolute magnitude for the donor of Aql X-1 of  $M_K = 3.0 \pm 0.8$ , which results in a distance of  $d = 6 \pm 2 \text{ kpc}$ . Our result is consistent with that derived from thermonuclear X-ray burst analysis ( $d < 6 \text{ kpc}$ ; Galloway et al. 2008). If we consider the interloper star to be a  $G9 \pm 2V$  and the extinction to be lower than that of Aql X-1, it places this object at  $d_{\text{int}} = 2.0\text{--}4.1 \text{ kpc}$ , in agreement with previous determinations (Chevalier et al. 1999).

The radial velocity curve of the Galaxy reported in Clemens (1985) and refined by Nakanishi & Sofue (2003) implies that the expected radial velocity of an object at the position of Aql X-1 would be  $68\text{--}92 \text{ km s}^{-1}$  ( $42\text{--}65 \text{ km s}^{-1}$  for the interloper star). From our spectra, we found a systemic velocity for the interloper of  $43 \pm 7 \text{ km s}^{-1}$ , which is fully consistent with the expected value. In the case of Aql X-1, we measure  $\gamma = 104 \pm 3 \text{ km s}^{-1}$ . This implies a natal kick in the radial direction of  $12\text{--}36 \text{ km s}^{-1}$ , in agreement with findings in others NS binaries (e.g. Cen X-4; González Hernández et al. 2005).

#### 4.2 Masses and inclination of Aql X-1

Our radial velocity curve, presented in Section 3, provides the first dynamical detection of the donor star in Aql X-1, revealing a projected velocity of  $K_2 = 136 \pm 4 \text{ km s}^{-1}$ . Previous attempts to measure the donor star orbital velocity in the optical regime were hampered by the presence of the interloper star. The so-called Bowen technique, which studies narrow emission lines (particularly the Bowen blend) arising from the inner, irradiated face of the companion star during the outburst, proposed  $K_2 \sim 250 \text{ km s}^{-1}$  (Cornelisse et al. 2007). Neither the obtained velocity amplitude (see e.g. Muñoz-Darias, Casares & Martínez-Pais 2005) nor the orbital phases are compatible with the solution presented here. Although the Bowen technique has proven to be valid in several systems (e.g. Steeghs & Casares 2002), a contaminating contribution to the Bowen blend by structures arising in other parts of the binary different from the irradiated face of the companion (e.g. hotspot) has been observed in some cases (e.g. Ser X-1; Hynes et al. 2004). This issue (as noted by the authors in Cornelisse et al. 2007) together with a limited orbital coverage probably concealed the donor star emission features in their spectra. A full optical spectroscopic study of Aquila X-1 in outburst will be presented in a forthcoming work (Jiménez-Ibarra et al., in preparation).

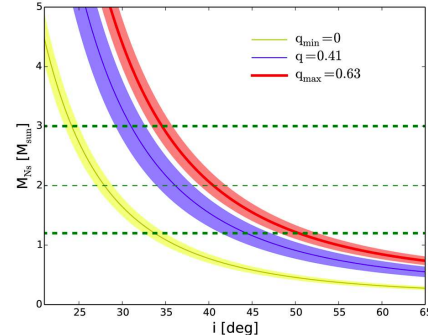


**Figure 5.** Neutron star mass versus orbital inclination. Horizontal, thick dashed lines correspond to the limits imposed to the NS mass ( $1.2$  and  $3 M_{\odot}$ ), whereas the thin dashed line marks the most massive NS found so far ( $2 M_{\odot}$ ; Antoniadis et al. 2013). The three solid lines represent our extreme (yellow and red lines) and preferred  $q$  values (blue line). The uncertainties (derived from  $K_2$  and  $P_{\text{orb}}$ ) are plotted as shaded regions.

The results derived in Section 3 ( $K_2$ ,  $P_{\text{orb}}$  and  $K_1$ ) produce a mass ratio  $q = \frac{M_{\text{donor}}}{M_{\text{NS}}} = \frac{K_1}{K_2} = 0.41 \pm 0.08$ , as well as a mass function:

$$f(M_{\text{NS}}) = \frac{M_{\text{NS}} \sin i^3}{(1+q)^2} = \frac{P_{\text{orb}} K_2^3}{2\pi G} = 0.21 \pm 0.02, \quad (2)$$

which does not significantly restrict the mass of the NS due to both the uncertainty in  $q$  and the unknown value of the orbital inclination ( $i$ ). The detection of both thermonuclear burst and pulsed emission indicates an NS accretor in Aql X-1, and thus its mass should be higher than  $M_{\text{NS}} > 1.2 M_{\odot}$  (Kiziltan et al. 2013). Similarly, the companion star has been classified as an evolved  $K4 \pm 2$  star; assuming that binary evolution does not significantly increase its mass (see Kolb, King & Baraffe 2001) then  $M_{\text{donor}} < 0.76 M_{\odot}$  (Cox 2000), which all together yields an upper limit to the mass ratio of  $q < 0.63$ . Using our  $K_2$  and  $P_{\text{orb}}$ , and considering a conservative constraint of  $M_{\text{NS}} < 3 M_{\odot}$ , the inclination parameter is restricted to  $23^\circ < i < 53^\circ$  (see Fig. 5). By including the proposed  $K_1$  and the upper limit imposed by the most massive NS found so far ( $M_{\text{NS}} \sim 2 M_{\odot}$ , PSR J0348+0432; Antoniadis et al. 2013), we obtain  $34^\circ < i < 47^\circ$ . On the other hand, photometric observations (Welsh, Robinson & Young 2000) constrain the orbital inclination to  $i > 36^\circ$ , which is fully consistent with our results. A canonical NS ( $M_{\text{NS}} = 1.4 M_{\odot}$ ) would require  $i = 42 \pm 3^\circ$ . Galloway et al. (2016) have very recently reported on the presence of intermittent X-ray dips on Aql X-1, which seem to be only present in  $\sim 10$  per cent of the orbital cycles. Our less constraining (i.e. more solid) upper limit ( $i < 53^\circ$  for  $M_{\text{NS}} > 1.2 M_{\odot}$ ) rules out a high orbital inclination as the origin of these events.

Casares (2015) found a linear correlation between  $K_2$  and the FWHM of the  $H\alpha$  line. The more general solution presented in the aforementioned Paper,

$$\frac{K_2}{\text{FWHM}} = \frac{\sqrt{\alpha f(q)}}{2}; \quad f(q) = \frac{0.49(1+q)^{-1}}{0.6 + q^{2/3} \ln(1 + q^{-1/3})} \quad (3)$$

assumes that the FWHM of the emission line is determined by the gas velocity at a characteristic disc radius  $R_W = \alpha R_{\text{L1}}$ , where  $R_{\text{L1}}$  is the distance from the compact object to the Lagrangian point L<sub>1</sub>. This empirical correlation implies that the  $H\alpha$  line is

## The donor of Aquila X-1 revealed L45

typically formed (in quiescence) at about  $0.42R_{\text{LJ}}$ . Following the same procedure but using  $\text{Br } \gamma$  instead of  $\text{H}\alpha$  together with our  $q$  and  $K_2$  values suggest that this line is formed at more external radii ( $0.54 \pm 0.11 \times R_{\text{LJ}}$ ), which is an expected feature supporting our results.

Finally, we note that the quiescent NIR emission of Aql X-1 shows significant long-term variability at 20 per cent level, but no apparent orbital modulation (Fig. 4). The latter could be due to both the relatively low inclination that we have derived and the presence of accretion related variability during the quiescent state (our observations were spanned over different epochs across more than a year). Spurious variability owing to a variable contribution from the interloper star is not expected since it only typically accounts for less than 5 per cent of the object flux (seeing  $\sim 0.2$ ; see Fig. 4). On the other hand, X-ray variability during the quiescence has been observed in Aql X-1 (Cackett et al. 2011), and optical variability is a common property of both quiescent black hole and NS transients (e.g. Zurita, Casares & Shahbaz 2003).

## 5 CONCLUSIONS

We used near-infrared IFS to single out Aquila X-1 from a nearby interloper star. The spectra reveal, for the first time, absorption features corresponding to a  $K4 \pm 2$  donor, veiled by  $\sim 36$  per cent in the  $K$  band, and moving at a projected orbital velocity of  $K_2 = 136 \pm 4 \text{ km s}^{-1}$ . We further refine the ephemerides of the system to  $T_0 = 2455\,810,387 \pm 0.005$  d and  $P_{\text{orb}} = 0.789\,5126 \pm 0.0000010 \text{ d}^{-1}$ , and constrain the orbital inclination to  $36^\circ < i < 47^\circ$ . Using the de-reddened  $K$ -band magnitude and the constraints on the spectral type, we infer a distance to the source of  $d = 6 \pm 2 \text{ kpc}$ .

## ACKNOWLEDGEMENTS

DMS acknowledges Fundación La Caixa for the financial support received in the form of a PhD contract. We also acknowledge support by the Spanish Ministerio de Economía y competitividad (MINECO) under grant AYA2013-42627. JC is supported from the Leverhulme Trust through the Visiting Professorship Grant VP2-2015-046. Based on observations made with ESO telescopes at the La Silla Paranal Observatory under program ID 085.D-0271. MOLLY software developed by T. R. Marsh is gratefully acknowledged.

## REFERENCES

- Al-Naimiy H. M., 1978, *Ap&SS*, 53, 181  
 Antoniadis J. et al., 2013, *Science*, 340, 448
- Cackett E. M., Fridriksson J. K., Homan J., Miller J. M., Wijnands R., 2011, *MNRAS*, 414, 3006  
 Campana S., Brivio F., Degenaar N., Mereghetti S., Wijnands R., D'Avanzo P., Israel G. L., Stella L., 2014, *MNRAS*, 441, 1984  
 Cardelli J. A., Clayton G. C., Mathis J. S., 1989, *ApJ*, 345, 245  
 Casares J., 2015, *ApJ*, 808, 80  
 Casella P., Altamirano D., Patruno A., Wijnands R., van der Klis M., 2008, *ApJ*, 674, L41  
 Chevalier C., Illovaiky S. A., Leisy P., Patat F., 1999, *A&A*, 347, L51  
 Clemens D. P., 1985, *ApJ*, 295, 422  
 Cornelisse R., Casares J., Steeghs D., Barnes A. D., Charles P. A., Hynes R. I., O'Brien K., 2007, *MNRAS*, 375, 1463  
 Cox A. N., 2000, *Allen's Astrophysical Quantities*. AIP Press, New York  
 Cushing M. C., Rayner J. T., Vacca W. D., 2005, *ApJ*, 623, 1115  
 Eggleton P. P., 1983, *ApJ*, 268, 368  
 Galloway D. K., Munoz M. P., Hartman J. M., Psaltis D., Chakrabarty D., 2008, *ApJS*, 179, 360  
 Galloway D. K., Ajayam A. N., Upjohn J., Stuart M., 2016, *MNRAS*, 461, 3847  
 Garcia M. R., Callanan P. J., McCarthy J., Eriksen K., Hjellming R. M., 1999, *ApJ*, 518, 422  
 González Hernández J. I., Rebolo R., Peñarrubia J., Casares J., Israelián G., 2005, *A&A*, 435, 1185  
 Hynes R. I., Robinson E. L., 2012, *ApJ*, 749, 3  
 Hynes R. I., Charles P. A., van Zyl L., Barnes A., Steeghs D., O'Brien K., Casares J., 2004, *MNRAS*, 348, 100  
 Kiziltan B., Kottas A., De Yoreo M., Thorsett S. E., 2013, *ApJ*, 778, 66  
 Kolb U., King A. R., Baraffe I., 2001, *MNRAS*, 321, 544  
 Kunze P. K., Durgaprasad N., Gokhale G. S., Iyengar V. S., Manchanda R. K., Sreekanth B. V., 1973, *Nat. Phys. Sci.*, 245, 37  
 Masana E., Jordi C., Ribas I., 2006, *A&A*, 450, 735  
 Mata Sánchez J., Muñoz-Darias T., Casares J., Steeghs D., Ramos Almeida C., Acosta Pulido J. A., 2015, *MNRAS*, 449, L1  
 Muñoz-Darias T., Casares J., Martínez-Pais I. G., 2005, *ApJ*, 635, 502  
 Muñoz-Darias T., Fender R. P., Motta S. E., Belloni T. M., 2014, *MNRAS*, 443, 3270  
 Nakanishi H., Sofue Y., 2003, *PASJ*, 55, 191  
 Rayner J. T., Cushing M. C., Vacca W. D., 2009, *ApJS*, 185, 289  
 Rousselot P., Lidman C., Cuby J.-G., Moreels G., Monnet G., 2000, *A&A*, 354, 1134  
 Shafter A. W., Szkody P., Thorstensen J. R., 1986, *ApJ*, 308, 765  
 Steeghs D., Casares J., 2002, *ApJ*, 568, 273  
 Wade R. A., Horne K., 1988, *ApJ*, 324, 411  
 Watson D., 2011, *A&A*, 533, A16  
 Welsh W. F., Robinson E. L., Young P., 2000, *AJ*, 120, 943  
 Zurita C., Casares J., Shahbaz T., 2003, *ApJ*, 582, 369

This paper has been typeset from a TeX/LaTeX file prepared by the author.

MNRASL 464, L41–L45 (2017)

Este documento incorpora firma electrónica, y es copia auténtica de un documento electrónico archivado por la ULL según la Ley 39/2015.  
*Su autenticidad puede ser contrastada en la siguiente dirección <https://sede.ull.es/validacion/>*

Identificador del documento:	970342	Código de verificación:	pkuTTaUi
Firmado por:	DANIEL MATA SÁNCHEZ UNIVERSIDAD DE LA LAGUNA	Fecha:	29/06/2017 10:41:42
	JORGE CASARES VELAZQUEZ UNIVERSIDAD DE LA LAGUNA		29/06/2017 11:14:09
	TEODORO MUÑOZ DARIAS UNIVERSIDAD DE LA LAGUNA		29/06/2017 12:50:38
	ERNESTO PEREDA DE PABLO UNIVERSIDAD DE LA LAGUNA		04/07/2017 18:28:11

# 6

## The 2015 outburst of the black hole transient V404 Cygni

In previous chapters, we have analysed LMXBs from different points of view and at different accretion stages. We first studied, through X-ray and optical spectroscopy, the recently discovered X-ray transient MAXI J1957+032. Then, we analysed the optical spectrum of the short-period black hole system Swift J1357.2-0933 during quiescence. In the third and fourth chapters, we revisited two classic systems harbouring neutron stars: the persistent Sco X-1 and the X-ray transient Aql X-1, and constrained the nature of their elusive donor stars. In the last chapter of the thesis, we will show our most recent work on the black hole LMXB V404 Cygni during its 2015 outburst. Here, we will present what is, to the best of our knowledge, the most complete optical spectroscopic campaign ever performed on a black hole transient. The chapter initially presents the results reported in Nature by our team (Muñoz-Darias et al. 2016; MD16 hereafter) to then focus on the new results to be published in Mata Sánchez et al. (2017c, in prep.).

### 6.1 Introduction

The low-mass X-ray binary V404 Cygni is a long-period system ( $P_{\text{orb}} = 6.5$  d) with the first dynamically confirmed stellar-mass BH (Casares, Charles & Naylor 1992). It has exhibited several outbursts along the years: 1938 (Wagner et al. 1991), 1956 (Richter 1989), 1989 (Makino 1989) and 2015 (Barthelmy et al. 2015a), with the last one followed by a mini-outburst only 6 months later (Barthelmy, Page & Palmer 2015b, Lipunov et al. 2015, Motta et al. 2015, Hardy et al. 2016). The 1938 event was historically known but misclassified as a classic nova (Duerbeck 1988), while the 1956 outburst was only discovered after the 1989 X-ray outburst, by inspection of earlier photographic plates (Richter 1989). Our group obtained optical spectroscopy from the 1989 and 2015 events (see Casares et al. 1991, MD16 and Muñoz-Darias et al. 2017).

The most recent outbursts (June and December 2015) were studied through an intensive spectro-photometric campaign led by our team, including simultaneous X-ray, radio and optical observations. We define the start of the June event at MJD = 57190.0 (2015 June 17, 00:00 UT);

any temporal reference is defined relative to this initial time. Our results (MD16, Muñoz-Darias et al. 2017) revealed the discovery of two outflow-features:

- P-Cygni profiles: P-Cygni features are typically observed in massive stars (in fact, they were first observed in the star P Cygni). These are associated with the presence of stellar winds expelling material away from the star. The material moving towards the observer produces a net absorption at blue-shifted wavelengths, while gas receding from the observer produces an excess of flux at red-shifted wavelengths. We observed this particular spectral shape, known as a P-Cygni profile (see Fig. 6.1) in several H and He I lines during the outburst of V404 Cygni, revealing the presence of a wind with a terminal velocity of up to  $\sim 3000 \text{ km s}^{-1}$ . Our analysis revealed not only the ubiquitous presence of winds throughout the entire outburst, but its simultaneity with the radio jet emission. A rough estimation of the total amount of material ejected during the outburst in the form of this cold wind returns similar values to that of the accreted mass, suggesting that the accretion process is actually regulated by the wind.

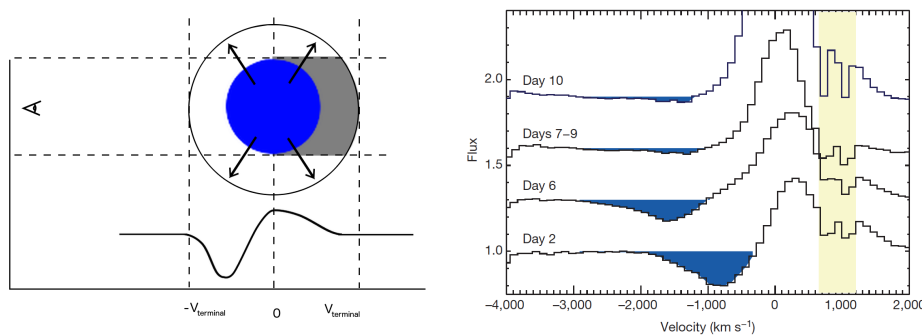


FIGURE 6.1— Left panel: diagram of the P-Cygni profile formation by a spherical expanding shell of material ejected from a hot, central source. Right panel: P-Cygni profiles observed in different days (2, 6, 7–9 and 10) during the outburst of V404 Cygni superimposed on the He I 5876 Å emission line. Yellow shading indicates regions contaminated by the Na I interstellar absorption doublet. From MD16.

- Nebular phase: after the peak of the outburst, the decay of the continuum flux was not linearly followed by the emission lines. The hydrogen Balmer series became relatively narrow, but with very extended wings. In particular, the H $\alpha$  line exhibited extreme equivalent widths (EWs, see below) and high Balmer decrements (BDs), which indicates the presence of an optically-thin nebula that contributes to the emission line as it cools, expands and the ionised hydrogen recombines (see Fig. 6.2).

In this chapter, we exploit the full spectroscopic optical database gathered by our team and collaborators during the June 2015 event with different telescopes and instruments. The obtained 651 spectra conform the most extensive optical data set of a BH XRT in outburst to date.

Este documento incorpora firma electrónica, y es copia auténtica de un documento electrónico archivado por la ULL según la Ley 39/2015.  
Su autenticidad puede ser contrastada en la siguiente dirección <https://sede.ull.es/validacion/>

Identificador del documento: 970342

Código de verificación: pkuTTaUi

Firmado por: DANIEL MATA SÁNCHEZ  
UNIVERSIDAD DE LA LAGUNA

Fecha: 29/06/2017 10:41:42

JORGE CASARES VELAZQUEZ  
UNIVERSIDAD DE LA LAGUNA

29/06/2017 11:14:09

TEODORO MUÑOZ DARIAS  
UNIVERSIDAD DE LA LAGUNA

29/06/2017 12:50:38

ERNESTO PEREDA DE PABLO  
UNIVERSIDAD DE LA LAGUNA

04/07/2017 18:28:11

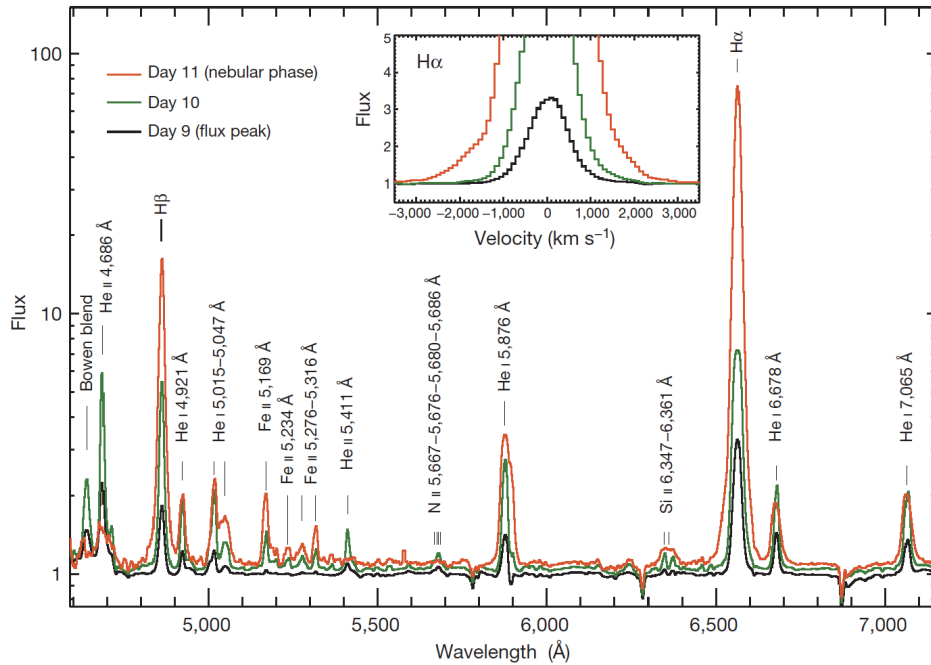


FIGURE 6.2— Averaged normalised spectra of V404 Cygni during the June 2015 outburst, corresponding to days 9 to 11. A logarithmic scale has been used to represent the extreme H $\alpha$  variation during the nebular phase (zoomed in the inset). Note that, because of the logarithmic scale, emission lines in the nebular phase seem broader than the rest but their FWHM values are actually smaller. An offset of 0.1 and 0.2 has been added to the day 10 and day 11 spectra, respectively.

## 6.2 Observations

We present the analysis of a total of 651 optical spectra covering the June 2015 outburst. The observation log is shown in Tab. 6.1 and 6.2. The telescopes used in this campaign are located at the Roque de Los Muchachos observatory (La Palma, Spain): Gran Telescopio Canarias (GTC) equipped with the Optical System for Imaging and low-Intermediate-Resolution Integrated Spectroscopy (OSIRIS); William Herschel Telescope (WHT) with the Intermediate dispersion Spectrograph and Imaging System (ISIS) attached; Nordic Optical Telescope (NOT), equipped with the Andalucia Faint Object Spectrograph and Camera (ALFOSC) and the Fibre-fed Echelle Spectrograph (FIES); and the Isaac Newton Telescope (INT) with the Intermediate Dispersion Spectrograph (IDS) attached.

This heterogeneous database has been reduced using semiautomatic routines developed by

Este documento incorpora firma electrónica, y es copia auténtica de un documento electrónico archivado por la ULL según la Ley 39/2015.  
Su autenticidad puede ser contrastada en la siguiente dirección <https://sede.ull.es/validacion/>

Identificador del documento: 970342

Código de verificación: pkuTTaUi

Firmado por: DANIEL MATA SÁNCHEZ  
UNIVERSIDAD DE LA LAGUNA

Fecha: 29/06/2017 10:41:42

JORGE CASARES VELAZQUEZ  
UNIVERSIDAD DE LA LAGUNA

29/06/2017 11:14:09

TEODORO MUÑOZ DARIAS  
UNIVERSIDAD DE LA LAGUNA

29/06/2017 12:50:38

ERNESTO PEREDA DE PABLO  
UNIVERSIDAD DE LA LAGUNA

04/07/2017 18:28:11

our team and based on IRAF<sup>1</sup>, PYTHON and MOLLY<sup>2</sup>. Each spectrum has been de-biased and flat-field corrected. For those exposures with two objects in the slit (when possible, the slit was rotated to include a field star simultaneously to V404 Cygni), a low-order spline function correction was applied along the spatial direction to account for large scale variability in the illumination. Individual arc spectra were extracted from the two-dimensional images at each object position (i.e. two different positions when the comparison star was present in the slit). Interpolated values from arcs obtained before and after the observation were used to obtain a precise wavelength calibration (when not available, the nearest arc was selected). The wavelength calibration was refined by comparing the observed position of sky emission lines with their corresponding rest wavelengths, from which we derived sub-pixel velocity drifts that were used to correct for mechanical flexure effects. Finally, the Earth relative velocity at the different epochs was also corrected from the spectra.

To obtain a reliable flux calibration, the spectra were initially calibrated relative to the comparison star included in the slit. The bright field star USNO-B1.0 1238-00435227 was employed during the most luminous phases of the outburst, while USNO-A2.0 1200-15039207 was used for the longer exposures, when the flux of V404 Cygni had dropped significantly. The spectra of both field stars were carefully flux-calibrated relative to the spectrophotometric standard star Wolf 1346 (Koen et al. 2010), and this absolute flux calibration was propagated to the whole database. A total of 622 spectra were observed under this configuration and therefore flux-calibrated. These were finally de-reddened using MOLLY routines and a reddening value of  $E(B - V) = 1.3$  (Chen, Shrader & Livio 1997, obtained during quiescence). Every flux-related measurement quoted in this work has been extracted from these final, unabsorbed spectra. We note, however, that additional absorption components (e.g. outflows) are present in the outburst data.

### 6.3 Methods

The emission lines present in the spectra vary significantly along the outburst. To study their evolution, and despite the different wavelength coverage of each instrument, we aimed at measuring parameters in a uniform way, as follows:

- EW: it is defined as the width (in Å) of a rectangle with area equal to that of a given spectral line, and height equal to unity. Therefore, it is measured on normalised spectra. Contrary to the usual convention, we defined EW as positive for emission features.
- Line flux: we measure the integrated flux of each emission line of the spectra after subtracting the continuum. This parameter is only available for flux-calibrated spectra.
- Unabsorbed  $r'$  magnitude: only the SDSS (Sloan Digital Sky Survey, Abazajian et al. 2009)  $r'$ -band is fully covered in a sufficient number of spectra to trace the outburst evolution. We multiplied every spectrum that covers the wavelength range  $\sim 5400 - 7100$  Å by the

<sup>1</sup>IRAF is distributed by the National Optical Astronomy Observatories, operated by the Association of Universities for Research in Astronomy, Inc., under contract with the National Science Foundation.

<sup>2</sup>MOLLY software developed by T. R. Marsh.

SDSS filter transmission profile of the  $r'$ -band filter. Given that the spectra are calibrated in flux density, we obtain the  $r'$ -band flux density using:

$$f_{r'} = \frac{\sum_{\nu} S_{\nu} \cdot T(r')_{\nu}}{\sum_{\nu} T(r')_{\nu}}$$

where  $S_{\nu}$  is the original spectrum flux density,  $T(r')_{\nu}$  is the transmission filter flux density (arbitrarily normalised, given that we include a normalisation factor in this expression) and  $f_{r'}$  the total flux density in the  $r'$ -band.

The correction between the SDSS  $r'$  magnitude and  $r'_{AB}$  is negligible (lower than 0.01, see Bohlin, Dickinson & Calzetti 2001). Therefore, we can directly apply the conversion between SDSS AB magnitudes and physical fluxes, where the zero-point flux density is defined to be 3631 Jy in every filter. This finally results in  $r'_{AB}$  (i.e.  $r'$ ) values for each flux calibrated spectrum. The quiescent observed magnitudes of V404 Cygni are:  $V = 18.42 \pm 0.02$ ,  $B = 20.63 \pm 0.05$  (Casares et al. 1993), which correspond to unabsorbed magnitudes of  $V = 14.26$  and  $B = 15.17$  (assuming the interstellar reddening law  $A_V = 3.2 E(B - V) = 4.16$  from Schild 1977). This implies an unabsorbed  $r' = 14.0 \pm 0.3$  quiescent magnitude (Jester et al. 2005), where the uncertainty reflects the optical variability observed in quiescence (Pavlenko et al. 1996). We note that all the unabsorbed  $r'$ -band magnitudes presented in this work are related to the observed  $r'$ -band magnitudes as:  $r' = r'_{obs} - 3.6$ .

- Gaussian fit: we fitted every emission line present in the spectra with a single Gaussian with height, full-width-at-half-maximum (FWHM) and velocity offset as free parameters. For every spectrum, the same fitting mask was applied to every particular line. For those lines with strong P-Cygni profiles and/or broad, extended wings (e.g. H $\alpha$ , He I 5876 Å), the applied mask was always wide enough to include them. We note that the H $\alpha$  FWHM measurements shown in this chapter have already been deconvolved from the instrumental resolution, measured on nearby sky lines for each instrumental configuration.
- Search for outflows: the most prominent P-Cygni profiles are observed in He I 5875.6 Å (He I-5876), while H $\alpha$  (the most intense line in the whole spectrum) sits on extended wings ( $\pm 3000 \text{ km s}^{-1}$ ) during the nebular phase. In order to detect outflows in these lines, we subtracted the Gaussian fit described above from the original spectra, keeping the normalised continuum level. We then measured the EW of the blue (-4000 to -1000  $\text{km s}^{-1}$ ) and red (1000 to 4000  $\text{km s}^{-1}$ ) halves of the residual to search for outflows. These are called EW blue and red excesses, respectively.

Este documento incorpora firma electrónica, y es copia auténtica de un documento electrónico archivado por la ULL según la Ley 39/2015.  
Su autenticidad puede ser contrastada en la siguiente dirección <https://sede.ull.es/validacion/>

Identificador del documento: 970342

Código de verificación: pkuTTaUi

Fecha: 29/06/2017 10:41:42

Firmado por: DANIEL MATA SÁNCHEZ  
UNIVERSIDAD DE LA LAGUNA

JORGE CASARES VELAZQUEZ  
UNIVERSIDAD DE LA LAGUNA

TEODORO MUÑOZ DARIAS  
UNIVERSIDAD DE LA LAGUNA

ERNESTO PEREDA DE PABLO  
UNIVERSIDAD DE LA LAGUNA

29/06/2017 11:14:09

29/06/2017 12:50:38

04/07/2017 18:28:11

#### 6.4 Results and discussion

We analysed the observed data set in a systematic way by measuring similar parameters on each spectrum. Their evolution through the event, as well as their correlations are presented in this section.

##### Evolution of the H $\alpha$ line

The H $\alpha$  line is the most intense optical emission line in almost every LMXB spectrum. Therefore, its analysis provides valuable results that can be compared with those from many other LMXBs in outburst.

###### *The nebular loops*

We first represent the EW versus the  $r'$ -band magnitude (see left panel of Fig. 6.3). There is an initial rise of the continuum flux, starting from the earlier phases of the outburst to the peak luminosities (days 1 to 9) with typical EWs in the range  $\sim 50\text{--}200\text{\AA}$ . The decay to quiescence is preceded by the so-called nebular phase (days 10 – 13), characterised by a dramatic drop in the continuum flux, and intense and a relatively narrow H $\alpha$  line (peaking  $\sim 100$  times above the continuum level) with extended wings (up to  $\pm \sim 3000\text{ km s}^{-1}$ ). This results in extremely large EWs (1000–2000  $\text{\AA}$ , see Fig. 6.3). After this stage, the system slowly returns to quiescent levels (defined by  $r' \sim 14$ ,  $\text{EW} = 19.0 \pm 5.2$ ; Casares 2015) over a timescale of  $\sim 40$  days (on day 41, the EW and  $r'$ -band magnitude are consistent with quiescence within  $2\sigma$ ). This evolution draws a clockwise loop pattern in the EW- $r'$  diagram, due to the presence of the nebular phase. Such a pattern is observed in the evolution of several parameters during the outburst, and will be referred to hereafter as the *nebular loop*.

The H $\alpha$  line flux (Fig. 6.3, right panel) follows a similar nebular loop. The decay of the H $\alpha$  flux during the nebular phase occurs at a slower rate than that of the continuum, exhibiting H $\alpha$  fluxes similar to those observed at much brighter outburst phases ( $\Delta r' \sim 3$ ). In fact, during the nebular phase (day 11: largest EW values), the contribution of this single line produces  $\sim 70\%$  of the integrated flux over the whole  $r'$ -band. This suggests that the main contribution to the emission line during this phase is not the accretion disc, but a cooling, expanding nebula (see MD16).

A similar nebular loop is seen when plotting the EW versus the H $\alpha$  line flux, as shown in Fig. 6.4 (top panel). When looking at this relation on a day-by-day basis, we also find smaller clockwise nebular loops in days 2 and 6 (see Fig. 6.4, lower panels). The timescales of these shorter loops are  $\sim 30\text{--}60$  min (when EW increases from 50 to 200  $\text{\AA}$ ), and they are observed simultaneously to the deepest P-Cygni profiles detected in the reference line He I-5876 throughout the outburst (see MD16).

Este documento incorpora firma electrónica, y es copia auténtica de un documento electrónico archivado por la ULL según la Ley 39/2015.  
Su autenticidad puede ser contrastada en la siguiente dirección <https://sede.ull.es/validacion/>

Identificador del documento: 970342

Código de verificación: pkuTTaUi

Fecha: 29/06/2017 10:41:42

Firmado por: DANIEL MATA SÁNCHEZ  
UNIVERSIDAD DE LA LAGUNA

JORGE CASARES VELAZQUEZ  
UNIVERSIDAD DE LA LAGUNA

TEODORO MUÑOZ DARIAS  
UNIVERSIDAD DE LA LAGUNA

ERNESTO PEREDA DE PABLO  
UNIVERSIDAD DE LA LAGUNA

29/06/2017 11:14:09

29/06/2017 12:50:38

04/07/2017 18:28:11

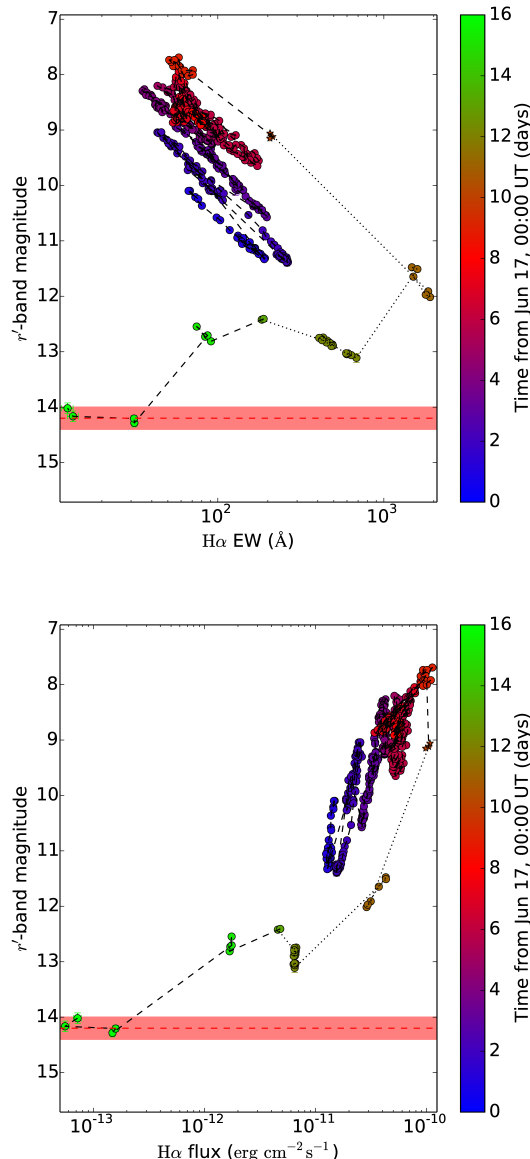


FIGURE 6.3— Top: EW of the H $\alpha$  line versus de-reddened  $r'$ -band magnitude. Bottom: H $\alpha$  line flux versus de-reddened  $r'$ -band magnitude. The quiescent magnitude is depicted as a red line, with a shaded region for the conservative 0.3 mag uncertainty. Colour bars refer to the observation date in days. From day 16 onwards, all the points have the same green colour. Star-shaped points refer to those where H $\alpha$  saturated the detector. The black-dashed line connects the consecutive points to depict the temporal evolution. In order to remarke those corresponding to the nebular phase (days 10–13) they have been conected with a black-dotted line.

Este documento incorpora firma electrónica, y es copia auténtica de un documento electrónico archivado por la ULL según la Ley 39/2015.  
Su autenticidad puede ser contrastada en la siguiente dirección <https://sede.ull.es/validacion/>

Identificador del documento: 970342

Código de verificación: pkuTTaUi

Firmado por: DANIEL MATA SÁNCHEZ  
UNIVERSIDAD DE LA LAGUNA

Fecha: 29/06/2017 10:41:42

JORGE CASARES VELAZQUEZ  
UNIVERSIDAD DE LA LAGUNA

29/06/2017 11:14:09

TEODORO MUÑOZ DARIAS  
UNIVERSIDAD DE LA LAGUNA

29/06/2017 12:50:38

ERNESTO PEREDA DE PABLO  
UNIVERSIDAD DE LA LAGUNA

04/07/2017 18:28:11

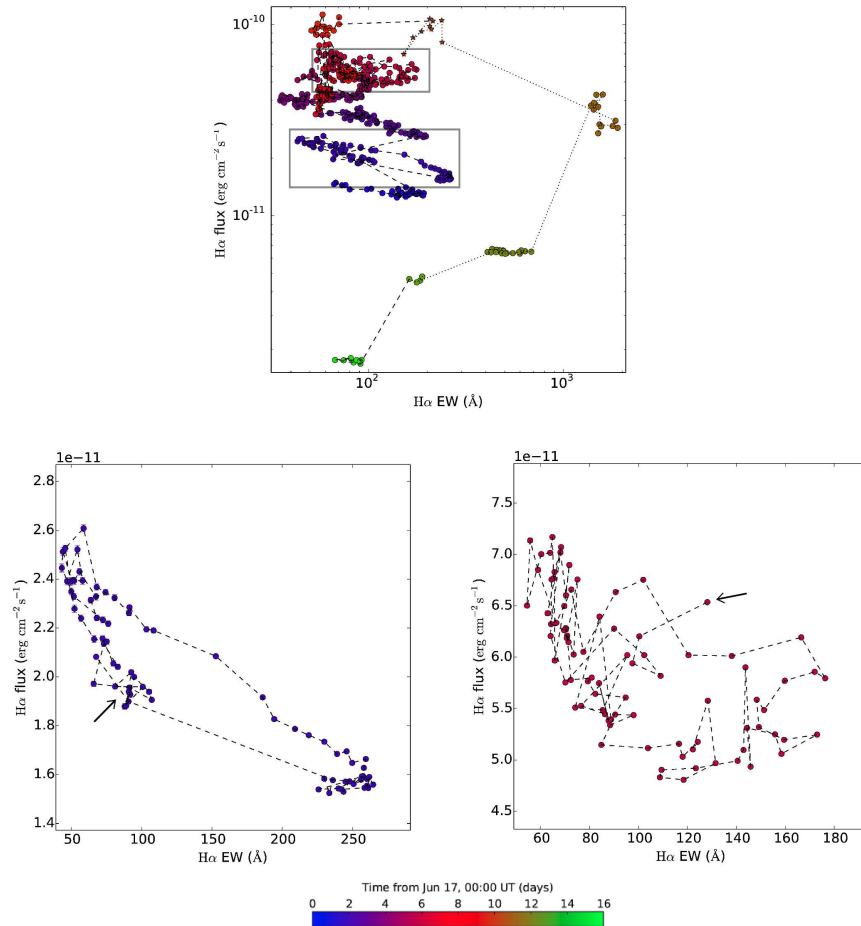


FIGURE 6.4— Top panel: EW versus flux for the H<sub>α</sub> line. The colour bar refers to the observation date in days. Only observations up to day 15 are depicted. As in Fig. 6.3, star-shaped points refer to those where H<sub>α</sub> saturated the detector. Bottom panels: zoom-in of top-left panel for days 2 (left) and day 6 (right), both marked by squares in the full diagram. The starting observation on each day has been marked with an arrow.

Este documento incorpora firma electrónica, y es copia auténtica de un documento electrónico archivado por la ULL según la Ley 39/2015.  
Su autenticidad puede ser contrastada en la siguiente dirección <https://sede.ull.es/validacion/>

Identificador del documento: 970342

Código de verificación: pkuTTaUi

Fecha: 29/06/2017 10:41:42

Firmado por: DANIEL MATA SÁNCHEZ  
UNIVERSIDAD DE LA LAGUNA

JORGE CASARES VELAZQUEZ  
UNIVERSIDAD DE LA LAGUNA

TEODORO MUÑOZ DARIAS  
UNIVERSIDAD DE LA LAGUNA

ERNESTO PEREDA DE PABLO  
UNIVERSIDAD DE LA LAGUNA

29/06/2017 11:14:09

29/06/2017 12:50:38

04/07/2017 18:28:11

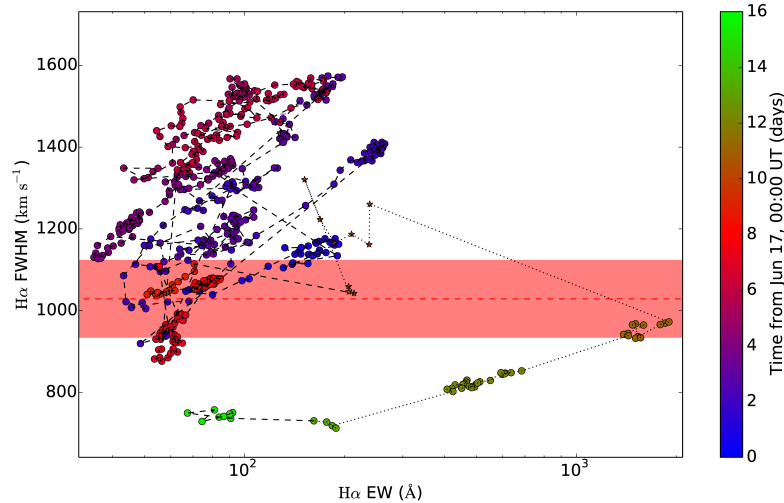


FIGURE 6.5— EW versus FWHM for the H $\alpha$  line. The colour bar refers to the observation date in days. Only observations up to day 15 are depicted. As in Fig. 6.3, star-shaped points refer to those where H $\alpha$  saturated the detector.

#### *The evolution of the FWHM*

A Gaussian fit to the H $\alpha$  line reveals clear changes in its FWHM. The classic picture considers that, during an outburst, the FWHM decreases as the disc expands and reaches areas of lower Keplerian velocities. However, during the initial and most active phases of the outburst, the FWHM of V404 Cygni is systematically larger than the quiescent value FWHM =  $1029 \pm 94$  km s $^{-1}$  (Casares 2015), as we show in Fig. 6.5. This unexpected increase in the FWHM can be explained if we consider that the nebular phase contributes to the emission line all through the outburst. Only at the end of the nebular phase, and for 9 days (from day 12 to 21) the FWHM drops below the quiescent level. However, the line flux remains high even if the continuum drops, so this cannot be a fully disc-dominated state, but still contaminated by the expanding nebula.

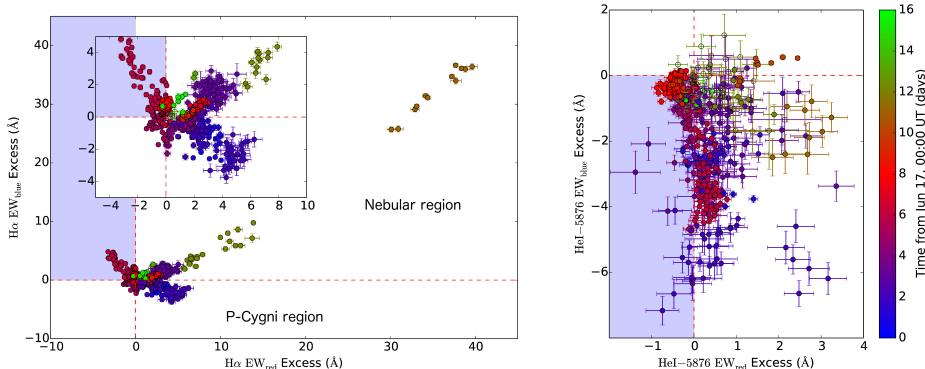


FIGURE 6.6— Left panel: EW excess (red vs blue halves) of the H $\alpha$  line residual after a Gaussian subtraction. The inset depicts a zoom in the figure. Those spectra where H $\alpha$  saturated the detector have been omitted. Right panel: analogous diagram for the He I-5876 line residuals. Only observations up to day 15 are shown. The colour bar refers to the observing date. Regions containing biased points (i.e. contaminated by other nearby line transitions) are marked with a blue shadow.

#### Search for outflows

In order to search for the presence of outflows, we subtracted the initial Gaussian fit to the H $\alpha$  line from every spectrum and studied the residuals. The EW excess of the two velocity halves, as defined in the previous section (blue and red, hereafter), can be used to classify the spectra in different groups (Fig. 6.6, left panel). A blue absorption combined with a red excess reveals the presence of P-Cygni profiles (e.g. day 2), while excess in both the blue and red halves are characteristic of the nebular phase (e.g. days 10–13). We note that the blue-shadowed region of the diagram (blue excess and red absorption) is populated by day 6 spectra. While the blue excess is not troubling (it marks the presence of the nebular phase), the red absorption is intriguing. After visual inspection of these spectra, we found the origin of this red absorption in the intense P-Cygni profiles of the nearby He I line at 6678.149 Å (see Fig. 6.7, left panel), which achieves in this day the maximum terminal velocity observed ( $3000 \text{ km s}^{-1}$ ) and contaminates the red excess of H $\alpha$ . The rest of the spectra are compatible with null excess in both the blue and red halves of H $\alpha$  (therefore, Gaussian profiles).

The same analysis was applied to He I-5876 line, which exhibits the most prominent P-Cygni profiles throughout the outburst. We note here that the mask defining the red ( $1250$  to  $4000 \text{ km s}^{-1}$ ) and blue ( $-500$  to  $-4000 \text{ km s}^{-1}$ ) halves is different from the one used for H $\alpha$ . This is due to both its narrower profile and the presence of an interstellar absorption (Na I  $5890 - 5896 \text{ Å}$ ; see Fig. 6.1). We note that this interstellar feature was masked when fitting the Gaussian. The resulting EW excess diagram (Fig. 6.6, right panel) reveals the deep blue absorptions (up to  $7 \text{ Å}$ ) of P-Cygni profiles (blue absorption and red emission). The nebular phase region (blue and red excess) is almost empty, with the remarkable exception of day 10 [between the peak of the outburst (day 9) and the main nebular phase event (day 11)]. We note

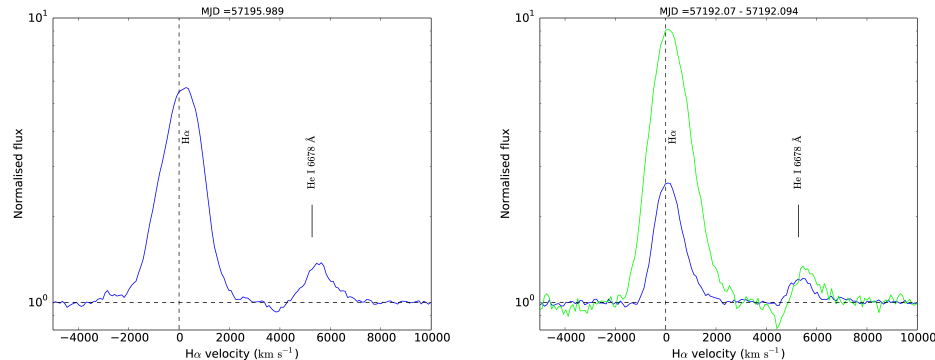


FIGURE 6.7— Left: individual spectra obtained in day 6 during the deepest P-Cygni profiles in He I lines. There is a P-Cygni absorption in He I 6678.149 Å, which contaminates the red wing of H<sub>α</sub>. Right: individual spectra obtained during a flare in day 2, corresponding to the peak (blue) and decay (green) of the flare. Note that the P-Cygni in He I 6678.149 Å has lower terminal velocities than in day 6, and does not affect the red wing of H<sub>α</sub>.

that the red excess is always underestimated (due to the interstellar band mentioned before) and produces the misplacement of some values in the blue-shaded region (red absorptions). The remaining spectra are compatible with null excess in both the blue and red halves of He I-5876 (therefore, Gaussian profiles).

Este documento incorpora firma electrónica, y es copia auténtica de un documento electrónico archivado por la ULL según la Ley 39/2015.  
*Su autenticidad puede ser contrastada en la siguiente dirección <https://sede.ull.es/validacion/>*

Identificador del documento: 970342

Código de verificación: pkuTTaUi

Firmado por: DANIEL MATA SÁNCHEZ  
 UNIVERSIDAD DE LA LAGUNA

Fecha: 29/06/2017 10:41:42

JORGE CASARES VELAZQUEZ  
 UNIVERSIDAD DE LA LAGUNA

29/06/2017 11:14:09

TEODORO MUÑOZ DARIAS  
 UNIVERSIDAD DE LA LAGUNA

29/06/2017 12:50:38

ERNESTO PEREDA DE PABLO  
 UNIVERSIDAD DE LA LAGUNA

04/07/2017 18:28:11

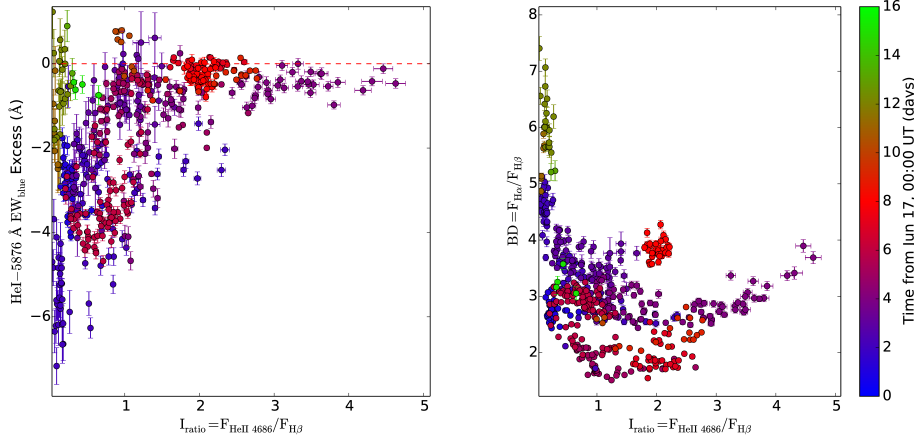


FIGURE 6.8— Left panel:  $I_{\text{ratio}}$  vs EW excess (blue half) of the He I-5876 line. Right panel: BD vs  $I_{\text{ratio}}$ . The colour bar defines the observation date. Only observations up to day 15 are depicted. Star-shaped points refer to those where H $\alpha$  saturated the detector.

#### Ionisation ratio and Balmer decrement

To trace the ionisation state of the outer disc, we computed the ionisation ratio ( $I_{\text{ratio}}$ ), defined as the flux ratio of He II 4685.8 Å (He II-4686) to H $\beta$ . When compared with the presence of P-Cygni profiles in the He I-5876 line, we find these are deeper for low  $I_{\text{ratio}}$  values (see Fig. 6.8, left panel). This implies that the ionising SED affecting the outer disc is also ionising the optical wind, thus preventing the observation of neutral P-Cygni absorptions. However, we find that a low  $I_{\text{ratio}}$  is not a sufficient condition to observe P-Cygni profiles. In particular, the main nebular phase event (day 11) occurs at  $I_{\text{ratio}} < 0.15$ , and does not show the presence of deep blue absorptions in He I-5876. This is due to the dominance of the broad wings associated to the nebula, which compensates for the blue absorption and it even rises a blue excess in the line (day 12). Besides, during the nebular phase the outflows gradually become optically thin as the flux decreases, diminishing the P-Cygni absorptions.

On the other hand, the Balmer decrement (BD), defined as the flux ratio of H $\alpha$  to H $\beta$ , varies greatly during the outburst (see Fig. 6.8, right panel). Typical values during the initial phase of the outburst are BD  $\sim 2 - 4$ , but during the main nebular phase (days 10–13) it reaches unprecedentedly high values (BD  $\sim 5 - 7$ ). These extreme values are similar to those observed in expanding nova shells during some stages (e.g. Iijima & Esenoglu 2003). This kind of event also exhibits emission lines from other atomic species such as Fe II and Si II, which are present in our nebular spectra as well (see Fig. 6.2). These transitions are also found in massive stars surrounded by low excitation nebulosities (e.g. Thackeray 1977).

Este documento incorpora firma electrónica, y es copia auténtica de un documento electrónico archivado por la ULL según la Ley 39/2015.  
Su autenticidad puede ser contrastada en la siguiente dirección <https://sede.ull.es/validacion/>

Identificador del documento: 970342

Código de verificación: pkuTTaUi

Fecha: 29/06/2017 10:41:42

Firmado por: DANIEL MATA SÁNCHEZ  
UNIVERSIDAD DE LA LAGUNA

JORGE CASARES VELAZQUEZ  
UNIVERSIDAD DE LA LAGUNA

TEODORO MUÑOZ DARIAS  
UNIVERSIDAD DE LA LAGUNA

ERNESTO PEREDA DE PABLO  
UNIVERSIDAD DE LA LAGUNA

29/06/2017 11:14:09

29/06/2017 12:50:38

04/07/2017 18:28:11

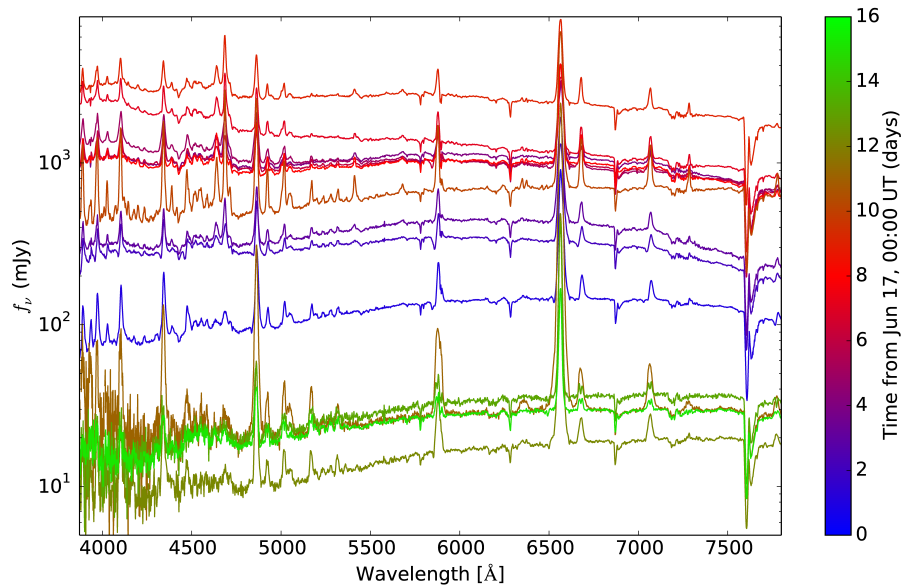


FIGURE 6.9—Day-averaged, flux-calibrated spectra, covering days 1 to 15 (except day 14). The colour bar marks the observation day. The flux density axis is in logarithmic scale to cover the extended range of flux variations.

#### The overall spectral evolution

We were able to follow the June 2015 outburst of V404 Cygni from day 1 to 15 (except day 14) with the same instrumental configuration (GTC+OSIRIS, R1000B; see Tab. 6.1).

The evolution of the flux-calibrated, day-averaged spectra reveals the extreme changes taking place in the system through the entire outburst (see Fig. 6.9). This contains dramatic changes in the line profiles, including P-Cygni features (Fig. 6.10, 6.11), broad emission line wings (Fig. 6.12) and double peaks (Fig. 6.13). The continuum exhibits changes both in flux density ( $\sim 10 - 3000$  mJy) and spectral slope (see Fig. 6.11).

When possible, we also analysed the evolution of the system within one day, using high time resolution data (one spectrum every 84 s), and found remarkable variations within our 0.5–2 h observing blocks. A day-by-day summary of the outburst evolution follows:

- On day 1, we observe a decay of more than 1 mag (i.e.  $r' = 10.2 - 11.4$ ) in  $\sim 1$  h, which suggests the presence of a flare before the observation started. The He I-5876 emission line (the most prolific in the exhibition of P-Cygni profiles along the outburst) exhibits P-Cygnis which become shallower (blue absorption depth of 3 – 12%) as the

Este documento incorpora firma electrónica, y es copia auténtica de un documento electrónico archivado por la ULL según la Ley 39/2015.  
Su autenticidad puede ser contrastada en la siguiente dirección <https://sede.ull.es/validacion/>

Identificador del documento: 970342

Código de verificación: pkuTTaUi

Fecha: 29/06/2017 10:41:42

Firmado por: DANIEL MATA SÁNCHEZ  
UNIVERSIDAD DE LA LAGUNA

JORGE CASARES VELAZQUEZ  
UNIVERSIDAD DE LA LAGUNA

TEODORO MUÑOZ DARIAS  
UNIVERSIDAD DE LA LAGUNA

ERNESTO PEREDA DE PABLO  
UNIVERSIDAD DE LA LAGUNA

29/06/2017 11:14:09

29/06/2017 12:50:38

04/07/2017 18:28:11

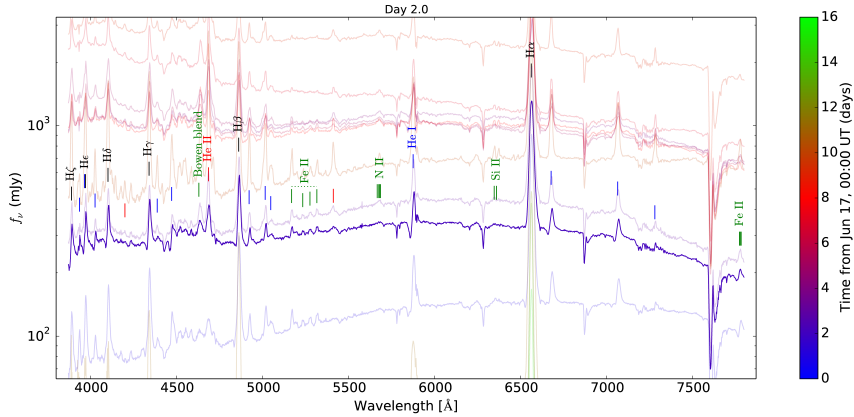


FIGURE 6.10— Same as Fig. 6.9 but focused on day 2 (the remaining spectra are plotted in the background), as it is the best example of P-Cygni profiles. The emission lines are marked with coloured lines: black for H, blue for He I, red for He II and green for other species (Si II, N II, Fe II and the Bowen blend).

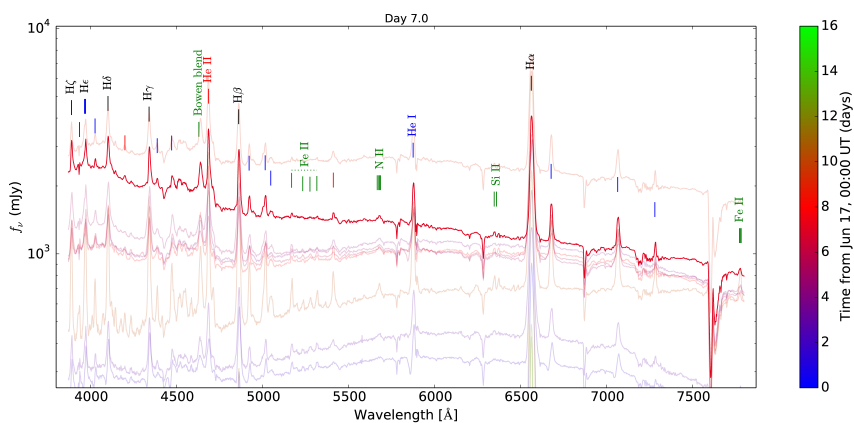


FIGURE 6.11— Same as Fig. 6.9 but focused on day 7.

Este documento incorpora firma electrónica, y es copia auténtica de un documento electrónico archivado por la ULL según la Ley 39/2015.  
Su autenticidad puede ser contrastada en la siguiente dirección <https://sede.ull.es/validacion/>

Identificador del documento: 970342

Código de verificación: pkuTTaUi

Fecha: 29/06/2017 10:41:42

Firmado por: DANIEL MATA SÁNCHEZ  
UNIVERSIDAD DE LA LAGUNA

JORGE CASARES VELAZQUEZ  
UNIVERSIDAD DE LA LAGUNA

TEODORO MUÑOZ DARIAS  
UNIVERSIDAD DE LA LAGUNA

ERNESTO PEREDA DE PABLO  
UNIVERSIDAD DE LA LAGUNA

29/06/2017 11:14:09

29/06/2017 12:50:38

04/07/2017 18:28:11

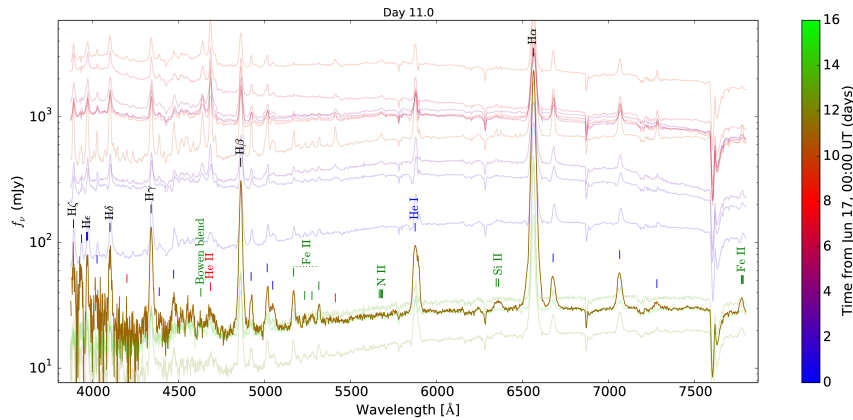


FIGURE 6.12— Same as Fig. 6.9 but focused on day 11, as the best example of nebular emission.

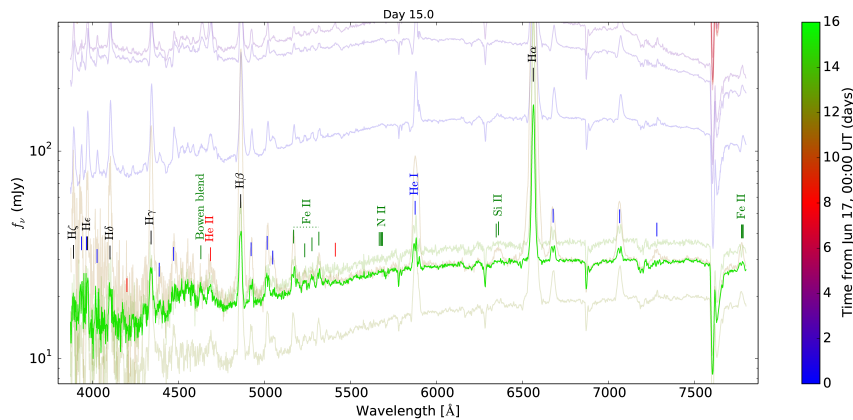


FIGURE 6.13— Same as Fig. 6.9 but focused on day 15, as the best example of double-peaked profiles (except for H $\alpha$  and H $\beta$ ).

Este documento incorpora firma electrónica, y es copia auténtica de un documento electrónico archivado por la ULL según la Ley 39/2015.  
Su autenticidad puede ser contrastada en la siguiente dirección <https://sede.ull.es/validacion/>

Identificador del documento: 970342

Código de verificación: pkuTTaUi

Firmado por: DANIEL MATA SÁNCHEZ  
UNIVERSIDAD DE LA LAGUNA

Fecha: 29/06/2017 10:41:42

JORGE CASARES VELAZQUEZ  
UNIVERSIDAD DE LA LAGUNA

29/06/2017 11:14:09

TEODORO MUÑOZ DARIAS  
UNIVERSIDAD DE LA LAGUNA

29/06/2017 12:50:38

ERNESTO PEREDA DE PABLO  
UNIVERSIDAD DE LA LAGUNA

04/07/2017 18:28:11

continuum flux decreases. Their terminal velocities are in the range  $1500 - 2000 \text{ km s}^{-1}$ . The  $I_{\text{ratio}} = 0.1 - 0.7$  is relatively low, while  $\text{BD} = 2.4 - 3.2$  and the EW of the  $\text{H}\alpha$  line varies between  $\text{EW} = 65 - 195 \text{ \AA}$ , (increasing as the  $r'$ -band brightness becomes fainter).

- Day 2 is characterised by some of the deepest P-Cygni profiles in He I-5876 (blue absorption depth of 8–30%). This observing block covers a full flare, including its rise, peak (shallower P-Cygni) and decay ( $r' = 9.0 - 11.3$ ). The decay from the peak to the lowest flux plateau occurs over similar time scales than in the previous day ( $\sim 1 \text{ h}$ ) despite the drop in flux is  $\sim 3$  times larger. After this decay, the deepest P-Cygnis observed during the outburst are seen. On the other hand, the initial rise seems to be slower than the decay ( $\sim 1 \text{ mag}$  in  $\sim 1 \text{ h}$ ). The ionisation ratio varies between  $I_{\text{ratio}} = 0.03 - 2.5$ , while  $\text{BD} = 0.9 - 5.1$ . A short nebular phase during the decay is observed ( $\text{H}\alpha$  exhibits  $\text{EW} = 40 - 270 \text{ \AA}$ , see Fig. 6.4 bottom-left panel). During this nebular phase (seen in  $\text{H}\alpha$ ), we also find simultaneous P-Cygni profiles in the He I lines, which suggests that the origin of both effects is the shell of expanding material (Fig. 6.6, right panel) produced by the wind.
- Day 3 exhibits a slow rise ( $\sim 1.75 \text{ h}$ ) in the continuum flux  $r' = 10.6 - 8.9$ , where P-Cygnis gradually disappear (no clear detection when  $r' < 9.5$ ). At the same time, He II-4686 and the Bowen blend become stronger, suggesting a higher ionisation of the disc material. Emission lines also exhibit broad wings at the beginning, extending up to  $2500 \text{ km s}^{-1}$  in the  $\text{H}\alpha$  line ( $\text{EW} \sim 200 \text{ \AA}$ ). The line becomes narrower as the flux steadily increases and returns to  $\sim 1500 \text{ km s}^{-1}$  ( $\text{EW} \sim 55 \text{ \AA}$ ), similar to values observed in previous nights. Indeed, excess in both red and blue  $\text{H}\alpha$  emission is measured in this data set (Fig. 6.6, left panel), confirming a faint nebular phase. The ionisation ratio is  $I_{\text{ratio}} = 0.2 - 1.7$ , and the high BD (up to 4.3) also supports this interpretation.
- Day 4 is a brighter version of day 1, exhibiting a slow decay of  $r' = 8.2 - 9.3$  in  $\sim 2 \text{ h}$ . The wings of the  $\text{H}\alpha$  line ( $\text{EW} = 35 - 92 \text{ \AA}$ , lower for higher fluxes) are not particularly broad (similar to day 1), which suggests that a necessary condition for the observation of the nebular phase is a relatively fast drop in flux. The ionisation ratio is  $I_{\text{ratio}} = 1.0 - 4.7$  (i.e. reaching the maximum value of the outburst), while BD is in the range  $2.4 - 4.0$ .
- Day 5 exhibits an initial ( $\sim 0.5 \text{ h}$ ) decay of  $r' = 8.2 - 9.2$ , ending in a plateau. The flux drop is not fast nor deep enough for a faint nebular phase to be observed ( $\text{EW} = 43 - 108 \text{ \AA}$ , lower for higher fluxes). The ionisation ratio is  $I_{\text{ratio}} = 0.6 - 2.6$  and  $\text{BD} = 1.5 - 2.2$  are consistent with the observed weak P-Cygnis in He I-5876 ( $\text{EW}_{\text{blue excess}} < 2.5 \text{ \AA}$ ).
- Day 6 starts with a flare, similar but brighter ( $r' = 8.1 - 9.7$ ) than the one observed in day 2, but with a faster decay ( $\sim 0.25 \text{ h}$ ). After this event, a slow rise analogous to that of day 3 is observed, starting with the nebular phase in  $\text{H}\alpha$  ( $\text{EW} = 53 - 177 \text{ \AA}$ ) which slowly fades as the flux increases. Deep P-Cygnis in He I-5876 (up to  $< 20\%$ ) are observed along the whole spectral set, being weaker at higher fluxes. Their terminal velocities are also higher than in previous days ( $\sim 3000 \text{ km s}^{-1}$ ). The ionisation ratio is  $I_{\text{ratio}} = 0.2 - 1.3$  while  $\text{BD} = 1.9 - 3.3$ .

Este documento incorpora firma electrónica, y es copia auténtica de un documento electrónico archivado por la ULL según la Ley 39/2015.  
Su autenticidad puede ser contrastada en la siguiente dirección <https://sede.ull.es/validacion/>

Identificador del documento: 970342

Código de verificación: pkuTTaUi

Fecha: 29/06/2017 10:41:42

Firmado por: DANIEL MATA SÁNCHEZ  
UNIVERSIDAD DE LA LAGUNA

JORGE CASARES VELAZQUEZ  
UNIVERSIDAD DE LA LAGUNA

TEODORO MUÑOZ DARIAS  
UNIVERSIDAD DE LA LAGUNA

ERNESTO PEREDA DE PABLO  
UNIVERSIDAD DE LA LAGUNA

29/06/2017 11:14:09

29/06/2017 12:50:38

04/07/2017 18:28:11

- Day 7 exhibits some of the faster ( $< 5$  min) but also weaker ( $r' = 7.9 - 8.9$ ) flares. This night is also characterised by a continuum shape significantly redder at the flares peak (see Fig. 6.11); there are flux density variations of  $880 - 1800$  mJy in the H $\alpha$  continuum, and  $2400 - 2800$  mJy near H $\gamma$  (4340.47 Å). Neither P-Cygni in He I-5876 nor the nebular phase in H $\alpha$  are detected through visual inspection. H $\alpha$  EW excesses (both in the red and blue halves) are present, suggesting a faint remaining of the nebular contribution. The ionisation ratio is  $I_{\text{ratio}} = 1.6 - 2.6$  and the Balmer decrement is BD =  $1.5 - 2.6$ .
- Day 8 shows a 1 h plateau at  $r' \sim 8.6 - 8.9$ , with no significant spectral changes. The null excess in the H $\alpha$  line suggests that neither nebular phase nor P-Cygnis are present. The most remarkable feature is the presence of high ionisation ratios  $I_{\text{ratio}} \sim 1.8 - 2.2$ , combined with BD =  $3.5 - 4.3$ .
- Day 9 corresponds to the peak of the outburst at  $r' \sim 7.7 - 8.0$ , but only  $\sim 0.5$  h worth of data were taken. Flares, P-Cygnis or nebular phases are not observed. Again, high ionisation features as the Bowen blend and He II-4686 prevail ( $I_{\text{ratio}} = 1.3 - 2.8$ ). The BD =  $2.0 - 2.8$  and EW of H $\alpha$  (EW =  $50 - 71$  Å), combined with null blue excess and small red excess in that line does not reveal any interesting feature. Similar results are found for He I-5876, where we only detect marginal P-Cygnis (EW<sub>blue excess</sub>  $\gtrsim -0.9$  Å).
- Day 10 corresponds to a transition stage at  $r' \sim 9.1$  at the begining of the main nebular phase event. The exposure time for these spectra was enough to saturate the peak of the H $\alpha$  line, but its broad wings confirm the nebular contribution. The ionisation ratio is  $I_{\text{ratio}} = 1.0 - 1.1$ , while BD >  $2.5 - 2.6$  and H $\alpha$  EW >  $205 - 215$  Å (note that measurements on H $\alpha$  are lower limits due to saturation). Hereafter, we will consider the following thresholds as indicators of the main nebular phase: H $\alpha$  EW  $\gtrsim 100$  Å, BD  $\gtrsim 5$ ,  $I_{\text{ratio}} < 1.2$ ; all these combined with the presence of blue and red excess in the H $\alpha$  line.
- Day 11 shows the highest H $\alpha$  EW values (EW =  $1472 - 1904$  Å) as well as the broadest wings (reaching up to  $\sim 3000$  km s $^{-1}$ , the wind terminal velocity of day 6). This is the result of a strong drop ( $r' \sim 12$ ) in the continuum flux (20 mJy) which is not immediately followed by the H $\alpha$  line flux (2000 mJy peak flux density). This extreme phenomenology is interpreted as caused by the presence of a cooling, expanding nebula (MD16). The ionisation ratio is extremely low  $I_{\text{ratio}} = 0.06 - 0.12$ , while BD =  $4.8 - 5.9$  reaches high values, as expected for hydrogen self-absorption (Drake & Ulrich 1980).
- Day 12 still exhibits nebular phase features in H $\alpha$  (BD =  $5.5 - 7.4$ ), but with lower EW =  $408 - 685$  Å, and narrower wings. On the other hand, the Bowen blend and He II high-excitation lines almost disappear at the lowest fluxes ( $I_{\text{ratio}} = 0.03 - 0.3$ ). Nevertheless, narrow (1500 km s $^{-1}$  terminal velocity) but clear P-Cygni features are present in the He I-5876 line, becoming deeper (up to  $< 15\%$ ) after a faint rebrightening of the system ( $r' = 13.1 - 12.8$ ). This shows that the wind is present even at very low luminosity outburst phases, in agreement with our results from the December 2015 mini outburst (see Muñoz-Darias et al. 2017).

Este documento incorpora firma electrónica, y es copia auténtica de un documento electrónico archivado por la ULL según la Ley 39/2015.  
Su autenticidad puede ser contrastada en la siguiente dirección <https://sede.ull.es/validacion/>

Identificador del documento: 970342

Código de verificación: pkuTTaUi

Fecha: 29/06/2017 10:41:42

Firmado por: DANIEL MATA SÁNCHEZ UNIVERSIDAD DE LA LAGUNA	29/06/2017 11:14:09
JORGE CASARES VELAZQUEZ UNIVERSIDAD DE LA LAGUNA	29/06/2017 12:50:38
TEODORO MUÑOZ DARIAS UNIVERSIDAD DE LA LAGUNA	04/07/2017 18:28:11
ERNESTO PEREDA DE PABLO UNIVERSIDAD DE LA LAGUNA	

- Day 13 to 15: double-peaked profiles appear in several lines, starting with He I (5876Å, 6678Å, 7065Å), and later also in Fe II (forest at 5150 – 5300Å), as the system starts returning to quiescence. Balmer lines remain single-peaked for a few more days. It is interesting to note that double-peaked profiles are observed at brighter  $r'$  magnitudes than on day 12. This is consistent with the interpretation that the nebula contributes to fill up the double peak. The ionisation ratio is  $I_{\text{ratio}} = 0.2$  and BD = 5.3 on day 13; and  $I_{\text{ratio}} = 0.3 - 0.7$  and BD = 3.0 – 3.6 on day 15. The corresponding EWs of H $\alpha$  are EW = 183 – 189 Å (on day 13) and EW = 74 – 91 Å (on day 15), with continuum fluxes of  $r' \sim 12.4$  and  $r' \sim 12.5 - 12.8$ , respectively. The threshold of EW  $\gtrsim 100$  Å and BD  $\gtrsim 5$ , as well as the presence of low blue and red excess in the H $\alpha$  line (EW<sub>excess</sub>  $\sim 1$  Å) on day 13 allow us to set the end of the nebular phase after this day. Despite of double-peaked profiles and low continuum fluxes, the presence of He II shows that there is still accretion activity in the system by day 15 ( $I_{\text{ratio}}$  is similar to day 1).

The summarised version of the outburst day-by-day evolution can be found in Tab. 6.3.

## 6.5 Conclusions and future work

We have presented a very detailed analysis of the spectroscopic campaign performed during the 2015 outburst of V404 Cygni. We find clear outflow signatures throughout the entire outburst. These include P-Cygni profiles (e.g. day 6), nebular phases (day 10–13) and a combination of both. We have constructed several diagrams in which the evolution of these wind-related features can be studied in detail. These would serve as a reference for future observations of BHs in outburst.

The extremely large database obtained for this outburst of V404 Cygni has prevented us from completing the analysis before the publication of this thesis. The complete analysis of the sample, as well as the comparison with both the December 2015 and the historic 1989 discovery outburst of V404 Cygni, will be performed in Mata Sánchez et al. (2017c, in prep.).

Este documento incorpora firma electrónica, y es copia auténtica de un documento electrónico archivado por la ULL según la Ley 39/2015.  
Su autenticidad puede ser contrastada en la siguiente dirección <https://sede.ull.es/validacion/>

Identificador del documento: 970342

Código de verificación: pkuTTaUi

Fecha: 29/06/2017 10:41:42

Firmado por: DANIEL MATA SÁNCHEZ  
UNIVERSIDAD DE LA LAGUNA

JORGE CASARES VELAZQUEZ  
UNIVERSIDAD DE LA LAGUNA

TEODORO MUÑOZ DARIAS  
UNIVERSIDAD DE LA LAGUNA

ERNESTO PEREDA DE PABLO  
UNIVERSIDAD DE LA LAGUNA

29/06/2017 11:14:09

29/06/2017 12:50:38

04/07/2017 18:28:11

## 6.6 Appendix

We present here the observation logs and a summary table with the main characteristics per day of the outburst.

TABLE 6.1— Observation log of the June 2015 outburst, containing 651 spectra (622 of them flux-calibrated). The employed acronyms are detailed below: Gran Telescopio Canarias (GTC), Optical System for Imaging and low-Intermediate-Resolution Integrated Spectroscopy (OSIRIS); William Herschel Telescope (WHT), Intermediate dispersion Spectrograph and Imaging System (ISIS); Nordic Optical Telescope (NOT), Andalucia Faint Object Spectrograph and Camera (ALFOSC), FIbre-fed Echelle Spectrograph (FIES); Isaac Newton Telescope (INT), Intermediate Dispersion Spectrograph (IDS).

Night	Tel./Inst.	Setup	$N_{\text{SPEC}}$	$T_{\text{EXP}} [\text{s}]$	Flux calibration	
2015 Jun 14	WHT/ISIS	R600B	2	600	N	
		R600R	2	600	N	
2015 Jun 15	GTC/OSIRIS	R1000B	1	600	N	
		R2500V	1	600	N	
		R2500I	1	600	N	
2015 Jun 16	NOT/FIES		1	1800	N	
2015 Jun 17	GTC/OSIRIS	R1000B	36	60	Y	
2015 Jun 18	GTC/OSIRIS	R1000B	75	60	Y	
		WHT/ACAM	CLEAR+V400	2	120	Y
		NOT/ALFOSC	Grism 7	2	600	N
		R1000B	75	60	Y	
2015 Jun 20	GTC/OSIRIS	R1000B	75	60	Y	
2015 Jun 21	GTC/OSIRIS	R1000B	40	60	Y	
2015 Jun 22	GTC/OSIRIS	R1000B	85	60	Y	
2015 Jun 23	GTC/OSIRIS	R1000B	36	60	Y	
2015 Jun 24	GTC/OSIRIS	R1000B	36	60	Y	
2015 Jun 25	GTC/OSIRIS	R1000B	17	60	Y	
2015 Jun 26	GTC/OSIRIS	R1000B	3	40	Y	
		R2500V	6	70	Y	
		R2500R	6	70	Y	
		R1000B	6	40	Y	
		R2500V	6	70	Y	
		R2500R	6	70	Y	
2015 Jun 27	GTC/OSIRIS	R1000B	19	20-120 <sup>a</sup>	Y	
		R2500V	3	360	Y	
		R2500R	3	120	Y	
2015 Jun 28	GTC/OSIRIS	R1000B	2	120	Y	
		R2500R	2	120	Y	
2015 Jun 29	GTC/OSIRIS					

<sup>a</sup> The exposure time for each spectrum varies within this range.

Este documento incorpora firma electrónica, y es copia auténtica de un documento electrónico archivado por la ULL según la Ley 39/2015.  
Su autenticidad puede ser contrastada en la siguiente dirección <https://sede.ull.es/validacion/>

Identificador del documento: 970342

Código de verificación: pkuTTaUi

Fecha: 29/06/2017 10:41:42

Firmado por: DANIEL MATA SÁNCHEZ  
UNIVERSIDAD DE LA LAGUNA

JORGE CASARES VELAZQUEZ  
UNIVERSIDAD DE LA LAGUNA

TEODORO MUÑOZ DARIAS  
UNIVERSIDAD DE LA LAGUNA

ERNESTO PEREDA DE PABLO  
UNIVERSIDAD DE LA LAGUNA

29/06/2017 11:14:09

29/06/2017 12:50:38

04/07/2017 18:28:11

TABLE 6.2— Continuation of table 6.1.

Night	Tel./Inst.	Setup	$N_{\text{SPEC}}$	$T_{\text{EXP}} [\text{s}]$	Flux calibration
2015 Jul 01	GTC/OSIRIS	R1000B	4	60-120 <sup>a</sup>	Y
		R2500R	4	60-120 <sup>a</sup>	Y
2015 Jul 04	GTC/OSIRIS	R2500R	2	130	Y
2015 Jul 07	WHT/ISIS	R300B	3	1375-1800 <sup>a</sup>	Y
		R600R	9	430-900 <sup>a</sup>	Y
2015 Jul 12	NOT/ALFOSC	Grism 7	1	900	N
		R300B	5	900	Y
		R600R	10	900	Y
2015 Jul 14	NOT/ALFOSC	Grism 7	2	900	N
2015 Jul 15	NOT/ALFOSC	Grism 7	1	900	N
2015 Jul 18	WHT/ISIS	R300B	3	900-1800 <sup>a</sup>	Y <sup>b</sup>
		R600R	4	900-1800 <sup>a</sup>	Y
2015 Jul 19	WHT/ISIS	R300B	10	900-1800 <sup>a</sup>	Y
		R600R	10	900-1800 <sup>a</sup>	Y
2015 Jul 20	INT/IDS	R632R	6	1800	Y
2015 Jul 21	WHT/ISIS	R300B	5	1800	N
		R600R	6	1800	Y
2015 Jul 27	WHT/ACAM	GG395+V400	2	900	Y
2015 Jul 31	GTC/OSIRIS	R2500R	2	139	Y
2015 Aug 06	WHT/ISIS	R1200R	6	1800	N
		NOT/ALFOSC	Grism 7	2	N
2015 Sep 01	WHT/ISIS	R300B	1	1800	Y
		R600R	2	900	Y
2015 Oct 28	WHT/ACAM	GG395+V400	2	900	Y

<sup>a</sup> The exposure time for each spectrum varies within this range.<sup>b</sup> Some exposures had the field star spectra at the edge of the chip, making flux calibration unreliable.

Este documento incorpora firma electrónica, y es copia auténtica de un documento electrónico archivado por la ULL según la Ley 39/2015.  
*Su autenticidad puede ser contrastada en la siguiente dirección <https://sede.ull.es/validacion/>*

Identificador del documento: 970342

Código de verificación: pkuTTaUi

Firmado por: DANIEL MATA SÁNCHEZ UNIVERSIDAD DE LA LAGUNA	Fecha: 29/06/2017 10:41:42
JORGE CASARES VELAZQUEZ UNIVERSIDAD DE LA LAGUNA	29/06/2017 11:14:09
TEODORO MUÑOZ DARIAS UNIVERSIDAD DE LA LAGUNA	29/06/2017 12:50:38
ERNESTO PEREDA DE PABLO UNIVERSIDAD DE LA LAGUNA	04/07/2017 18:28:11

TABLE 6.3— Summary table with the main characteristics per day of the outburst.

Day	$r'$ -band magnitude	BD	$I_{ratio}$	EW of H $\alpha$ (Å)	Others
1	10.2 – 11.4	2.4 – 3.2	0.1 – 0.7	65 – 195	Slow decay.
2	9.0 – 11.3	0.9 – 5.1	0.03 – 2.5	40 – 270	Full flare, nebular loop and deep P-Cygni.
3	10.6 – 8.9	2.5 – 4.3	0.2 – 1.7	55 – 200	Slow rise.
4	8.2 – 9.3	2.4 – 4.0	1.0 – 4.7	35 – 92	Slow decay.
5	8.2 – 9.2	1.5 – 2.2	0.6 – 2.6	43 – 105	Decay and plateau.
6	8.1 – 9.7	1.9 – 3.3	0.2 – 1.3	53 – 177	Full flare, nebular loop and deep P-Cygni.
7	7.9 – 8.9	1.5 – 2.6	1.6 – 2.6	53 – 67	Fast, red flares.
8	8.6 – 8.9	3.5 – 4.3	1.8 – 2.2	71 – 84	Bright plateau.
9	7.7 – 8.0	2.0 – 2.8	1.3 – 2.8	50 – 71	Flux peak.
10	9.1	> 2.5	1.0 – 1.1	> 205	Nebular phase starts.
11	12.0	4.8 – 5.9	0.06 – 0.12	1472 – 1904	Nebular phase.
12	13.1 – 12.8	5.5 – 7.4	0.03 – 0.3	408 – 685	Nebular phase.
13	12.4 – 11.4	5.3	0.2	183 – 189	Nebular phase ends, double-peaked lines.
15	12.5 – 12.8	3.0 – 3.6	0.3 – 0.7	74 – 91	Double-peaked lines.

Este documento incorpora firma electrónica, y es copia auténtica de un documento electrónico archivado por la ULL según la Ley 39/2015.  
*Su autenticidad puede ser contrastada en la siguiente dirección <https://sede.ull.es/validacion/>*

Identificador del documento: 970342

Código de verificación: pkuTTaUi

Firmado por: DANIEL MATA SÁNCHEZ  
 UNIVERSIDAD DE LA LAGUNA

Fecha: 29/06/2017 10:41:42

JORGE CASARES VELAZQUEZ  
 UNIVERSIDAD DE LA LAGUNA

29/06/2017 11:14:09

TEODORO MUÑOZ DARIAS  
 UNIVERSIDAD DE LA LAGUNA

29/06/2017 12:50:38

ERNESTO PEREDA DE PABLO  
 UNIVERSIDAD DE LA LAGUNA

04/07/2017 18:28:11

Este documento incorpora firma electrónica, y es copia auténtica de un documento electrónico archivado por la ULL según la Ley 39/2015.  
*Su autenticidad puede ser contrastada en la siguiente dirección <https://sede.ull.es/validacion/>*

Identificador del documento: 970342

Código de verificación: pkuTTaUi

Firmado por: DANIEL MATA SÁNCHEZ UNIVERSIDAD DE LA LAGUNA	Fecha: 29/06/2017 10:41:42
JORGE CASARES VELAZQUEZ UNIVERSIDAD DE LA LAGUNA	29/06/2017 11:14:09
TEODORO MUÑOZ DARIAS UNIVERSIDAD DE LA LAGUNA	29/06/2017 12:50:38
ERNESTO PEREDA DE PABLO UNIVERSIDAD DE LA LAGUNA	04/07/2017 18:28:11

---

# 7

---

## Conclusions

**I**N this thesis, we analyse multiwavelength observations of five low-mass X-ray binaries. The application of different techniques has provided new insights into both their dynamical parameters and the relevant accretion-related physical processes at work.

### MAXI J1957+032

- Based on the short duration ( $< 5$  d) and frequent recurrence of its outbursts (4 in  $\sim 16$  months), as well as its featureless optical spectrum, our analysis suggests that the recently discovered X-ray transient MAXI J1957+032 may be a short orbital period low-mass X-ray binary.
- The observed X-ray softening of this source during its decay to quiescence allows us to constrain its distance to  $d < 13$  kpc. This, combined with the non-detection of its quiescent counterpart, points towards a donor star spectral type later than G8.
- After considering the properties of other known X-ray transients, we find similarities with accreting millisecond pulsars, which would place MAXI J1957+032 at  $d \sim 5$  kpc.

### Swift J1357.2-0933

- We use optical spectra obtained with the 10.4-m Gran Telescopio Canarias to constrain the non-stellar contribution to the optical emission in quiescence. This yields more restrictive lower limits to the distance ( $d > 2.29$  kpc) and height over the Galactic plane ( $z > 1.75$  kpc), placing Swift J1357.2-0933 in the Galactic thick disc.
- We detect variability in the H $\alpha$  profile modulated with the orbital period  $P_{\text{orb}} = 0.11 \pm 0.04$  d, confirming the result obtained during the outburst.

- We find that this system harbours one of the most massive black holes known in our Galaxy,  $M_{\text{BH}} > 9.3 M_{\odot}$ . Our analysis favours a mass ratio of  $q \sim 0.04$  and a companion mass of  $M_2 \sim 0.4 M_{\odot}$ .

### Sco X-1

- We perform a Monte Carlo analysis to constrain the dynamical parameters of the prototypical X-ray binary Sco X-1. We obtain the following constraints, at 90 per cent confidence level:

$$M_1 < 1.73 M_{\odot}; \quad 0.28 < q < 0.51; \quad 0.28 M_{\odot} < M_2 < 0.70 M_{\odot}$$

A possible set of parameters would be a canonical neutron star of  $M_1 \sim 1.4 M_{\odot}$ , an orbital inclination of  $i \sim 36^{\circ}$  and a disc opening angle of  $\sim 11^{\circ}$ .

- We present the best near-infrared spectrum of the source to date. Despite the non-detection of donor star features due to the high veiling ( $X > 0.66$ ) in the K-band, our deep observations constrain the spectral type of the donor to be later than K4 and luminosity class IV.

### Aql X-1

- We use near-infrared integral field spectroscopy obtained with an adaptive optics module to single out Aquila X-1 from a nearby field star. These spectra reveal, for the first time, absorption features corresponding to a K4  $\pm$  2 donor, veiled by  $\sim 36$  per cent in the K band, and moving with a radial velocity semi-amplitude of  $K_2 = 136 \pm 4 \text{ km s}^{-1}$ .
- We further refine the ephemeris of the system to  $T_0 = 2455810.387 \pm 0.005 \text{ d}$  and  $P_{\text{orb}} = 0.7895126 \pm 0.0000010 \text{ d}$ . We constrain the orbital inclination to be in the range  $36^{\circ} < i < 47^{\circ}$ .
- Using the de-reddened K-band magnitude and the constraints on the spectral type, we infer a distance to the source of  $d = 6 \pm 2 \text{ kpc}$ .

### V404 Cygni

- We present the most extensive spectroscopic database ever performed on a X-ray transient outburst to the best of our knowledge. It includes 651 spectra (622 of them flux-calibrated) obtained with different telescopes and instruments.

Este documento incorpora firma electrónica, y es copia auténtica de un documento electrónico archivado por la ULL según la Ley 39/2015.  
Su autenticidad puede ser contrastada en la siguiente dirección <https://sede.ull.es/validacion/>

Identificador del documento: 970342

Código de verificación: pkuTTaUi

Fecha: 29/06/2017 10:41:42

Firmado por: DANIEL MATA SÁNCHEZ  
UNIVERSIDAD DE LA LAGUNA

JORGE CASARES VELAZQUEZ  
UNIVERSIDAD DE LA LAGUNA

TEODORO MUÑOZ DARIAS  
UNIVERSIDAD DE LA LAGUNA

ERNESTO PEREDA DE PABLO  
UNIVERSIDAD DE LA LAGUNA

29/06/2017 11:14:09

29/06/2017 12:50:38

04/07/2017 18:28:11

- We find outflows in the form of P-Cygni profiles (wind), as well as broad wings in the emission lines, in particular in H $\alpha$  (nebular phase). The HeI 5876 Å emission line reveals P-Cygnis all through the outburst, at different depths and terminal velocities of 1500 – 3000 km s $^{-1}$ .
- We report on the evolution of the spectral parameters during the outburst. We find *nebular loops* indicating the presence of an expanding nebula through the entire outburst, especially important during the so-called nebular phase on day 11, but also at smaller scale during the flares observed on days 2 and 6.

### Future work

The techniques presented in this thesis will be applied to other LMXBs. In particular, given the great success obtained in Aql X-1, we will use the VLT telescope equipped with SINFONI to spatially resolve the black-hole X-ray transient IGR J17091-3624 from a nearby interloper. We also plan to extend this strategy by studying a number of highly-reddened quiescent X-ray transients in crowded regions of the Galactic plane, selected from the Black-CAT catalogue (Corral-Santana et al. 2016).

We will also exploit the complete V404 Cygni database, including observations of the 2015 December mini-outburst (only 6 months after the June event), as well as spectra obtained during the historic 1989 outburst. The results of this analysis and the comparison between outbursts will be published in Mata Sánchez et al. (2017c, in prep.). We also plan to search for the presence of spectroscopic wind/outflow features in new outburst events of other black-hole transients, and already have approved ToO proposals on 8-m and 10-m class telescopes (VLT, GTC).

Este documento incorpora firma electrónica, y es copia auténtica de un documento electrónico archivado por la ULL según la Ley 39/2015.  
Su autenticidad puede ser contrastada en la siguiente dirección <https://sede.ull.es/validacion/>

Identificador del documento: 970342

Código de verificación: pkuTTaUi

Firmado por: DANIEL MATA SÁNCHEZ  
UNIVERSIDAD DE LA LAGUNA

Fecha: 29/06/2017 10:41:42

JORGE CASARES VELAZQUEZ  
UNIVERSIDAD DE LA LAGUNA

29/06/2017 11:14:09

TEODORO MUÑOZ DARIAS  
UNIVERSIDAD DE LA LAGUNA

29/06/2017 12:50:38

ERNESTO PEREDA DE PABLO  
UNIVERSIDAD DE LA LAGUNA

04/07/2017 18:28:11

Este documento incorpora firma electrónica, y es copia auténtica de un documento electrónico archivado por la ULL según la Ley 39/2015.  
*Su autenticidad puede ser contrastada en la siguiente dirección <https://sede.ull.es/validacion/>*

Identificador del documento: 970342

Código de verificación: pkuTTaUi

Firmado por: DANIEL MATA SÁNCHEZ  
UNIVERSIDAD DE LA LAGUNA

Fecha: 29/06/2017 10:41:42

JORGE CASARES VELAZQUEZ  
UNIVERSIDAD DE LA LAGUNA

29/06/2017 11:14:09

TEODORO MUÑOZ DARIAS  
UNIVERSIDAD DE LA LAGUNA

29/06/2017 12:50:38

ERNESTO PEREDA DE PABLO  
UNIVERSIDAD DE LA LAGUNA

04/07/2017 18:28:11

## Bibliography

- Abadie J., et al., 2011, *Physical Review Letters*, **107**, 271102
- Abazajian K. N., et al., 2009, *ApJS*, **182**, 543
- Applegate J. H., 1992, *ApJ*, **385**, 621
- Armas Padilla M., Degenaar N., Wijnands R., 2013, *MNRAS*, **434**, 1586
- Armas Padilla M., Ueda Y., Hori T., Shidatsu M., Muñoz-Darias T., 2017, *MNRAS*, **467**, 290
- Barthelmy S. D., D'Ai A., D'Avanzo P., Krimm H. A., Lien A. Y., Marshall F. E., Maselli A., Siegel M. H., 2015a, GRB Coordinates Network, [17929](#)
- Barthelmy S. D., Page K. L., Palmer D. M., 2015b, GRB Coordinates Network, [18716](#)
- Belczynski K., Wiktorowicz G., Fryer C. L., Holz D. E., Kalogera V., 2012, *ApJ*, **757**, 91
- Belloni T. M., Motta S. E., Muñoz-Darias T., 2011, Bulletin of the Astronomical Society of India, **39**, 409
- Blaauw A., 1961, Bulletin of the Astronomical Institutes of the Netherlands, **15**, 265
- Bohlin R. C., Dickinson M. E., Calzetti D., 2001, *The Astronomical Journal*, **122**, 2118
- Burderi L., Di Salvo T., Riggio A., Papitto A., Iaria R., D'Aì A., Menna M. T., 2010, *A&A*, **515**, A44
- Cannizzo J. K., Shafter A. W., Wheeler J. C., 1988, *ApJ*, **333**, 227
- Cantrell A. G., Bailyn C. D., McClintock J. E., Orosz J. A., 2008, *ApJL*, **673**, L159
- Casares J., 2015, *ApJ*, 808, 80
- Casares J., Charles P. A., 1994, *MNRAS*, **271**, L5
- Casares J., Jonker P. G., 2014, *Space Science Reviews*, **183**, 223
- Casares J., Charles P. A., Jones D. H. P., Rutten R. G. M., Callanan P. J., 1991, *MNRAS*, **250**, 712

- Casares J., Charles P. A., Naylor T., 1992, *Nature*, **355**, 614
- Casares J., Charles P. A., Naylor T., Pavlenko E. P., 1993, *MNRAS*, **265**, 834
- Casares J., Negueruela I., Ribó M., Ribas I., Paredes J. M., Herrero A., Simón-Díaz S., 2014, *Nature*, **505**, 378
- Casares J., Jonker P. G., Israelian G., 2017, preprint, ([arXiv:1701.07450](https://arxiv.org/abs/1701.07450))
- Chaty S., Haswell C. A., Malzac J., Hynes R. I., Shrader C. R., Cui W., 2003, *MNRAS*, **346**, 689
- Chen W., Shrader C. R., Livio M., 1997, *ApJ*, **491**, 312
- Chevalier C., Illovaisky S. A., Leisy P., Patat F., 1999, *A&A*, **347**, L51
- Coriat M., Fender R. P., Dubus G., 2012, *MNRAS*, **424**, 1991
- Cornelisse R., Heise J., Kuulkers E., Verbunt F., in't Zand J. J. M., 2000, *A&A*, **357**, L21
- Cornelisse R., Casares J., Muñoz-Darias T., Steeghs D., Charles P., Hynes R., O'Brien K., Barnes A., 2008, in Bandyopadhyay R. M., Wachter S., Gelino D., Gelino C. R., eds, American Institute of Physics Conference Series Vol. 1010, A Population Explosion: The Nature & Evolution of X-ray Binaries in Diverse Environments. pp 148–152 ([arXiv:0801.3367](https://arxiv.org/abs/0801.3367)), doi:10.1063/1.2945024
- Corral-Santana J. M., Casares J., Muñoz-Darias T., Rodríguez-Gil P., Shahbaz T., Torres M. A. P., Zurita C., Tyndall A. A., 2013, *Science*, **339**, 1048
- Corral-Santana J. M., Casares J., Muñoz-Darias T., Bauer F. E., Martínez-Pais I. G., Russell D. M., 2016, *A&A*, **587**, A61
- Cox A. N., 2000, Allen's astrophysical quantities
- Demorest P. B., Pennucci T., Ransom S. M., Roberts M. S. E., Hessels J. W. T., 2010, *Nature*, **467**, 1081
- Downes R. A., Webbink R. F., Shara M. M., Ritter H., Kolb U., Duerbeck H. W., 2006, VizieR Online Data Catalog, **5123**
- Drake S. A., Ulrich R. K., 1980, *ApJS*, **42**, 351
- Duerbeck H. W., 1988, Bulletin d'Information du Centre de Donnees Stellaires, **34**, 127
- Faulkner J., Flannery B. P., Warner B., 1972, *ApJL*, **175**, L79
- Fender R. P., 2001, *X-ray Astronomy: Stellar Endpoints, AGN, and the Diffuse X-ray Background*, **599**, 101

Este documento incorpora firma electrónica, y es copia auténtica de un documento electrónico archivado por la ULL según la Ley 39/2015.  
*Su autenticidad puede ser contrastada en la siguiente dirección <https://sede.ull.es/validacion/>*

Identificador del documento:	970342	Código de verificación:	pkuTTaUi
Firmado por:	DANIEL MATA SÁNCHEZ UNIVERSIDAD DE LA LAGUNA	Fecha:	29/06/2017 10:41:42
JORGE CASARES VELAZQUEZ UNIVERSIDAD DE LA LAGUNA			29/06/2017 11:14:09
TEODORO MUÑOZ DARIAS UNIVERSIDAD DE LA LAGUNA			29/06/2017 12:50:38
ERNESTO PEREDA DE PABLO UNIVERSIDAD DE LA LAGUNA			04/07/2017 18:28:11

- Fender R., Muñoz-Darias T., 2016, in Haardt F., Gorini V., Moschella U., Treves A., Colpi M., eds, Lecture Notes in Physics, Berlin Springer Verlag Vol. 905, Lecture Notes in Physics, Berlin Springer Verlag. p. 65 ([arXiv:1505.03526](https://arxiv.org/abs/1505.03526)), doi:10.1007/978-3-319-19416-5\_3
- Frank J., King A. R., Lasota J.-P., 1987, *A&A*, **178**, 137
- Fujimoto M. Y., Hanawa T., Miyaji S., 1981, *ApJ*, **247**, 267
- Gallo E., Fender R. P., Pooley G. G., 2004, *Nuclear Physics B Proceedings Supplements*, **132**, 363
- Galloway D. K., Munoz M. P., Hartman J. M., Psaltis D., Chakrabarty D., 2008, *ApJS*, **179**, 360
- Galloway D. K., Premachandra S., Steeghs D., Marsh T., Casares J., Cornelisse R., 2014, *ApJ*, **781**, 14
- Giacconi R., Gursky H., Paolini F. R., Rossi B. B., 1962, *Physical Review Letters*, **9**, 439
- González Hernández J. I., Rebolo R., Israelian G., Filippenko A. V., Chornock R., Tominaga N., Umeda H., Nomoto K., 2008, *ApJ*, **679**, 732
- González Hernández J. I., Suárez-Andrés L., Rebolo R., Casares J., 2017, *MNRAS*, **465**, L15
- Hardy L., Gandhi P., Dhillon V., Littlefair S., Butterley T., Wilson R., 2016, *The Astronomer's Telegram*, **8501**
- Hasinger G., van der Klis M., 1989, *A&A*, **225**, 79
- Hobbs G., Lorimer D. R., Lyne A. G., Kramer M., 2005, *MNRAS*, **360**, 974
- Horne K., Marsh T. R., 1986, *MNRAS*, **218**, 761
- Iijima T., Esenoglu H. H., 2003, *A&A*, **404**, 997
- Jester S., et al., 2005, *The Astronomical Journal*, **130**, 873
- Jonker P. G., Nelemans G., 2004, *MNRAS*, **354**, 355
- Jonker P. G., van der Klis M., Groot P. J., 2003, *MNRAS*, **339**, 663
- Kalogera V., Baym G., 1996, *ApJL*, **470**, L61
- King A. R., Kolb U., Burderi L., 1996, *ApJL*, **464**, L127
- Kiziltan B., Kottas A., De Yoreo M., Thorsett S. E., 2013, *ApJ*, **778**, 66
- Knigge C., 2011, in Schmidtobreick L., Schreiber M. R., Tappert C., eds, Astronomical Society of the Pacific Conference Series Vol. 447, Evolution of Compact Binaries. p. 3 ([arXiv:1108.4716](https://arxiv.org/abs/1108.4716))
- Koen C., Kilkenny D., van Wyk F., Marang F., 2010, *MNRAS*, **403**, 1949

Este documento incorpora firma electrónica, y es copia auténtica de un documento electrónico archivado por la ULL según la Ley 39/2015.  
*Su autenticidad puede ser contrastada en la siguiente dirección <https://sede.ull.es/validacion/>*

Identificador del documento: 970342

Código de verificación: pkuTTaUi

Fecha: 29/06/2017 10:41:42

Firmado por: DANIEL MATA SÁNCHEZ  
*UNIVERSIDAD DE LA LAGUNA*

29/06/2017 11:14:09

JORGE CASARES VELAZQUEZ  
*UNIVERSIDAD DE LA LAGUNA*

TEODORO MUÑOZ DARIAS  
*UNIVERSIDAD DE LA LAGUNA*

ERNESTO PEREDA DE PABLO  
*UNIVERSIDAD DE LA LAGUNA*

29/06/2017 12:50:38

04/07/2017 18:28:11

- Kraft R. P., Mathews J., Greenstein J. L., 1962, *ApJ*, **136**, 312
- Kreidberg L., Bailyn C. D., Farr W. M., Kalogera V., 2012, *ApJ*, **757**, 36
- Krimm H. A., et al., 2011, The Astronomer's Telegram, **3138**, 1
- Krimm H. A., et al., 2013, *ApJS*, **209**, 14
- Kudritzki R.-P., Puls J., 2000, *Annual Review of Astronomy and Astrophysics*, **38**, 613
- Kuulkers E., van der Klis M., Oosterbroek T., Asai K., Dotani T., van Paradijs J., Lewin W. H. G., 1994, *A&A*, **289**, 795
- Kuulkers E., et al., 2007, *A&A*, **466**, 595
- Lasota J.-P., 2001, *New Astronomy Reviews*, **45**, 449
- Leibowitz E. M., Ney A., Drissen L., Grandchamps A., Moffat A. F. J., 1991, *MNRAS*, **250**, 385
- Lipunov V., et al., 2015, The Astronomer's Telegram, **8453**
- Liu Q. Z., van Paradijs J., van den Heuvel E. P. J., 2007, *A&A*, **469**, 807
- Makino F., 1989, IAU Circ., **4782**
- Markoff S., Nowak M. A., Wilms J., 2005, *ApJ*, **635**, 1203
- Markoff S., et al., 2015, *ApJL*, **812**, L25
- Marsh T. R., 1988, *MNRAS*, **231**, 1117
- Marsh T. R., Horne K., Shipman H. L., 1987, *MNRAS*, **225**, 551
- Mata Sánchez D., Muñoz-Darias T., Casares J., Steeghs D., Ramos Almeida C., Acosta Pulido J. A., 2015a, *MNRAS*, **449**, L1
- Mata Sánchez D., Muñoz-Darias T., Casares J., Corral-Santana J. M., Shahbaz T., 2015b, *MNRAS*, **454**, 2199
- Mata Sánchez D., Muñoz-Darias T., Casares J., Jiménez-Ibarra F., 2017a, *MNRAS*, **464**, L41
- Mata Sánchez D., Charles P. A., Armas Padilla M., Buckley D. A. H., Israel G. L., Linares M., Muñoz-Darias T., 2017b, *MNRAS*, **468**, 564
- Matsuoka M., et al., 2009, *PASJ*, **61**, 999
- Matthews J. H., Knigge C., Long K. S., Sim S. A., Higginbottom N., 2015, *MNRAS*, **450**, 3331
- McClintock J. E., Canizares C. R., Tarter C. B., 1975, *ApJ*, **198**, 641
- Mirabel I. F., Rodriguez L. F., Cordier B., Paul J., Lebrun F., 1992, *Nature*, **358**, 215

Este documento incorpora firma electrónica, y es copia auténtica de un documento electrónico archivado por la ULL según la Ley 39/2015.  
*Su autenticidad puede ser contrastada en la siguiente dirección <https://sede.ull.es/validacion/>*

Identificador del documento: 970342	Código de verificación: pkTTaUi
Firmado por: DANIEL MATA SÁNCHEZ UNIVERSIDAD DE LA LAGUNA	Fecha: 29/06/2017 10:41:42
JORGE CASARES VELAZQUEZ UNIVERSIDAD DE LA LAGUNA	29/06/2017 11:14:09
TEODORO MUÑOZ DARIAS UNIVERSIDAD DE LA LAGUNA	29/06/2017 12:50:38
ERNESTO PEREDA DE PABLO UNIVERSIDAD DE LA LAGUNA	04/07/2017 18:28:11

- Mitsuda K., Inoue H., Nakamura N., Tanaka Y., 1989, PASJ, **41**, 97
- Motta S. E., 2016, *Astronomische Nachrichten*, **337**, 398
- Motta S. E., et al., 2015, The Astronomer's Telegram, **8462**
- Motta S. E., Rouco-Escorial A., Kuulkers E., Muñoz-Darias T., Sanna A., 2017, MNRAS, **468**, 2311
- Muñoz-Darias T., 2009, *Publications of the Astronomical Society of the Pacific*, **121**, 935
- Muñoz-Darias T., Casares J., Martínez-Pais I. G., 2005, ApJ, **635**, 502
- Muñoz-Darias T., Motta S., Belloni T. M., 2011, MNRAS, **410**, 679
- Muñoz-Darias T., Fender R. P., Motta S. E., Belloni T. M., 2014, MNRAS, **443**, 3270
- Muñoz-Darias T., et al., 2016, Nature, **534**, 75
- Muñoz-Darias T., et al., 2017, MNRAS, **465**, L124
- Negueruela I., 1998, A&A, **338**, 505
- Neilsen J., Lee J. C., 2009, Nature, **458**, 481
- Nelemans G., Tauris T. M., van den Heuvel E. P. J., 1999, A&A, **352**, L87
- O'Donoghue D., Charles P. A., 1996, MNRAS, **282**, 191
- Osaki Y., 1974, PASJ, **26**, 429
- Özel F., Psaltis D., Narayan R., McClintock J. E., 2010, ApJ, **725**, 1918
- Paczynski B., 1971, *Annual Review of Astronomy and Astrophysics*, **9**, 183
- Paczynski B., 1976, in Eggleton P., Mitton S., Whelan J., eds, IAU Symposium Vol. 73, Structure and Evolution of Close Binary Systems. p. 75
- Palmer D. M., Barthelmy S. D., Cummings J. R., Gehrels N., Krimm H. A., Markwardt C. B., Sakamoto T., Tueller J., 2005, The Astronomer's Telegram, **546**
- Papitto A., di Salvo T., Burderi L., Menna M. T., Lavagetto G., Riggio A., 2007, MNRAS, **375**, 971
- Pavlenko E. P., Martin A. C., Casares J., Charles P. A., Ketsaris N. A., 1996, MNRAS, **281**, 1094
- Ponti G., Fender R. P., Begelman M. C., Dunn R. J. H., Neilsen J., Coriat M., 2012, MNRAS, **422**, L11
- Ponti G., De K., Muñoz-Darias T., Stella L., Nandra K., 2017, MNRAS, **464**, 840

Este documento incorpora firma electrónica, y es copia auténtica de un documento electrónico archivado por la ULL según la Ley 39/2015.  
*Su autenticidad puede ser contrastada en la siguiente dirección <https://sede.ull.es/validacion/>*

Identificador del documento: 970342

Código de verificación: pkUTTaUi

Fecha: 29/06/2017 10:41:42

Firmado por: DANIEL MATA SÁNCHEZ  
 UNIVERSIDAD DE LA LAGUNA

JORGE CASARES VELAZQUEZ  
 UNIVERSIDAD DE LA LAGUNA

TEODORO MUÑOZ DARIAS  
 UNIVERSIDAD DE LA LAGUNA

ERNESTO PEREDA DE PABLO  
 UNIVERSIDAD DE LA LAGUNA

29/06/2017 11:14:09

29/06/2017 12:50:38

04/07/2017 18:28:11

- Proga D., 2000, *ApJ*, **538**, 684
- Remillard R. A., McClintock J. E., 2006, *Annual Review of Astronomy and Astrophysics*, **44**, 49
- Repetto S., Davies M. B., Sigurdsson S., 2012, *MNRAS*, **425**, 2799
- Repetto S., Igoshev A. P., Nelemans G., 2017, *MNRAS*, **467**, 298
- Rhoades C. E., Ruffini R., 1974, *Physical Review Letters*, **32**, 324
- Richter G. A., 1989, *Information Bulletin on Variable Stars*, **3362**
- Schachter J., Filippenko A. V., Kahn S. M., 1989, *ApJ*, **340**, 1049
- Schild R. E., 1977, *The Astronomical Journal*, **82**, 337
- Shahbaz T., Kuulkers E., 1998, *MNRAS*, **295**, L1
- Shahbaz T., Russell D. M., Zurita C., Casares J., Corral-Santana J. M., Dhillon V. S., Marsh T. R., 2013, *MNRAS*, **434**, 2696
- Shahbaz T., Watson C. A., Dhillon V. S., 2014, *MNRAS*, **440**, 504
- Shklovsky I. S., 1967, *ApJL*, **148**, L1
- Steeghs D., Casares J., 2002, *ApJ*, **568**, 273
- Steeghs D., McClintock J. E., Parsons S. G., Reid M. J., Littlefair S., Dhillon V. S., 2013, *ApJ*, **768**, 185
- Steiner J. F., McClintock J. E., Reid M. J., 2012, *ApJL*, **745**, L7
- Thackeray A. D., 1977, *MNRAS*, **180**, 95
- Udalski A., Kaluzny J., 1991, *Publications of the Astronomical Society of the Pacific*, **103**, 198
- Ugliano M., Janka H.-T., Marek A., Arcones A., 2012, *ApJ*, **757**, 69
- Wade R. A., Horne K., 1988, *ApJ*, **324**, 411
- Wagner R. M., Bertram R., Starrfield S. G., Howell S. B., Kreidl T. J., Bus S. J., Cassatella A., Fried R., 1991, *ApJ*, **378**, 293
- Warner B., 1995, *Cambridge Astrophysics Series*, **28**
- White N. E., Mason K. O., 1985, *Space Science Reviews*, **40**, 167
- Witte M. G., Savonije G. J., 2001, *A&A*, **366**, 840
- Zurita C., Casares J., Shahbaz T., 2003, *ApJ*, **582**, 369
- Zurita C., Corral-Santana J. M., Casares J., 2015, *MNRAS*, **454**, 3351

Este documento incorpora firma electrónica, y es copia auténtica de un documento electrónico archivado por la ULL según la Ley 39/2015.  
*Su autenticidad puede ser contrastada en la siguiente dirección <https://sede.ull.es/validacion/>*

Identificador del documento: 970342

Código de verificación: pkuTTaUi

Fecha: 29/06/2017 10:41:42

Firmado por: DANIEL MATA SÁNCHEZ  
*UNIVERSIDAD DE LA LAGUNA*

JORGE CASARES VELAZQUEZ  
*UNIVERSIDAD DE LA LAGUNA*

TEODORO MUÑOZ DARIAS  
*UNIVERSIDAD DE LA LAGUNA*

ERNESTO PEREDA DE PABLO  
*UNIVERSIDAD DE LA LAGUNA*

29/06/2017 11:14:09

29/06/2017 12:50:38

04/07/2017 18:28:11